Hungarian Geographical Bulletin

Volume 72 Number 4 2023

Research Centre for Astronomy and Earth Sciences
GEOGRAPHICAL INSTITUTE

HUNGARIAN GEOGRAPHICAL BULLETIN

Quarterly Journal of the
GEOGRAPHICAL INSTITUTE
RESEARCH CENTRE FOR ASTRONOMY AND EARTH SCIENCES

Indexed by Elsevier-GEOBASE®, Elsevier-SCOPUS®,
EBSCO Information Services, CAB Abstracts, Current Geographical Publications,
Scimago Journal & Country Rank, Google Scholar

HUNGARIAN GEOGRAPHICAL BULLETIN 72 2023 (4)

CONTENT

György Varga, Ágnes Rostási, Aida Meiramova, Pavla Dagsson-Waldhauserová and *Fruzsina Gresina:* Increasing frequency and changing nature of Saharan dust storm events in the Carpathian Basin (2019–2023) – the new normal? 319

Fatemeh Nooshin Nokhandan, Kaveh Ghahraman and *Erzsébet Horváth:* Erosion susceptibility mapping of a loess-covered region using Analytic Hierarchy Process – A case study: Kalat-e-Naderi, northeast Iran..... 339

Balázs Víg, Gábor Varga, Richárd Balogh, Dénes lóczy, László Nagyváradi and *Szabolcs Ákos Fábián:* Channel-reach morphometric analysis on a headwater stream in a low-mountainous region: A case study from Mecsek Hills 365

Nizom Farmonov, Khilola Amankulova, Shahid Nawaz Khan, Mokhigul Abdurakhimova, József Szatmári, Tukhtaeva Khabiba, Radjabova Makhliyo, Meiliyeva Khodicha and *László Mucsi:* Effectiveness of machine learning and deep learning models at county-level soybean yield forecasting..... 383

Adam Piasecki: European Green Deal + Poland + hydroelectric plants = Future? 399

Book review section

Nowak, M.J. et al.: Spatial Planning Systems in Central and Eastern European Countries. Review and Comparison of Selected Issues *(Olena Denysenko)* 415

Flint Ashery, S.: Micro-residential Dynamics: A Case Study of Whitechapel, London *(Ramóna Vámos)* 419

DOI: 10.15201/hungeobull.72.4.1 Hungarian Geographical Bulletin **72** 2023 (4) 319–337.

Increasing frequency and changing nature of Saharan dust storm events in the Carpathian Basin (2019–2023) – the new normal?

György VARGA[1,2,3], Ágnes ROSTÁSI[2,4], Aida MEIRAMOVA[2,4], Pavla DAGSSON-WALDHAUSEROVÁ[5,6] and Fruzsina GRESINA[1,3]

Abstract

The number and intensity of Saharan dust storm events identified in Europe has been increasing over the last decade. This can be explained by the role of ongoing climate change. An extension of previous studies covering a 40-year period is presented in this paper, with new data on the frequency, synoptic meteorological background, source areas, grain size, grain shape and general mineralogy of deposited dust for the period 2019–2023 in the Carpathian Basin. A total of 55 dust storm episodes have been identified in the region over the five-year period, which is significantly higher than the long-term average. The classification based on synoptic meteorological background clearly showed that the frequency of circulation types with a more pronounced meridional component increased and dust material reached further north more frequently than before. In several cases, large amounts of dust were deposited, from which samples were collected and subjected to detailed granulometric analysis. The varied grain size data showed that coarse silt (20–62.5 μm) and sand (62.5 < μm) fractions were also present in large quantities in the transported dust material.

Keywords: Saharan dust, climate change, Carpathian Basin, grain size

Received October 2023, accepted December 2023.

Introduction

The changing climate has increased the importance of atmospheric research in recent decades. The combined study of the many interconnected components of the Earth system is necessary to gain a deeper understanding of the scale and rate of change in the atmosphere, and to unravel the interconnections between them, on a scale and at a rate not previously known in human history (Easterling, D.R. *et al*. 2000; Shepherd, T.G. 2014; IPCC, 2022). A key part of this is the study of atmospheric components traveling with the major circulations and the winds driven by these airflow systems over long distances (Harrison, S.P. *et al.* 2001; Kohfeld, K.E. and Tegen, I. 2007; Maher, B.A. *et al.* 2010; Pósfai, M. and Buseck, P.R. 2010).

Over the past decades, atmospheric mineral dust has been in the focus of climate and environmental research. The emission, transport and deposition of particulate matter has an impact on our environment

[1] Geographical Institute, HUN-REN Research Centre for Astronomy and Earth Sciences, Budaörsi út 45. H-1112 Budapest, Hungary. Corresponding author's e-mail: varga.gyorgy@csfk.org
[2] Research Institute of Biomolecular and Chemical Engineering, University of Pannonia, Veszprém, Hungary.
[3] ELTE Department of Meteorology, Institute of Geography and Earth Sciences, ELTE Eötvös Loránd University, Budapest, Hungary.
[4] Air Chemistry Research Group, Research Institute of Biomolecular and Chemical Engineering, University of Pannonia, Veszprém, Hungary.
[5] Faculty of Environmental and Forest Sciences, Agricultural University of Iceland, Reykjavik, Iceland.
[6] Department of Water Resources and Environmental Modelling, Faculty of Environmental Sciences, Czech University of Life Sciences Prague, Prague, Czech Republic.

locally, regionally and globally (Monteiro, A. *et al.* 2022). Mineral particles with a wide variety of material properties are released into the atmosphere and scatter, reflect and absorb radiation from the sun, directly modifying the irradiance patterns (Arimoto, R. 2001). The role of particulate matter in cloud formation is considered as an indirect radiative effect (Nickovic, S. *et al.* 2016; Rieger, D. *et al.* 2017; Weger, M. *et al.* 2018; Adebiyi, A.A. *et al.* 2023). For a given water vapour content, the increased atmospheric particle number also increases the number of condensation nuclei required for cloud and ice formation, thus contributing to the formation of more but smaller cloud elements (Hoose, C. *et al.* 2008; Nickovic, S. *et al.* 2016; Ginoux, P. 2017; Kok, J.F. *et al.* 2017; Ansmann, A. *et al.* 2019). This will result in the formation of lighter but longer-lived clouds due to the dust-loaded air masses. Other environmental effects of long-range mineral particles at the point of deposition are also significant: in soil formation (see e.g., Terra rossa soils of the Mediterranean – MacLeod, D.A. [1980]; Jackson, M.L. *et al.* [1982]; Jahn, R. *et al.* [1991]; Atalay, I. [1997]; Muhs, D.R. *et al.* [2010]); in the carbon cycle through the iron and phosphorus supply to ocean and marine ecosystems (Ridgwell, A.J. 2002); in the modification of precipitation pH (Rodá, F. *et al.* 1993; Rogora, M. *et al.* 2004; Čanić, K.Š. *et al.* 2009) and in many other processes (for details, see e.g., Meinander, O. *et al.* 2022; Monteiro, A. *et al.* 2022).

Every year, billions of tons of mineral dust are picked up by the winds from arid semi-arid regions and transported, sometimes thousands of kilometres (Tegen, I. and Lacis, A.A. 1996; Mahowald, N.M. *et al.* 1999, 2006; Ginoux, P. *et al.* 2001). The main source areas are in the Sahara, from where the dust is transported to the Atlantic (as far as the Americas); northwards to Europe; and eastwards to the Middle East.

The frequency of dust transport to Europe has changed in recent years (Varga, Gy. 2020; Hrabcak, P. 2022; Salvador, P. *et al.* 2022; Cuevas-Agulló, E. *et al.* 2023; Kok, J.F. *et al.* 2023). In Spain, France, Central Europe, the Carpathian Basin and even at higher latitudes such as Greenland (Francis, D. *et al.* 2018), Iceland (Varga, Gy. *et al.* 2021), and Finland (Varga, Gy. *et al.* 2023), the changing flow patterns and the occurrence of African dust have been noticed. The general picture of the Saharan dust masses and dust storm events reaching the Carpathian Basin over the last 40 years has been described in great detail in previous publications (Varga, Gy. *et al.* 2013; Varga, Gy. 2020). In this paper, we present the frequency and intensity variations observed in the last few years, including the characteristics of the grain size and particle size distribution of the transported dust.

Material and methods

Study area

We investigate Saharan dust events reaching the Carpathian Basin (45°–48.5° N, 16°–23° E). This closed basin in central Europe is bounded by the Alps, Carpathians and Dinarides mountain ranges. The climate and weather are determined by three meteorological regimes: Atlantic, Continental and Mediterranean. Previous research by Varga, Gy. (2020) on dust storm events from the Sahara has shown that air masses of African origin typically transport desert dust into the region in spring and summer. Winter dust storm events have also increased in the last decade, sometimes accompanied by significant deposition and muddy rain. From 1979 to 2018, 218 Saharan dust storm events have reached the Carpathian Basin, with a clear increasing trend in the time series.

Identification of dust storm events

For reasons of consistency with previous research, the same methodology was used as before. Potential dust storm events were identified using standardised values from

daily TOMS, EP and OMI Aerosol Index data available since 1979. Verification of the potential events was based on a multi-step procedure using satellite imagery, modelling of the air trajectory propagation by HYSPLIT back-trajectory (HYbrid Single-Particle Lagrangian Integrated Trajectory – Stein, A.F. *et al.* 2015), CALIPSO aerosol v4.10 subtype vertical profiles (https://www-calipso.larc.nasa.gov/) to verify the presence of mineral dust in the air column, and the MERRA-2 Dust Column Mass Density dataset available since 1980 (Area-Averaged of Dust Column Mass Density [M2T1NXAER v5.12.4] – Gelaro, R. *et al.* [2017] – data were obtained from Giovanni application for visualisation and access Earth science remote sensing data platform [https://giovanni.gsfc.nasa.gov/giovanni/]). Also from the MERRA-2 database are the wet and dry dust deposition data (Dust Dry Deposition Bin-all: M2TMNXADG v5.12.4; Dust Wet Deposition Bin-all: M2TMNXADG v5.12.4; Dust Dry+Wet Deposition Bin-all: M2TMNXADG v5.12.4).

In addition to the areal averages of the MERRA-2 datasets, we also used spatial flux data of dust dispersion and the Barcelona Supercomputing Center NMMB/BSC model (Pérez, C. *et al.* 2011; Klose, M. *et al.* 2021), where dust load, dry and wet deposition values were estimated using the SDS-WAS (Sand and Dust Storm Warning Advisory and Assessment System) interface.

Synoptic meteorology

Synoptic meteorology-based typing of individual events was based on the Daily Mean Composite application of NOAA Earth System Research Laboratory (http://www.esrl.noaa.gov/psd/) using the NCEP/NCAR (National Centers for Environmental Protection / National Center for Atmospheric Research) Reanalysis Project dataset (Kalnay, E. *et al.* 1996) 700 hPa potential level, meridional and zonal wind components, and wind vectors. The use of the 700 hPa level as a vertical level, also considered as a typical transport altitude, has been shown to be characteristic in previous studies (Alpert, P. *et al.* 2004; Barkan, J. *et al.* 2005; Varga, Gy. *et al.* 2013). To analyse the possible role of high-altitude eddy-driven polar jet stream flow and its changing patterns, data for the 250 hPa level were also examined.

Granulometric analyses

Mineral dust samples collected during dust storm events coinciding with intense deposition were analysed using automated static image processing technology with a Malvern Morphologi G3-IDSE. During the study, the size and shape parameters of tens of thousands (typically 50,000) of individual grains are automatically recorded during scanning with a 40 pixel per μm^2 resolution objective.

Among the available parameters, we used the circle-equivalent diameter, high-sensitivity circularity, convexity, aspect ratio, solidity and grayscale intensity determined as a function of transmittance. Circle-equivalent diameter is calculated as the diameter of a circle with the same area as the projected two-dimensional particle image.

The shape parameters are highly dependent on the size of the grain (partly for measurement-technical reasons), so the 5–40 μm range was investigated for shape-analyses. An accurate indicator of the circularity property is the high sensitivity (HS) circularity, which is calculated by the instrument as the ratio of the projected area of the grain to the square of its circumference. Solidity value is given by the ratio of the area of the investigated object to the area enclosed by the convex hull, while aspect ratio is the ratio of the width to the length of a given particle. The value of convexity is determined by dividing the circumference of the convex hull by the circumference of the grain. The perimeter of the convex hull is the smallest convex polygon containing the area of the grain.

In addition to automated image processing, mineral composition studies were also performed using a Raman spectrom-

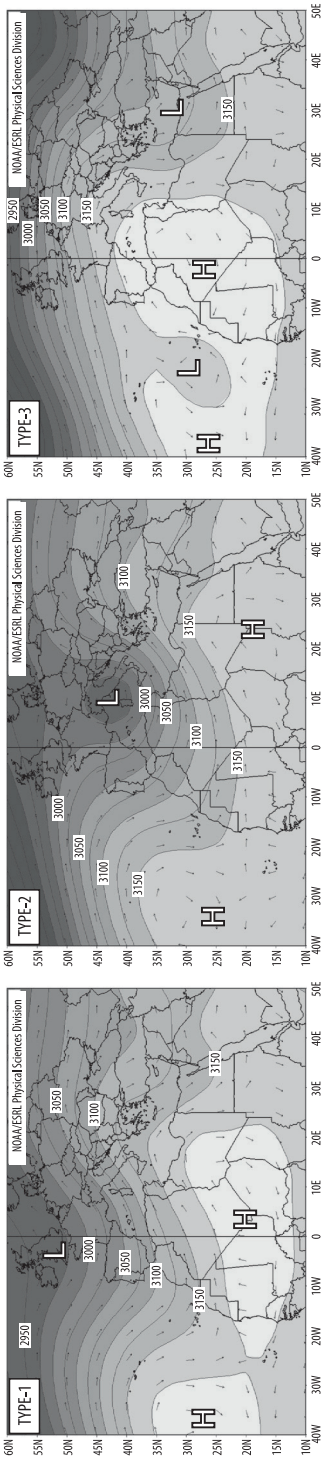

Fig. 1. Synoptic meteorological background (mean geopotential height map and wind vectors at 700 hPa) of different types of Saharan dust events.
Source: Varga, Gy. 2020.

eter (Kaiser Optical Systems Raman Rxn1 Spectrometer, 785 nm, < 500 mW) as part of the instrument, after correlating the recorded spectra of selected grains with a reference database (BioRad-KnowItAll Informatics System 2017, Raman ID Expert).

Results

Saharan dust storm events in the Carpathian Basin

The identified dust storm events were classified into three main groups based on their synoptic meteorological background and closely related air mass trajectories. A detailed description of the classification can be found in Varga, Gy. (2020). The most frequent events (about two thirds of all events) are associated with the southward flow of the high-altitude atmospheric trough over the Eastern Atlantic basin, and mainly Saharan dust storm events transported over the Western Mediterranean basin are placed in this cluster. African air masses arriving into the Carpathian Basin over the Central Mediterranean basin with the frontal flow of the Mediterranean cyclones were classified as Type-2, accounting for a quarter of all episodes. The relatively rare Type-3 events, under which conditions dust material was drifting over the Atlantic Ocean and then became long-range dust transport episodes with westerly winds, accounted for 8 percent of all events over the last four and a half decades *(Figure 1).*

The previously published database has been extended to November 2023, and now contains 273 identified Saharan dust storm events from 1979 onwards. The time series and seasonality distributions, completed with MERRA-2 deposition data, are shown in *Figure 2* and *Table 1*. The data clearly demonstrate that the number of dust storm events in the region has increased over the last decade and a half. During the first three decades of the period under study, an average of 3–5 episodes per year hit the Carpathian Basin. This number increased to

Table 1. Decadal, seasonal and type-specific frequencies of Saharan dust storm events in the Carpathian Basin between 1979 and 2023

Types and seasons			Decades					
			1998–2008	1989–1998	1999–2008	2009–2018	2019–2023*	*Total*
Type-1	Seasons	spring	14	10	15	17	10	*66*
		summer	14	4	15	24	10	*67*
		autumn	2	2	3	9	10	*26*
		winter	2	–	2	13	5	*22*
	T1 total		32	16	35	63	35	*181*
Type-2	Seasons	spring	7	6	8	7	6	*34*
		summer	–	–	2	2	2	*6*
		autumn	3	1	2	4	1	*11*
		winter	4	–	2	7	1	*14*
	T2 total		14	7	14	20	10	*65*
Type-3	Seasons	spring	–	1	–	2	–	3
		summer	1	–	–	5	6	12
		autumn	1	–	3	–	2	6
		winter	–	3	1	–	2	6
	T3 total		2	4	4	7	10	27
Total			*48*	*27*	*53*	*90*	*55*	*273*

*Refers to a half-decade period.

an average of 9 in the 2010s, and to 11 in the 2019–2023 period, which is examined below in detail. According to surface observations and European reports (e.g., Salvador, P. *et al.* 2022; Cuevas-Agulló, E. *et al.* 2023), the intensity of each event (the amount of transported and deposited dust) also increased during this period. This is confirmed by the increasing frequency of local muddy rain events, which regularly receive considerable media coverage.

A detailed analysis of the dust storm events of the fifth (half)decade of the 45-year database has been undertaken in this article. This included the identification of 55 new episodes between 2019 and 2023. In addition to the increased number of events, it was striking that the occurrence of Type-3 episodes increased significantly, especially in 2022 and 2023. During the five-year period, 10 such episodes were recorded, compared to a total of 17 in the previous 40 years. However, based on surface observations, MERRA-2 Dust Column Mass Density data and dust load data from the BSC operational forecast, there have been changes in intensity in recent years (*Figures 3* and *4*).

Characteristics of some selected events

To illustrate the changing intensity of dust transport and increasing frequency of Type-3 episodes, 11 events were selected *(Figure 5)*, the main characteristics of which are presented in the following:

SDE #1: 23 April 2019.
The most intense and widespread Saharan dust storm event in decades hit Europe in April 2019. By 19 April, atmospheric dust forecast models were already predicting large amounts of dust over the Iberian Peninsula, with a steady supply from the African continent. The cut-off low of 20 April 2019 (a closed circulation system formed from an upper-level trough in the preceding days) determined the synoptic situation of North Africa, and the cyclonic flow lifted a huge mass of desert dust into the atmosphere. The dust-loaded air masses drifted north and northeast (to the western Mediterranean, Spain, southern France and Italy, then towards the Balkans, central and western Europe, the British Isles), and on 23–24 April atmospheric dust was observed over the continent from almost

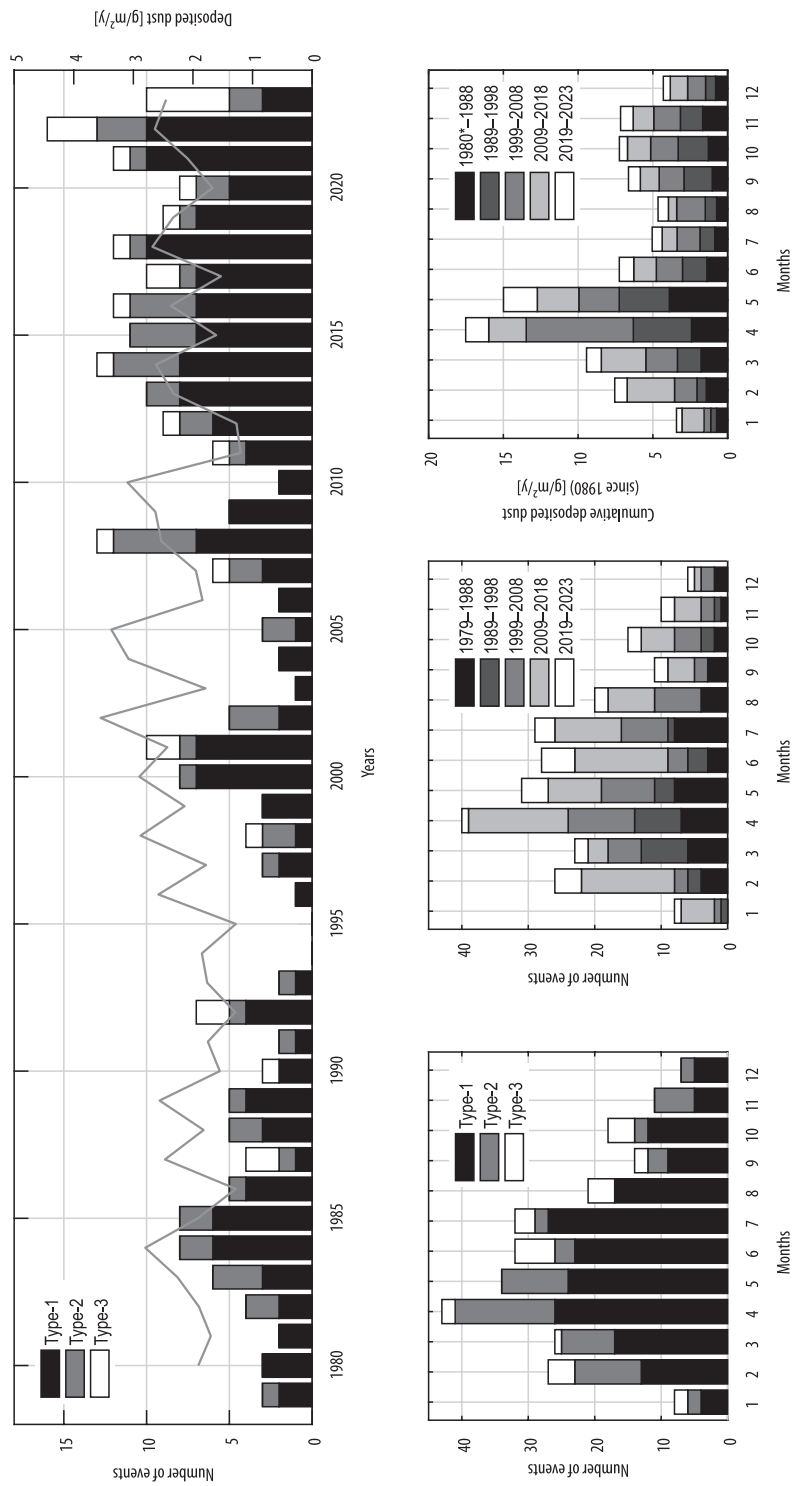

Fig. 2. Frequency of Saharan dust storm events by type and temporal changes in modelled values of deposition in the Carpathian Basin between 1979 and 2023. *Source:* Authors' own elaboration.

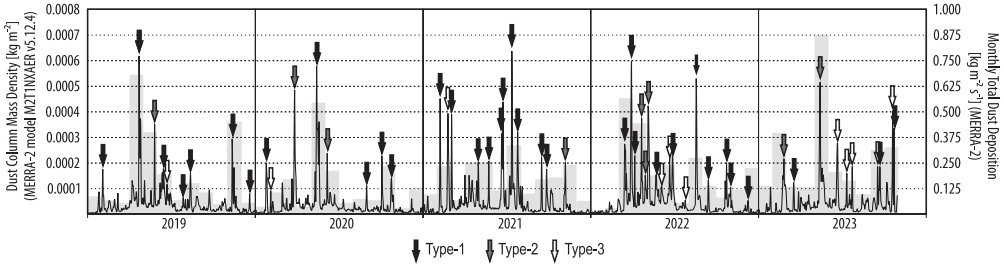

Fig. 3. MERRA-2 daily Dust Column Mass Density and monthly deposition data, and identified Saharan dust storm events by type, 2019 to 2023. *Source:* Authors' own elaboration.

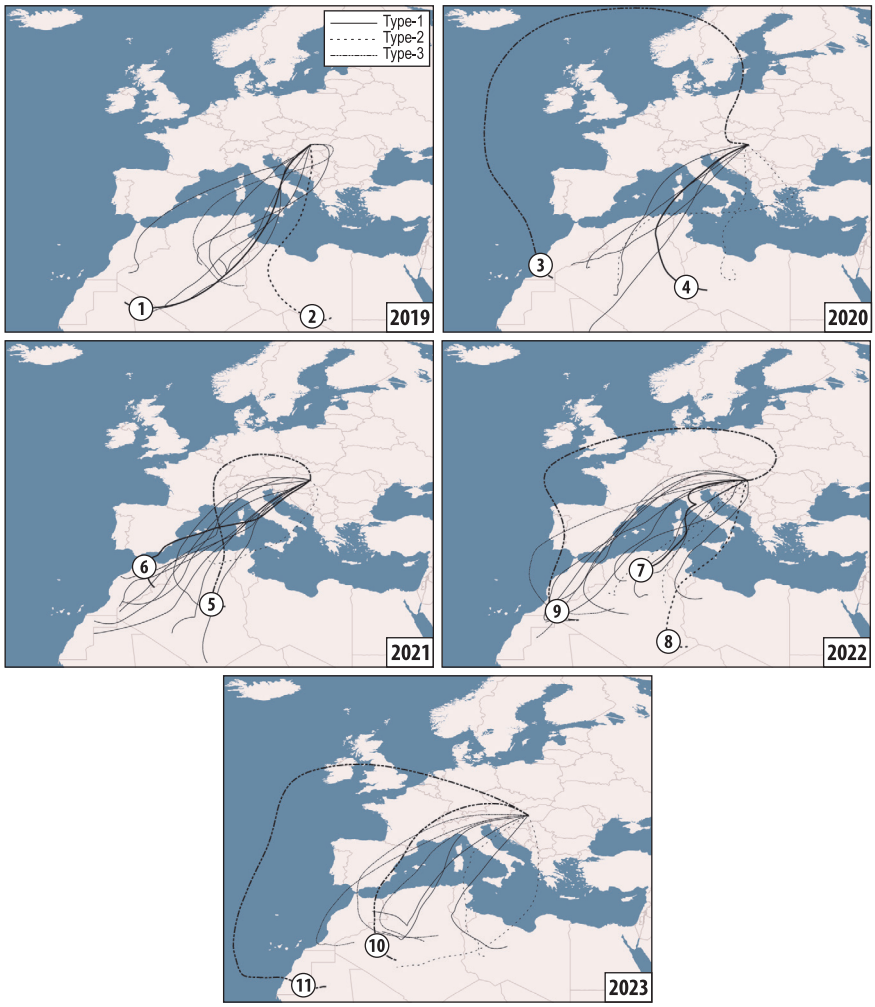

Fig. 4. Dust transport pathways of Saharan dust storm events reaching the Carpathian Basin by year between 2019 and 2023. (Numbered and bolded trajectories of selected episodes are described in the text). *Source:* Authors' own elaboration.

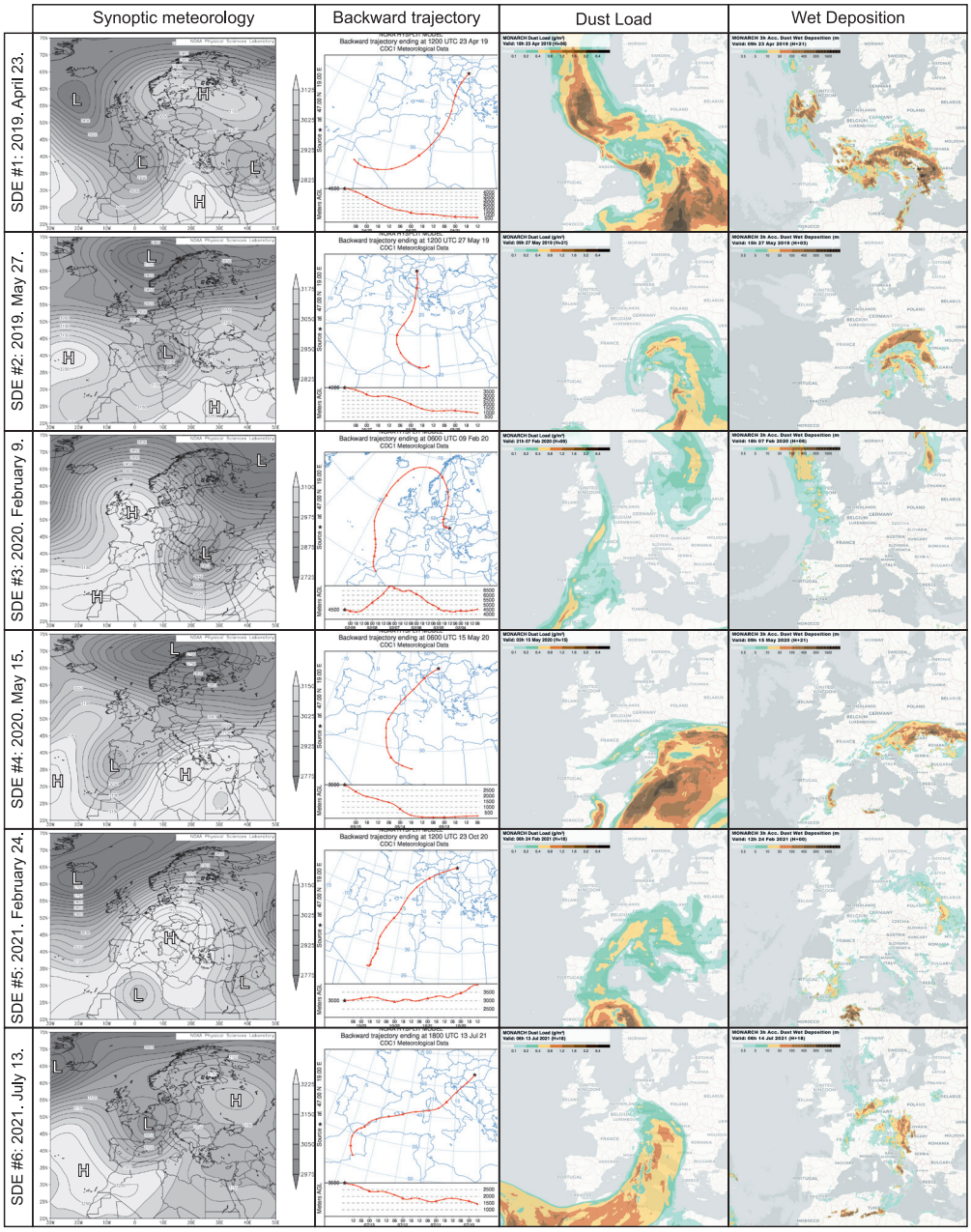

Fig. 5. Synoptic meteorological background (700 hPa geopotential height); backward trajectories of dust-loaded air masses; modelled dust load and wet dust deposition. *Data source:* WMO Barcelona Dust Regional Center and the partners of the Sand and Dust Storm Warning Advisory and Assessment System (SDS-WAS) for Northern Africa, the Middle East and Europe.

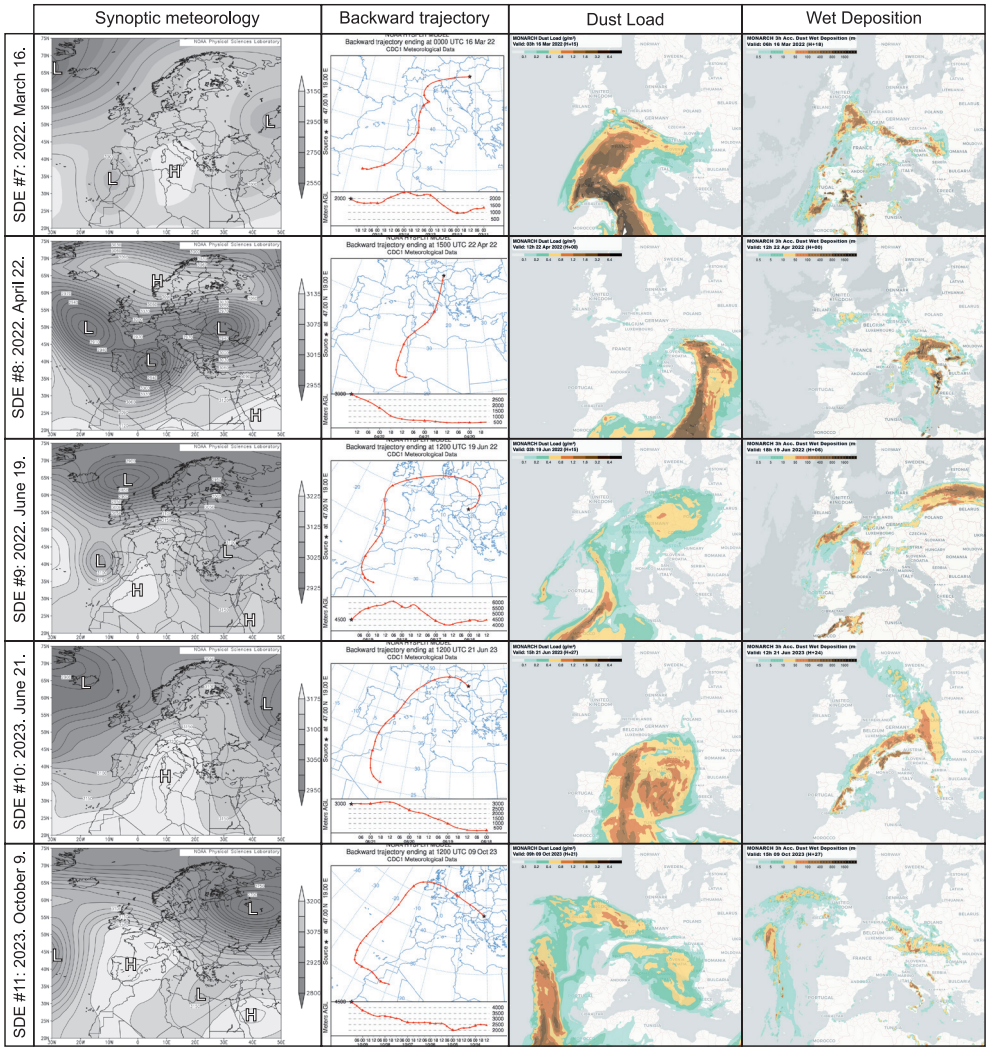

Fig. 5. – Continued.

Iceland to southern Turkey. The meteorological background to the event is a cut-off low resulting from the southward movement of a high-altitude atmospheric trough over the eastern Atlantic basin. The intense southerly flow formed on the foreward side of the eastward moving low pressure plume, which then spread from NW Europe to the eastern Mediterranean Sea due to the blocking effect of the anticyclone over the continent.

SDE #2: 27 May 2019.

The strong southerly flow (meridional wind component above 20 < m/s at the typical dust transport height of 700 hPa) of the foreward side of the cyclone that formed over the western Mediterranean Sea and then deepened over the central sub-basin drifted the Saharan dust over the Carpathian Basin in late May 2019. During the precipitation events associated with the Mediterranean cyclone,

large amounts of dust were washed out over central Europe. An extensive cirrus canopy was observed in satellite imagery and in cloud subtype analyses of CALIPSO vertical profiles, the formation of which is assumed to be driven by increased dust concentration and condensation nuclei number.

SDE #3: 9 February 2020.
The transport path of the Saharan dust storm event identified in February 2020 is the longest trajectory identified in recent decades, with desert dust reaching the Carpathian Basin atmosphere after a transport of about 7,500 km. The episode associated with the Western Sahara dust plume initially headed towards the Atlantic Ocean, driven by the clockwise flow regime of a large-scale anticyclone over the southern Iberian Peninsula and the north-western Sahara. Dust drifting over the ocean was carried northwestward by the circulation system of the high-pressure atmospheric object and then moved towards Europe in the westerly wind belt. During this period, the unusually southerly position of the polar jet stream contributed to the formation of several Atlantic depressions and their associated storms, violent cyclones and synoptic situations dominated by meridional wind components. The former Iberian anticyclone led to the formation of a western European omega block, which was of fundamental importance in controlling the direction of dust transport. It should be mentioned that the present episode is also included in the catastrophe of Saharan dust storm events reaching Iceland, as well as the April 2019 episode (Varga, Gy. *et al.* 2021).

SDE #4: 15 May 2020.
Intense dust storms developed in the southern foothills of the Atlas Mountains during the powerful wind gusts of a cold drop from the high amplitude southerly wave of the polar jet stream. African air masses, driven by a southwesterly flow driven by a pressure gradient generated by a frontal trough crossing Europe in a southwesterly-northeasterly direction and a pressure gradient between a southeastern European high-pressure blockage, reached the Carpathian Basin in mid-May 2020. The huge amounts of particulate matter were transported from the southern Atlas foothills, from unconsolidated sediments of its mountain foothills, from the deposits of its intermittent water flows and from the sediments of its salt lakes, which also have a hectic water flow, so from relatively nearby Saharan source areas. Dust deposition has been reported from many countries (Garofalide, S. *et al.* 2022), and the deposited dust was clearly observed on car windscreens, roof windows and other outdoor surfaces.

The particle size of the samples collected from the deposited particulate matter varied over a wide range, with both the finest (fine silt) and sand fractions appearing on the distribution curve, with a mode of 32.6 μm.

SDE #5: 24 February 2021.
The large-scale circulation conditions of the event were determined by a central European atmospheric ridge and the omega blocking situation formed by the troughs on either side. The western trough appeared more prominent on the pressure maps than the eastern one and extended as far northwest as Africa, where a cut-off low was also formed. This meteorological situation persisted for days and in this stationary state the Saharan dust transport over the western Mediterranean basin flowed directly northwards towards higher latitudes. In the atmospheric trough flow regime, the transport of dust at latitudes N50° deviated from the meridional direction and followed the isohips towards the Carpathian Basin. Both the enhanced, above-average meridionality and the extreme amount of dust transport associated with this event have been discussed in detail by Francis, D. *et al.* (2023). Intense dust deposition from southwestern Europe to Finland has created opportunities for citizen science campaigns in many places (e.g., Meinander, O. *et al.* 2023). The results of a highly successful project to collect the dust deposited in the French Alps in connection with the event were published in Dumont, M. *et al.* (2023).

The particle size of the samples deposited in the Carpathian Basin was found to be particularly coarse-grained, with a mode size of 98.2 μm in the distribution curve during our measurements, and smaller particles barely appearing in the sample.

SDE #6: 13 July 2021.
On 9 July 2021, intense dust storms developed in the Tidikelt depression (surrounded by plateaus (Tanezrouft, Plateau du Tademait) and mountains (Ahaggar, Tassili-n-Ajjer), with dust material drifting northwards due to the flow system of a low-pressure atmospheric formation moving eastwards from the Canary Islands. The Saharan dust-loaded air masses were transported eastwards from western Europe by a cyclonic cold front into the central European atmosphere, where an intense washout episode was again observed.

SDE #7: 16 March 2022.
Another Saharan dust storm event affecting almost all of Europe hit our region in March 2022. Images of orange-coloured snowfields in the Pyrenees and the Alps attracted a lot of press coverage, but even in Finland there was significant washout (Meinander, O. *et al.* 2023; Varga, Gy. *et al.* 2023). The synoptic meteorological background of the event was similar to that of the previous ones: the cut-off low from the high-altitude trough, generated by an unusually high-amplitude southern wave of the polar jet stream, caused violent dust storm to pass through the Atlas, with dust material drifting along the northward branch towards the higher latitudes of Europe.

The deposited fine-grained dust samples had a mode size of 12.1 μm, which is the smallest of our Saharan dust samples collected so far.

SDE #8: 22 April 2022.
A powerful cyclone over the Iberian Peninsula advected large amounts of particulate matter into the Mediterranean Sea from the Atlas forelands on 20 April 2022. Two days later, as the low-pressure formation drifted eastwards, its frontal meridional flow brought dust-loaded air masses to the atmosphere of central Europe.

Precipitation-washed particulate matter once again appeared as muddy rain in the Carpathian Basin, with the mode of the samples occurring at 26 μm on the volume-based size distribution curve.

SDE #9: 19 June 2022.
The steep pressure gradient between the cut-off low from the high-latitude trough along the Atlantic coast of the Iberian Peninsula and northwest Africa and the extensive anticyclone that dominates the weather of southwestern Europe was responsible for the atmospheric transport of Saharan dust, which flowed northward in association with the circulation system. The Saharan dust reached the Carpathian Basin along the northern edge of the dissipating anticyclone, with its clockwise flow passing the British Isles, northern Germany and Poland.

SDE #10: 21 June 2023..
The weather of the European continent was dominated by an omega-block low-high-low pressure system with an anticyclonic centre over the central Mediterranean basin. The southerly flow of the western low-pressure system transported particulate matter from the intermountain basins of the Atlas northwards, where the circulation of the northern edge of the anticyclonic system carried air masses towards the Carpathian Basin.

SDE #11: 9 October 2023.
The weather in western Europe and northwest Africa was dominated by a powerful anticyclone in early October 2023. Large amounts of dust were released from the Atlantic coastal West African source areas as a result of localised heavy dust storms, which drifted over the ocean and then northwards. In the North Atlantic region, a series of cyclones deepened and the steep pressure gradient between the prevailing atmospheric pressure regimes allowed the further long-range transport of air masses containing large amounts of dust. Dust also reached the Irish region and then flowed towards Central Europe via northwesterly currents.

Temperature changes during dust storm events

The intrusion of African air masses into the temperate zone necessarily leads to warming. The variability in seasonality, synoptic background, intensity, transport path and frequency of Saharan dust storm events by type all play a role in the observed temperature changes during episodes over time.

During Type-1 SDEs, the major warming effect is mainly observed in autumn and winter, but the average temperature increase is above 1.5 °C in about all seasons *(Table 2).* Type-2 events associated with Mediterranean cyclones also typically cause above-average warming in autumn and winter, but over the whole period there has been an increase in the spring warming effect on decadal averages. However, just in the last few years, this effect has again been reduced.

In the last five-year period examined in detail, the number of Type-3 events has increased, but the low number of cases means that average effects are not worth talking about for earlier periods. Due to the longest transport path, the warm advection influence of this type could be the weakest, but due to the synoptic meteorological background, i.e., the need for anticyclonic effects in the study area prior to the arrival of dust, a relatively large average temperature increase has been observed in the recent past for summer events.

Granulometric and mineral characteristics

Granulometric analyses of dust samples collected during intense deposition events reveal a high degree of heterogeneity *(Figure 6).* The particle size of the dust material varies widely,

Table 2. Average surface temperature increase in the Carpathian Basin during the Saharan dust events by decades and synoptic type

Decades	Types	Seasons				Annual mean
		spring	summer	autumn	winter	
1979–1988	Type-1	2.7	1.7	6.6	3.6	2.6
	Type-2	-0.6	–	2.2	2.0	0.8
	Type-3	–	-2.2	2.9	–	0.3
	Decadal mean	*1.6*	*1.4*	*3.8*	*2.5*	*2.0*
1989–1998	Type-1	3.7	3.6	4.4	–	3.8
	Type-2	1.0	–	3.3	–	1.3
	Type-3	9.6	–	–	2.4	4.2
	Decadal mean	*3.1*	*3.6*	*4.1*	*2.4*	*3.2*
1999–2008	Type-1	3.3	3.7	6.6	0.0	3.6
	Type-2	2.0	4.4	5.4	7.4	3.6
	Type-3	–	–	5.7	4.1	5.3
	Decadal mean	*2.8*	*3.8*	*6.0*	*3.8*	*3.7*
2009–2018	Type-1	2.6	3.6	4.8	4.1	3.6
	Type-2	4.4	1.6	5.9	4.6	4.5
	Type-3	2.3	4.0	–	–	3.6
	Decadal mean	*3.0*	*3.6*	*5.1*	*4.3*	*3.8*
2019–2023*	Type-1	1.4	4.0	5.4	6.9	4.1
	Type-2	0.4	1.9	3.1	1.6	1.0
	Type-3	–	3.3	0.3	1.1	2.3
	Decadal mean	*1.0*	*3.6*	*4.5*	*4.8*	*3.2*
Total	Type-1	2.7	3.3	5.4	4.3	3.5
	Type-2	1.5	2.8	4.3	4.0	2.6
	Type-3	4.7	3.2	3.4	2.3	3.2
	Mean	*2.4*	*3.2*	*4.8*	*3.9*	*3.3*

*Refers to a half-decade period.

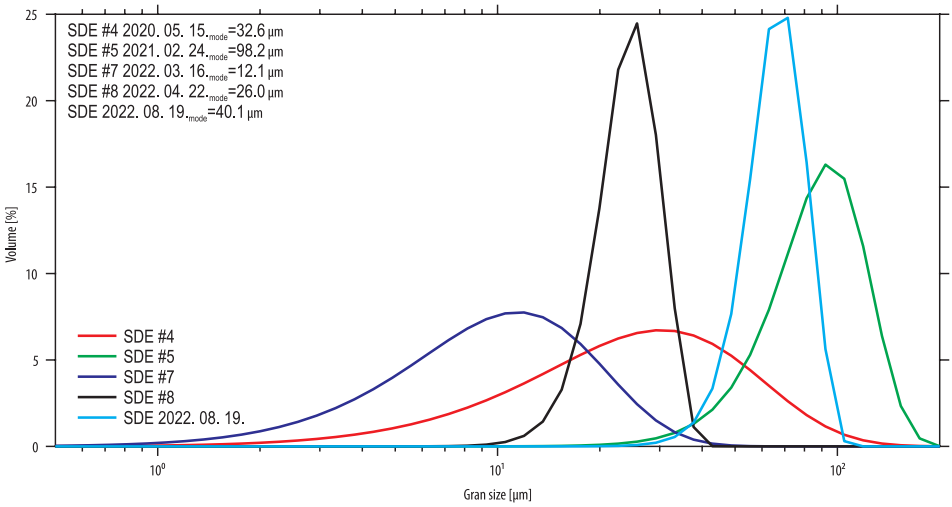

Fig. 6. Grain size distributions of Saharan dust material deposited in Hungary. *Source:* Authors' own elaboration.

with relatively coarse particles often observed, exceeding 20–30 µm. For the samples studied, the modes of the volume distribution curves varied from 12.1 µm to 98.2 µm. In some events, the size distributions spanned a wide range.

This variability was less observed in the shape parameters. Although we have limited the size dependence of the parameters by analysing only the 5–40 µm range, it is still evident that the largest grain size sample of the 24 February 2021 event shows a different character (with significantly smaller convexity and HS circularity values). It is also observed that the dimensionless Intensity mean values, which are also closely related to size and depend on the light transmittance, also vary in a large range (73.4–117.0). Nevertheless, the shape characteristics of the other samples showed very small differences *(Table 3).* The high convexity (0.97–0.98) and solidity (0.94–0.98) parameters clearly support the eolian origin.

Our Raman spectroscopy measurements, which do not provide enough data for detailed mineralogical analysis, identified quartz, feldspar, calcite, dolomite and gypsum in the samples. In addition, other minerals are obviously present in the deposited material, but the technology used is currently not suitable for their detection *(Table 4).*

However, from the information available, it is clear that quartz and feldspars make up the largest proportion of the samples. The number of quartz grains is closely related to the average grain size, with the samples containing the coarsest grains showing the highest number of quartz. In general, it was also observed that gypsum was mainly observed in samples from the Tunisian chotts and the southeastern foreland of the Atlas. However, it is also clear that these mineralogical data do not allow the possible sources to be precisely determined. It is also notable that the sample associated with the strong dust storm event of March 2022, which affected the largest area, was heterogeneous in mineralogical terms, presumably due to the combined emission of several dust sources that were acive at the same time and the mixing of dust material.

Discussion

Changing dust transport mechanisms – the new normal?

We have highlighted in our previous studies that the number and intensity of Saharan dust storm events in Central Europe (Varga, Gy.

Table 3. Shape properties of mineral particles sampled during dust deposition events in Hungary (D[4,3] – Volume Moment Mean – De Brouckere Mean)

Sample name	SDE #4 15 May 2020	SDE #5 24 February 2021	SDE #7 16 March 2022	SDE #8 22 April 2022	SDE 19 August 2022
Aspect Ratio D[4,3]	0.78	0.77	0.77	0.77	0.78
Convexity D[4,3]	0.97	0.86	0.98	0.97	0.98
Elongation D[4,3]	0.45	0.45	0.46	0.45	0.54
HS Circularity D[4,3]	0.81	0.63	0.82	0.82	0.86
Solidity D[4,3]	0.96	0.94	0.96	0.96	0.98
Mean Intensity D[4,3]	77.56	117.00	78.19	73.39	93.47
Intensity STDV D[4,3]	26.85	25.52	23.21	22.40	19.12

Table 4. General mineralogical properties of the Saharan dust samples collected in Hungary

SDE	Quartz	Feldspar	Calcite	Dolomite	Gypsum
	%				
SDE #4 – 15 May 2020	74.7	15.2	6.3	1.3	2.5
SDE #5 – 24 February 2021	85.6	4.1	1.0	9.3	0.0
SDE #7 – 16 March 2022	68.1	10.1	7.2	5.8	8.7
SDE #8 – 22 April 2022	74.1	17.9	5.6	0.6	1.9
SDE – 19 August 2022	75.7	14.3	1.4	4.3	4.3
Mean	*75.9*	*13.0*	*4.4*	*3.8*	*2.9*

et al. 2013; Varga, Gy. 2020; Rostási, Á. *et al.* 2022) has increased in the last 10–15 years. These findings have been confirmed by several other studies across Europe, which also report more frequent (Salvador, P. *et al.* 2022; Cuevas-Agulló, E. *et al.* 2023; Kok, J.F. *et al.* 2023) and intense Saharan dust storm events. It was also striking that North African dust is not only reaching the southern regions of the European continent, but is also becoming more frequent in more northerly regions (e.g., Greenland – Francis, D. *et al.* 2018; Iceland – Varga, Gy. *et al.* 2021; Finland – Meinander, O. *et al.* 2023; Varga, Gy. *et al.* 2023).

This is supported by data from the last five years, which are presented in this article. Both the significantly higher number of events than long-term averages and the changing synoptic background fit well into the context of the previously raised idea that climate change is driving significant changes in atmospheric transport processes. One manifestation of this is the increased warming of the Arctic, i.e. the jet stream pattern modifying effect of Arctic amplification (Francis, J.A. and Vavrus, S.J. 2012). This spatially differentiated warming results in a decreasing temperature contrast between higher and lower latitudes, which difference drives the jet stream, and thus determines its trajectory to deviate more from the west-east flow direction, which is clearly characterized by zonal components, and to become wavier (the role of meridional wind components is increased). In general, a meridional pattern of wind vectors was observed at high altitudes during the intense episodes. The low-pressure atmospheric systems that blew through the Atlas Mountains (driven by the jet), causing severe dust storms there, turned northwards under the influence of the dominant flow and reached central and northern Europe. Similar synoptic situations have been described by Francis, D. *et al.* (2023) for Saharan dust storm events associated with atmospheric river situations in the Alps, which can coexist with severe melting. In another publication (Francis, D. *et al.* 2018), they reported on this meteorological situation in the context of the transport of African dust-loaded air masses reaching Greenland.

This type of increased meridional flow due to climate change will lead to extreme weather events. Atmospheric flows driven by the wavy jet stream cross zones with fundamentally different climatic parameters in their general characteristics, sometimes causing cold spells from the Arctic and, as shown in this paper, warm advection from the hot subtropical climatic zones.

Effects of giant dust transport on mineral dust-related interpretations

The particle size data reported in our observations and measurements also fit well into the range of recent papers on particle size of particulate matter. Previous observations and concepts suggest that the typical grain size of particulate matter reaching Europe (and regions generally further away from source areas) should not be larger than 10–20 μm. As is well illustrated by the European measurement datasets collected by Goudie, A.S. and Middleton, N.J. (2001): Crete: 8–30 μm (mode; Mattson, J.O. and Nihlén, T. 1996), 4–16 μm (median); Spain: 4–30 μm (mean; Sala, J.Q. *et al.* 1996); Germany: 2.2–16 μm (median); Italy: 16.8 μm (modal), 14.6 μm (median; Ozer, P. *et al.* 1998); South France: 4–12.7 μm (median; Bücher, A. and Lucas, G. 1984), 8–11 μm (median; Coudé-Gaussen, G. 1991); France (Paris Basin): 8 μm (Coudé-Gaussen, G. *et al.* 1988); Swiss Alps: 4.5 ± 1.5 μm (median; Wagenbach, D. and Geis, K. 1989); and Central Mediterranean: 2–8 μm (mode; Tomadin, L. and Lenaz, R. 1989). These values are also used as upper bounds in the dust dispersion models (GEOS-5; MACC_II; MASINGAR; MetUM; NGAC; NMMB/BSC-Dust; CHIMERE; CMAQ-KOSA; COAMPS; CUACE/Dust; BSC-DREAM8b; DREAM8-NMME-MACC; TAQM_KOSA – Benedetti, A. *et al.* 2014).

In recent years, the number of papers on long-range transport of large particulate matter has increased significantly, and they report that sometimes 200–300 μm particles can be transported up to thousands of kilometres (Ryder, C.L. *et al.* 2018; Van der Does, M. *et al.* 2018; Adebiyi, A.A. *et al.* 2023). Our reported data also significantly exceed the particle size that was previously considered typical.

This also has a major impact on, for example, the highly underestimated dust deposition data in the models, where the mass of the deposited particulate is related to the third power of the particle size, so a slight upward shift in the size range has a significant impact on the dust flux data (Adebiyi, A.A. and Kok, J.F. 2020). The (paleo)environmental interpretation of the deposition data is thus greatly modified. The importance of eolian dust deposits in climate reconstructions is of particular importance in some regions (e.g., in regions covered by loess). In these data sets, there has so far been no marked inclusion of long-range dust.

Conclusions

In the paper, we completed our previous long-term (1979–2018) analysis of Saharan dust storm events in the Carpathian Basin with an analysis of the period 2019–2023. The 218 dust storm events previously identified for a 40-year period have been complemented by 55 additional events. The number of events over the five-year period was significantly higher than the long-term average, and this fits well with the picture already indicated by the 2010 studies, i.e. that both the number and intensity of dust storm events have increased significantly.

Classification based on the analysis of the synoptic background of dust storm events revealed that the typical meteorological background of these events has been modified. Among the atmospheric flow conditions defined by the wavy jet stream, circulation patterns with a more pronounced meridional wind component were dominant during the more intense dust storm events. It was clearly observed that the dust material was moving further north within the European domain and was also regularly observed in Germany, Poland and Finland. Circulation patterns across climatic belts are also as-

sociated with marked weather changes, so that extreme weather events are regularly observed; warm spells, muddy rain and wet washouts during Saharan dust storm events.

Detailed grain size and particle shape analyses of samples of the deposited particulate matter showed that the atmospheric dust material is very diverse. A large amount of coarse-grained fraction was observed in the samples analysed. Among the mineral grains, in some samples, coarse rock flour and sand fractions were dominant. Our knowledge of the long-range transport of this coarse fraction is significantly incomplete, as the range above 20 μm is not even parameterised in climate and dust transport models, i.e. calculations of the amount of transported and deposited dust significantly underestimate the actual values. The data on the long-range transport of large particles also point to the need for revision of (paleo)environmental reconstructions and the role of particulate matter of Saharan origin in sediment and soil formation.

Acknowledgement: The research was supported by the NRDI projects FK138692. This work has been implemented by the National Multidisciplinary Laboratory for Climate Change (RRF-2.3.1-21-2022-00014) project within the framework of Hungary's National Recovery and Resilience Plan supported by the Recovery and Resilience Facility of the European Union. The research was funded by the Sustainable Development and Technologies National Programme of the Hungarian Academy of Sciences (FFT NP FTA). Images were provided by the WMO Barcelona Dust Regional Center and the partners of the Sand and Dust Storm Warning Advisory and Assessment System (SDS-WAS) for Northern Africa, the Middle East and Europe.

REFERENCES

Adebiyi, A.A. and Kok, J.F. 2020. Climate models miss most of the coarse dust in the atmosphere. *Science Advances* 6. Doi:10.1126/sciadv.aaz9507

Adebiyi, A.A., Kok, J.F., Murray, B.J., Ryder, C.L., Stuut, J.-B.W., Kahn, R.A., Knippertz, P., Formenti, P., Mahowald, N.M., Pérez García-Pando, C., Klose, M., Ansmann, A., Samset, B.H., Ito, A., Balkanski, Y., di Biagio, C., Romanias, M.N., Huang, Y. and Meng, J. 2023. A review of coarse mineral dust in the Earth system. *Aeolian Research* 60. 100849. Doi:https://doi.org/10.1016/j.aeolia.2022.100849

Alpert, P., Kishcha, P., Shtivelman, A., Krichak, S.O. and Joseph, J.H. 2004. Vertical distribution of Saharan dust based on 2.5-year model predictions. *Atmospheric Research* 70. 109–130. Doi:10.1016/j.atmosres.2003.11.001

Ansmann, A., Mamouri, R.-E., Bühl, J., Seifert, P., Engelmann, R., Hofer, J., Nisantzi, A., Atkinson, J.D., Kanji, Z.A., Sierau, B., Vrekoussis, M. and Sciare, J. 2019. Ice-nucleating particle versus ice crystal number concentrationin altocumulus and cirrus layers embedded in Saharan dust: A closure study. *Atmospheric Chemistry and Physics* 19. 15087–15115. Doi:10.5194/acp-19-15087-2019

Arimoto, R. 2001. Eolian dust and climate: Relationships to sources, tropospheric chemistry, transport and deposition. *Earth-Science Reviews* 54. 29–42. Doi:https://doi.org/10.1016/S0012-8252(01)00040-X

Atalay, I. 1997. Red Mediterranean soils in some karstic regions of Taurus mountains, Turkey. *Catena* 28. 247–260. Doi:10.1016/S0341-8162(96)00041-0

Barkan, J., Alpert, P., Kutiel, H. and Kishcha, P. 2005. Synoptics of dust transportation days from Africa toward Italy and central Europe. *Journal of Geophysical Research* 110. D07208. Doi:10.1029/2004JD005222

Benedetti, A., Baldasano, J.M., Basart, S., Benincasa, F., Boucher, O., Brooks, M.E., Chen, J.-P., Colarco, P.R., Gong, S., Huneeus, N., Jones, L., Lu, S., Menut, L., Morcrette, J.-J., Mulcahy, J., Nickovic, S., Pérez García-Pando, C., Reid, J.S., Sekiyama, T.T., Tanaka, T.Y., Terradellas, E., Westphal, D.L., Zhang, X.-Y. and Zhou, C.-H. 2014. Operational dust prediction. In *Mineral Dust: A Key Player in the Earth System*. Eds.: Knippertz, P. and Stuut, J.-B.W., Dordrecht, Springer Netherlands, 223–265. Doi:10.1007/978-94-017-8978-3_10

Bücher, A. and Lucas, G. 1984. Sédimentation éolienne intercontinentale, poussières sahariennes et géologie. *Bulletin des Centres de Recherches Exploration* 8. 151–165.

Čanić, K.Š., Vidič, S. and Klaić, Z.B. 2009. Precipitation chemistry in Croatia during the period 1981–2006. *Journal of Environmental Monitoring* 11. 839–851. Doi:10.1039/B816432K

Coudé-Gaussen, G., Désiré, E. and Regrain, R. 1988. Particularité de poussières sahariennes distales tombées sur la Picardie et l'Ile-de-France le 7 Mai 1988. *Hommes et Terres du Nord* 4. 246–251.

Coudé-Gaussen, G. 1991. *Les Poussières Sahariennes: Cycle Sédimentaire et Place dans les Environments et Paléoenvironments Désertiques*. Montrouge, John Libby Eurotext.

Cuevas-Agulló, E., Barriopedro, D., García, R.D., Alonso-Pérez, S., González-Alemán, J.J., Werner, E., Suárez, D., Bustos, J.J., García-Castrillo, G., Garcíia, O., Barreto, Á. and Basart, S. 2023. Sharp increase of Saharan dust intrusions over the Western Mediterranean and Euro-Atlantic

region in winters 2020–2022 and associated atmospheric circulation. *EGUsphere* 2023. 1749. 1–39. Doi:10.5194/egusphere-2023-1749

Dumont, M., Gascoin, S., Réveillet, M., Voisin, D., Tuzet, F., Arnaud, L., Bonnefoy, M., Bacardit Peñarroya, M., Carmagnola, C., Deguine, A., Diacre, A., Dürr, L., Evrard, O., Fontaine, F., Franki, A., Fructus, M., Gandois, L., Gouttevin, I., Gherab, A., Hagenmuller, P., Hansson, S., Herbin, H., Josse, B., Jourdain, B., Lefevre, I., Le Roux, G., Libois, Q., Liger, L., Morin, S., Petitprez, D., Robledano, A., Schneebeli, M., Salze, P., Six, D., Thibert, E., Trachsel, J., Vernay, M., Viallon-Galinier, L. and Voiron, C. 2023. Spatial variability of Saharan dust deposition revealed through a citizen science campaign. *Earth System Science Data* 15. 3075–3094. Doi:10.5194/essd-15-3075-2023

Easterling, D.R., Meehl, G.A., Parmesan, C., Changnon, S.A., Karl, T.R. and Mearns, L.O. 2000. Climate extremes: Observations, modeling, and impacts. *Science* 289. 2068–2074. Doi:10.1126/science.289.5487.2068

Francis, D., Eayrs, C., Chaboureau, J., Mote, T. and Holland, D.M. 2018. Polar jet associated circulation triggered a Saharan cyclone and derived the poleward transport of the African dust generated by the cyclone. *Journal of Geophysical Research: Atmospheres* 123. 11899–11917. Doi:10.1029/2018JD029095

Francis, D., Fonseca, R., Nelli, N., Bozkurt, D., Cuesta, J. and Bosc, E. 2023. On the Middle East's severe dust storms in spring 2022: Triggers and impacts. *Atmospheric Environment* 296. 119539. Doi:https://doi.org/10.1016/j.atmosenv.2022.119539

Francis, J.A. and Vavrus, S.J. 2012. Evidence linking Arctic amplification to extreme weather in mid-latitudes. *Geophysical Research Letters* 39. 6. 1029. Doi:10.1029/2012GL051000

Garofalide, S., Postolachi, C., Cocean, A., Cocean, G., Motrescu, I., Cocean, I., Munteanu, B.S., Prelipceanu, M., Gurlui, S. and Leontie, L. 2022. Saharan dust storm aerosol characterization of the event (9 to 13 May 2020) over European AERONET sites. *Atmosphere* 13. (3): 493. Doi:10.3390/atmos13030493

Gelaro, R., McCarty, W., Suárez, M.J., Todling, R., Molod, A., Takacs, L., Randles, C.A., Darmenov, A., Bosilovich, M.G., Reichle, R., Wargan, K., Coy, L., Cullather, R., Draper, C., Akella, S., Buchard, V., Conaty, A., da Silva, A.M., Gu, W., Kim, G.K., Koster, R., Lucchesi, R., Merkova, D., Nielsen, J.E., Partyka, G., Pawson, S., Putman, W., Rienecker, M., Schubert, S.D., Sienkiewicz, M. and Zhao, B. 2017. The modern-era retrospective analysis for research and applications, version 2 (MERRA-2). *Journal of Climate* 30. 5419–5454. Doi:10.1175/JCLI-D-16-0758.1

Ginoux, P., Chin, M., Tegen, I., Prospero, J.M., Holben, B., Dubovik, O. and Lin, S.-J. 2001. Sources and distributions of dust aerosols simulated with the GOCART model. *Journal of Geophysical Research: Atmospheres* 106. 20255–20273. Doi:10.1029/2000JD000053

Ginoux, P. 2017. Warming or cooling dust? *Nature Geoscience* 10. 246–248. Doi:10.1038/ngeo2923

Goudie, A.S. and Middleton, N.J. 2001. Saharan dust storms: Nature and consequences. *Earth-Science Reviews* 56. 179–204. Doi:10.1016/S0012-8252(01)00067-8

Harrison, S.P., Kohfeld, K.E., Roelandt, C. and Claquin, T. 2001. The role of dust in climate changes today, at the last glacial maximum and in the future. *Earth-Science Reviews* 54. 43–80. Doi:https://doi.org/10.1016/S0012-8252(01)00041-1

Hoose, C., Lohmann, U., Erdin, R. and Tegen, I. 2008. The global influence of dust mineralogical composition on heterogeneous ice nucleation in mixed-phase clouds. *Environmental Research Letters* 3. 025003. Doi:10.1088/1748-9326/3/2/025003

Hrabcak, P. 2022. Saharský prach nad slovenskom v rokoch 2015–2020 (Saharan dust over Slovakia in the years 2015–2020). *Meteorologický Časopis* 25. 3–17.

IPCC 2022. *AR5 Climate Change 2013: The Physical Science Basis.* IPCC, WWW Document. Available at https://www.ipcc.ch/report/ar5/wg1/

Jackson, M.L., Clayton, R.N., Violante, A. and Violante, P. 1982. Eolian influence on terra rossa soils of Italy traced by quartz oxygen isotopic ratio. *Developments in Sedmentology* 28. 293–301.

Jahn, R., Zarei, M. and Stahr, K. 1991. Genetic implications of quartz in ''Terra Rossa'' soils in Portugal. In *Proceedings of 7th Euroclay Conference.* Eds.: Störr, M., Hennig, K.-H. and Adolphi, P., Dresden, Ernst-Moritz-Arndt-Universität, 541–546.

Kalnay, E., Kanamitsu, M., Kistler, R., Collins, W., Deaven, D., Gandin, L., Iredell, M., Saha, S., White, G., Woollen, J., Zhu, Y., Chelliah, M., Ebisuzaki, W., Higgins, W., Janowiak, J., Mo, K.C., Ropelewski, C., Wang, J., Leetmaa, A., Reynolds, R., Jenne, R. and Joseph, D. 1996. The NCEP/NCAR 40-year reanalysis project. *Bulletin of the American Meteorological Society* 77. 437–471. Doi:10.1175/1520-0477(1996)077<0437:TNYRP>2.0.CO;2

Klose, M., Jorba, O., Gonçalves Ageitos, M., Escribano, J., Dawson, M.L., Obiso, V., di Tomaso, E., Basart, S., Montané Pinto, G., Macchia, F., Ginoux, P., Guerschman, J., Prigent, C., Huang, Y., Kok, J.F., Miller, R.L. and Pérez García-Pando, C. 2021. Mineral dust cycle in the Multiscale Online Nonhydrostatic AtmospheRe CHemistry model (MONARCH) Version 2.0. *Geoscientific Model Development* 14. 6403–6444. Doi:10.5194/gmd-14-6403-2021

Kohfeld, K.E. and Tegen, I. 2007. 4.13 – Record of mineral aerosols and their role in the earth system. In *Treatise on Geochemistry*. Eds.: Holland, H.D. and Turekian, K.K.B.T. Oxford, Pergamon, 1–26. Doi:https://doi.org/10.1016/B978-008043751-4/00236-4

Kok, J.F., Ridley, D.A., Zhou, Q., Miller, R.L., Zhao, C., Heald, C.L., Ward, D.S., Albani, S. and Haustein, K. 2017. Smaller desert dust cooling effect estimated from analysis of dust size and abundance. *Nature Geoscience* 10. 274–278. Doi:10.1038/ngeo2912

Kok, J.F., Storelvmo, T., Karydis, V.A., Adebiyi, A.A., Mahowald, N.M., Evan, A.T., He, C. and Leung, D.M., 2023. Mineral dust aerosol impacts on global climate and climate change. *Nature Reviews Earth & Environment* 4. 71–86. Doi:10.1038/s43017-022-00379-5

MacLeod, D.A. 1980. The origin of the red Mediterranean soils in Epirus, Greece. *Journal of Soil Science* 31. 125–136. Doi:10.1111/j.1365-2389.1980.tb02070.x

Maher, B.A., Prospero, J.M., Mackie, D., Gaiero, D., Hesse, P.P. and Balkanski, Y. 2010. Global connections between aeolian dust, climate and ocean biogeochemistry at the present day and at the last glacial maximum. *Earth-Science Reviews* 99. 61–97. Doi:https://doi.org/10.1016/j.earscirev.2009.12.001

Mahowald, N.M., Kohfeld, K., Hansson, M., Balkanski, Y., Harrison, S.P., Prentice, I.C., Schulz, M. and Rodhe, H. 1999. Dust sources and deposition during the last glacial maximum and current climate: A comparison of model results with paleodata from ice cores and marine sediments. *Journal of Geophysical Research: Atmospheres* 104. 15895–15916. Doi:https://doi.org/10.1029/1999JD900084

Mahowald, N.M., Muhs, D.R., Levis, S., Rasch, P.J., Yoshioka, M., Zender, C.S. and Luo, C. 2006. Change in atmospheric mineral aerosols in response to climate: Last glacial period, preindustrial, modern, and doubled carbon dioxide climates. *Journal of Geophysical Research: Atmospheres* 111. D10. Doi:https://doi.org/10.1029/2005JD006653

Mattsson, J.O. and Nihlén, T. 1996. The transport of Saharan dust to southern Europe: A scenario. *Journal of Arid Environments* 32. 111–119. Doi:https://doi.org/10.1006/jare.1996.0011

Meinander, O., Dagsson-Waldhauserova, P., Amosov, P., Aseyeva, E., Atkins, C., Baklanov, A., Baldo, C., Barr, S.L., Barzycka, B., Benning, L.G., Cvetkovic, B., Enchilik, P., Frolov, D., Gassó, S., Kandler, K., Kasimov, N., Kavan, J., King, J., Koroleva, T., Krupskaya, V., Kulmala, M., Kusiak, M., Lappalainen, H.K., Laska, M., Lasne, J., Lewandowski, M., Luks, B., McQuaid, J.B., Moroni, B., Murray, B., Möhler, O., Nawrot, A., Nickovic, S., O'Neill, N.T., Pejanovic, G., Popovicheva, O., Ranjbar, K., Romanias, M., Samonova, O., Sanchez-Marroquin, A., Schepanski, K., Semenkov, I., Sharapova, A., Shevnina, E., Shi, Z., Sofiev, M., Thevenet, F., Thorsteinsson, T., Timofeev, M., Umo, N.S., Uppstu, A., Urupina, D., Varga, G., Werner, T., Arnalds, O. and Vukovic Vimic, A. 2022. Newly identified climatically and environmentally significant high-latitude dust sources. *Atmospheric Chemistry and Physics* 22. 11889–11930. Doi:10.5194/acp-22-11889-2022

Meinander, O., Kouznetsov, R., Uppstu, A., Sofiev, M., Kaakinen, A., Salminen, J., Rontu, L., Welti, A., Francis, D., Piedehierro, A.A., Heikkilä, P., Heikkinen, E. and Laaksonen, A. 2023. African dust transport and deposition modelling verified through a citizen science campaign in Finland. *Scientific Reports* 13. 21379. Doi:10.1038/s41598-023-46321-7

Monteiro, A., Basart, S., Kazadzis, S., Votsis, A., Gkikas, A., Vandenbussche, S., Tobias, A., Gama, C., García-Pando, C.P., Terradellas, E., Notas, G., Middleton, N., Kushta, J., Amiridis, V., Lagouvardos, K., Kosmopoulos, P., Kotroni, V., Kanakidou, M., Mihalopoulos, N., Kalivitis, N., Dagsson-Waldhauserová, P., El-Askary, H., Sievers, K., Giannaros, T., Mona, L., Hirtl, M., Skomorowski, P., Virtanen, T.H., Christoudias, T., di Mauro, B., Trippetta, S., Kutuzov, S., Meinander, O. and Nickovic, S. 2022. Multi-sectoral impact assessment of an extreme African dust episode in the Eastern Mediterranean in March 2018. *Science of The Total Environment* 843. 156861. Doi:https://doi.org/10.1016/j.scitotenv.2022.156861

Muhs, D.R., Budahn, J., Avila, A., Skipp, G., Freeman, J. and Patterson, D.A. 2010. The role of African dust in the formation of Quaternary soils on Mallorca, Spain and implications for the genesis of Red Mediterranean soils. *Quaternary Science Reviews* 29. 2518–2543. Doi:10.1016/j.quascirev.2010.04.013

Nickovic, S., Cvetkovic, B., Madonna, F., Rosoldi, M., Pejanovic, G., Petkovic, S. and Nikolic, J. 2016. Cloud ice caused by atmospheric mineral dust. Part 1: Parameterization of ice nuclei concentration in the NMME-DREAM model. *Atmospheric Chemistry and Physics* 16. 11367–11378. Doi:10.5194/acp-16-11367-2016

Ozer, P., Erpicum, M., Cortemiglia, G.C. and Lucchetti, G. 1998. A dustfall event in November 1996 in Genoa, Italy. *Weather* 53. 140–145. Doi:https://doi.org/10.1002/j.1477-8696.1998.tb03982.x

Pérez, C., Haustein, K., Janjic, Z., Jorba, O., Huneeus, N., Baldasano, J.M., Black, T., Basart, S., Nickovic, S., Miller, R.L., Perlwitz, J.P., Schulz, M. and Thomson, M. 2011. Atmospheric dust modeling from meso to global scales with the online NMMB/BSC-Dust model. Part 1: Model description, annual simulations and evaluation. *Atmospheric Chemistry and Physics* 11. 13001–13027. Doi:10.5194/acp-11-13001-2011

Pósfai, M. and Buseck, P.R. 2010. Nature and climate effects of individual tropospheric aerosol particles. *Annual Review of Earth and Planetary Sciences* 38. 17–43. Doi:10.1146/annurev.earth.031208.100032

Ridgwell, A.J. 2002. Dust in the Earth system: The biogeochemical linking of land, air and sea. *Philosophical Transactions of the Royal Society A* 360. 2905–2924. Doi:10.1098/rsta.2002.1096

Rieger, D., Steiner, A., Bachmann, V., Gasch, P., Förstner, J., Deetz, K., Vogel, B. and Vogel, H. 2017. Impact of the 4 April 2014 Saharan dust outbreak on the photovoltaic power generation in Germany. *Atmospheric Chemistry and Physics* 17. 13391–13415. Doi:10.5194/acp-17-13391-2017

Rodá, F., Bellot, J., Avila, A., Escarré, A., Piñol, J. and Terradas, J. 1993. Saharan dust and the atmospheric inputs of elements and alkalinity to mediterranean ecosystems. *Water, Air, & Soil Pollution* 66. 277–288. Doi:10.1007/BF00479851

Rogora, M., Mosello, R. and Marchetto, A. 2004. Long-term trends in the chemistry of atmospheric deposition in Northwestern Italy: the role of increasing Saharan dust deposition. *Tellus B: Chemical and Physical Meteorology* 56. 426–434. Doi:10.3402/tellusb.v56i5.16456

Rostási, Á., Topa, B.A., Gresina, F., Weiszburg, T.G., Gelencsér, A. and Varga, G. 2022. Saharan dust deposition in Central Europe in 2016. A representative year of the increased north African dust removal over the last decade. *Frontiers in Earth Science* 10. 1–18. Doi:10.3389/feart.2022.869902

Ryder, C.L., Marenco, F., Brooke, J.K., Estelles, V., Cotton, R., Formenti, P., McQuaid, J.B., Price, H.C., Liu, D., Ausset, P., Rosenberg, P.D., Taylor, J.W., Choularton, T., Bower, K., Coe, H., Gallagher, M., Crosier, J., Lloyd, G., Highwood, E.J. and Murray, B.J. 2018. Coarse-mode mineral dust size distributions, composition and optical properties from AER-D aircraft measurements over the tropical eastern Atlantic. *Atmospheric Chemistry and Physics* 18. 17225–17257. Doi:10.5194/acp-18-17225-2018

Sala, J.Q., Cantos, J.O. and Chiva, E.M. 1996. Red dust rain within the Spanish Mediterranean area. *Climatic Change* 32. 215–228. Doi:10.1007/BF00143711

Salvador, P., Pey, J., Pérez, N., Querol, X. and Artíñano, B. 2022. Increasing atmospheric dust transport towards the western Mediterranean over 1948–2020. *Climate and Atmospheric Science* 5. (1): 34. Doi:10.1038/s41612-022-00256-4

Shepherd, T.G. 2014. Atmospheric circulation as a source of uncertainty in climate change projections. *Nature Geoscience* 7. 703–708. Doi:10.1038/ngeo2253

Stein, A.F., Draxler, R.R., Rolph, G.D., Stunder, B.J.B., Cohen, M.D. and Ngan, F. 2015. Noaa's hysplit atmospheric transport and dispersion modeling system. *Bulletin of the American Meteorological Society* 96. (12): 2059–2077. Doi:10.1175/BAMS-D-14-00110.1

Tegen, I. and Lacis, A.A. 1996. Modeling of particle size distribution and its influence on the radiative properties of mineral dust aerosol. *Journal of Geophysical Research: Atmospheres* 101. 19237–19244. Doi:10.1029/95JD03610

Tomadin, L. and Lenaz, R. 1989. Eolian dust over the Mediterranean and their contribution to the present sedimentation. In *Paleoclimatology and Paleometeorology: Modern and Past Patterns of Global Atmospheric Transport*. Eds.: Leinen, M. and Sarnthein, M., Dordrecht, Springer Netherlands, 267–282. Doi:10.1007/978-94-009-0995-3_11

Van der Does, M. Knippertz, P., Zschenderlein, P., Giles Harrison, R. and Stuut, J.-B.W. 2018. The mysterious long-range transport of giant mineral dust particles. *Science Advances* 4. eaau2768. Doi:10.1126/sciadv.aau2768

Varga, Gy., Kovács, J. and Újvári, G. 2013. Analysis of Saharan dust intrusions into the Carpathian Basin (Central Europe) over the period of 1979–2011. *Global and Planetary Change* 100. 333–342. Doi:10.1016/j.gloplacha.2012.11.007

Varga, Gy. 2020. Changing nature of Saharan dust deposition in the Carpathian Basin (Central Europe): 40 years of identified North African dust events (1979–2018). *Environment International* 139. (June): 105712. Doi:10.1016/j.envint.2020.105712

Varga, Gy., Dagsson-Waldhauserová, P., Gresina, F. and Helgadottir, A. 2021. Saharan dust and giant quartz particle transport towards Iceland. *Scientific Reports* 11. 11891. Doi:10.1038/s41598-021-91481-z

Varga, Gy., Meinander, O., Rostási, Á., Dagsson-Waldhauserova, P., Csávics, A. and Gresina, F. 2023. Saharan, Aral-Caspian and Middle East dust travels to Finland (1980–2022). *Environment International* 180. 108243. Doi:https://doi.org/10.1016/j.envint.2023.108243

Wagenbach, D. and Geis, K. 1989. The mineral dust record in a high alpine glacier (Colle Gnifett, Swiss Alps). In *Paleoclimatology and Paleometeorology: Modern and Past Patterns of Global Atmospheric Transport*. Eds.: Leinen, M. and Sarnthein, M., Dordrecht, Springer Netherlands, 543–564.

Weger, M., Heinold, B., Engler, C., Schumann, U., Seifert, A., Fössig, R., Voigt, C., Baars, H., Blahak, U., Borrmann, S., Hoose, C., Kaufmann, S., Krämer, M., Seifert, P., Senf, F., Schneider, J. and Tegen, I. 2018. The impact of mineral dust on cloud formation during the Saharan dust event in April 2014 over Europe. *Atmospheric Chemistry and Physics* 18. 17545–17572. Doi:10.5194/acp-18-17545-2018

DOI: 10.15201/hungeobull.72.4.2 Hungarian Geographical Bulletin **72** 2023 (4) 339–364.

Erosion susceptibility mapping of a loess-covered region using Analytic Hierarchy Process – A case study: Kalat-e-Naderi, northeast Iran

Fatemeh NOOSHIN NOKHANDAN[1], Kaveh GHAHRAMAN[1] and Erzsébet HORVÁTH[1]

Abstract

In this study, the Analytic Hierarchy Process (AHP) is applied to generate erosion susceptibility maps in four basins of Kalat-e-Naderi county, namely Archangan, Kalat, Qaratigan, and Chahchaheh basins, situated in northeast Iran. The Kalat-e-Naderi region is characterized by a partial coverage of loess. Given the agricultural significance of loess and its susceptibility to erosion, this research focuses specifically on regions covered by loess. Geographic Information System (GIS) tools, including ArcMap and Quantum Geographic Information System (QGIS), were utilized to facilitate the creation of erosion susceptibility maps. Seven factors, including slope, aspect, elevation, drainage density, lithology, the Normalized Difference Vegetation Index (NDVI), and precipitation were selected for consideration. Recognizing the variability of precipitation and vegetation cover across different seasons, seasonal data for the specified factors were employed. Consequently, erosion susceptibility maps were generated on a seasonal basis. Pairwise comparison tables revealed that precipitation, lithology, and slope emerged as the dominant factors contributing to erosion susceptibility in this region. The resultant maps distinctly delineate basins with higher precipitation values, unresistant lithology (such as loess, characterized by high porosity and permeability), and steeper slopes, exhibiting heightened susceptibility to erosion (Archangan and Kalat basins). The credibility of the research findings was examined through on-site observations. The outcomes of this study may provide pertinent insights for decision-makers and planners. This information can be effectively employed in formulating strategies aimed at conserving soil quality in areas vulnerable to erosion hazards.

Keywords: Analytic Hierarchy Process (AHP), erosion susceptibility on loess, GIS, Kalat-e-Naderi

Received July 2023, accepted November 2023.

Introduction

Soil erosion stands as a critical global environmental challenge, exerting far-reaching impacts on agricultural productivity, natural resources, and socio-economic development (Jebur, M.N. *et al.* 2014; Zhao, J. *et al.* 2016; Li, Y. *et al.* 2020; Vanmaercke, M. *et al.* 2021; Cen, Y. *et al.* 2022). Soil erosion is speeded up by a complex interplay of environmental factors, such as topography, soil characteristics, climate, and vegetation, as well as human activities like deforestation, farming, and construction (Lukić, T. *et al.* 2018, 2019; Thomas, J. *et al.* 2018; Abbas, S. *et al.* 2022). To mitigate soil erosion, diverse strategies, ranging from conservation tillage to the implementation of hydraulic structures, have been developed (Morgan, R. 1995; Barbera, V. *et al.* 2012; Lukić, T. *et al.* 2016). Due to the importance of soil erosion, researchers have been investigating soil erosion using different models, including Agricultural Non-point Source Pollution Model (AGNPS) (Young, R. *et al.* 1989; Zhu, K.-W. *et al.* 2020; Zou, L. *et al.* 2020; Huang, C. *et al.* 2022), Soil and Water

[1] Department of Physical Geography, ELTE Eötvös Loránd University, Pázmány Péter sétány 1/C, H-1117, Budapest, Hungary. E-mails: fatimanooshin@gmail.com, kevingh70@gmail.com, erzsebet.horvath@ttk.elte.hu

Assessment Tool (SWAT) (Neitsch, S.L. *et al.* 2011; Bhattacharya, R.K. *et al.* 2020; Echogdali, F.Z. *et al.* 2022), European Soil Erosion Model (EUROSEM) (Morgan, R. *et al.* 1998; Pandey, S. *et al.* 2021; Raza, A. *et al.* 2021; Shen, N. *et al.* 2023), Erosion Potential Model (EPM) (Ahmadi, M. *et al.* 2020; Ennaji, N. *et al.* 2022; Aleksova, B. *et al.* 2023), and Revised Universal Soil Loss Equation (RUSLE) (Kebede, Y.S. *et al.* 2021; Aswathi, J. *et al.* 2022; Micić Ponjiger, T. *et al.* 2023). Besides the mentioned methods, the AHP (Saaty, T.L. 1980) is widely used to investigate soil erosion and to map the erosion susceptible areas (Saha, S. *et al.* 2019; Das, B. *et al.* 2020; Kucuker, D.M. and Giraldo, D.C. 2022). However, among these advancements, challenges persist in predicting the spatial distribution of soil erosion, including constraints related to time, cost, facilities, and result accuracy (Kucuker, D.M. and Giraldo, D.C. 2022). Recent years have witnessed the integration of remote sensing techniques and Geographic Information Systems (GIS), overcoming these limitations and enabling the prediction of soil erosion in larger areas with reasonable cost and accuracy (Aslam, B. *et al.* 2021; Alam, N.M. *et al.* 2022; Alizadeh, M. *et al.* 2022; Kucuker, D.M. and Giraldo, D.C. 2022; Hayatzadeh, M. *et al.* 2023).

The investigated area, Kalat-e-Naderi county, located in a partially loess-covered region in northeast Iran, becomes the focal point of our study. Some areas of the county are dedicated to agriculture, while crop production is active on less steep slopes, emphasizing the need to address soil erosion, particularly in loess-covered regions, for sustainable food production. Loess is an eolian (windblown) pale yellow sediment (Pye, K. and Tsoar, H. 1987; Fenn, K. *et al.* 2022), which besides its agricultural importance, serves as a crucial repository of Quaternary climate changes (Xu, J. *et al.* 2022), offering a comprehensive terrestrial record of interglacial-glacial cycles. It stands out as a significant geological formation that captures the dynamic shifts in environmental conditions over time (Marković, S.B. *et al.* 2014). Defined as sediment entrained, transported, and deposited by the wind, and diagenetised *in situ*, loess is characterized by the predominance of silt-sized particles (Wang, X. *et al.* 2017), ranging from 2 μm to 50 μm in diameter (Smalley, I. *et al.* 2011). While most loess deposits exhibit a composition that includes measurable amounts of sand (> 50 μm) and clay (< 2 μm), the distinctive feature of loess lies in its prevalent content of silt-sized particles, typically ranging from 60 to 90 percent (Muhs, D.R. 2007). Due to its elevated porosity and silt content, loess is acknowledged as one of the most fertile forms of unconsolidated sedimentary rock. The inherent porosity of loess facilitates the absorption of gases containing carbon and nitrogen, enabling the provision of water and dissolved nutrients to plants through capillary rise during dry periods (Richthofen, F. 1872; Emerson, W.W. and McGarry, D. 2003). However, the susceptibility of loess to erosion is evident, as it can be easily eroded by surface water, making it prone to the formation of subcutaneous hollow landforms (Pécsi, M. 1990; Wu, Q. *et al.* 2019). Consequently, the sensitivity of loess landforms to erosion highlights their significance in the context of natural hazards and related issues.

While numerous studies have delved into the well-known northern loess regions of Iran (e.g., Aqband, Neka, Maraveh Tappeh, etc.) (Khormali, F. *et al.* 2009; Asadi, S. *et al.* 2013; Ghafarpour, A. *et al.* 2016, 2023; Gharibreza, M. *et al.* 2020; Sharifigarmdareh, J. *et al.* 2020) few investigations have specifically focused on the Kalat-e-Naderi loess region (Okhravi, R. and Amini, A. 2001; Karimi, A. *et al.* 2011), particularly in terms of erosion and with a geomorphological approach.

Against the backdrop of the unique characteristics and challenges posed by loess-covered areas, this study has two aims: 1) to generate soil erosion susceptibility maps in the less known, and less investigated loess-covered region of northeast Iran using the AHP method, and 2) to analyse the role of soil erosion in shaping various geomorphological landforms within the study area, employing a geomorphological approach.

Material and methods

Study area

The study area is located near the Iran-Turkmenistan border and is recognized as one of the loess-covered regions within the Khorasan-e-Razavi province. This region encompasses four basins including Archangan, Kalat, Qaratigan, and Chahchaheh basins, arranged from northwest to southeast *(Figure 1).* Loess regions in the study area share a common chronological relationship with the loesses in the Caspian Lowlands, despite a more than 500 km between the two areas (Karimi, A. *et al.* 2011). In the Kalat-e-Naderi region, the loess occurs in a patchy distribution with a thickness of up to 12 metres ((Karimi, A. *et al.* 2011), which is notably less than the thickness of loesses in the Caspian Lowlands in the northern part of Iran (Frechen, M. *et al.* 2009; Kehl, M. *et al.* 2021; Feizi, V. *et al.* 2023). As reported by Karimi, A. *et al.* (2011), the sand, silt, clay, gypsum, and carbonate contents of Kalat-e-Naderi sections are 10–18, 67–86, 4–16, 11–25, and 2–12 percent, respectively, showing the typical loess characteristics (Pécsi, M. 1990). Loess deposits are predominantly distributed on the north-eastern slopes of the Kopeh Dagh mountain range, covering a plateau-like geomorphic surface within a synclinal structure (Karimi, A. *et al.* 2011).

The Kopeh Dagh mountain range demonstrates a northwest-southeast orientation. From a structural geological standpoint, the region showcases numerous folds, faults, and fissures, with the primary fault direction oriented northwest-southeast. The formation of synclines and anticlines in this area can be attributed to the predominant northwest-southeast directional pressure. According to the Digital Elevation Model (DEM) of the study area, the

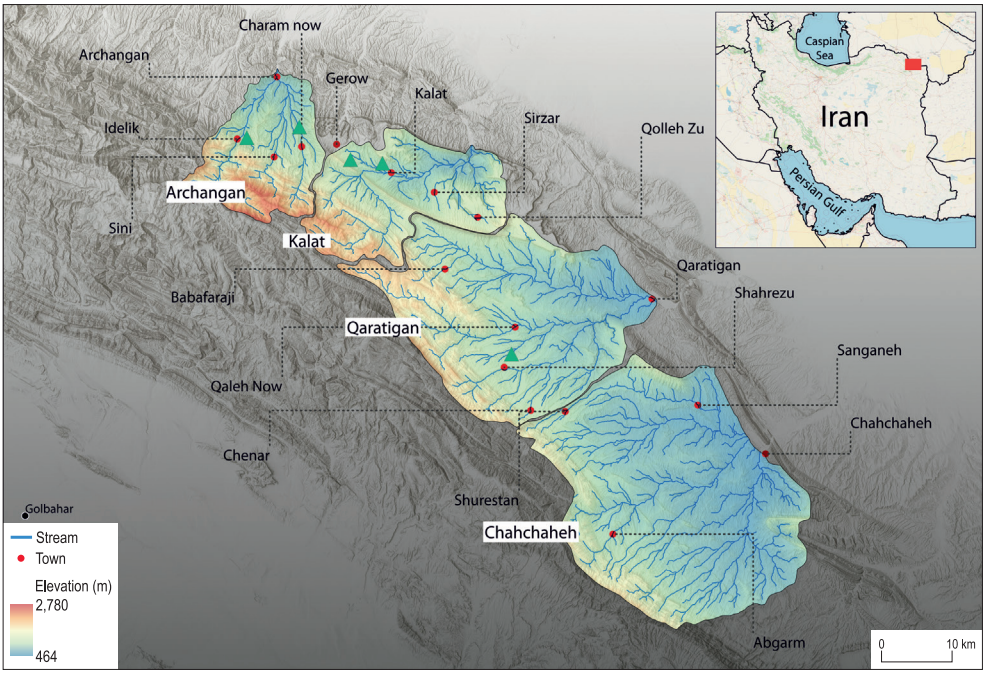

Fig. 1. The location of the studied basins in northeast Iran. The green rectangles indicate the positions of the visiting sites, as depicted in photos 1 through 5. *Source:* Authors' own elaboration.

highest and lowest elevations are recorded at 460 m and 2,780 m, respectively.

According to Köppen's climate classification, Kalat-e-Naderi falls into the cold semi-arid (BSk) category (Köppen, W. 1900). Climatic data from the Qaratigan watershed indicate a mean annual precipitation of 287 mm and a temperature of 12.2 °C (Amini, A. 1995). Historical climatic data for the area and its surroundings reveal significant seasonal variations in precipitation. The highest amounts (averaging 46.6 mm) occur between late January and the end of April, while the lowest precipitation values are observed between June and October (0.2 mm in August). Due to the arid and semi-arid climate, precipitation characteristics differ from more humid regions. In such arid and semi-arid regions, precipitation typically manifests as short but intense rainfall events (Ghahraman, K. and Nagy, B. 2023).

Overall, in pursuit of our objectives, we employed the AHP methodology, coupled with remotely sensed data (e.g., digital elevation models and optical satellite imagery), GIS tools (e.g., ArcGIS and QGIS), and field surveys.

*Table 1. Pairwise comparison scale**

Rating scale	Numerical	Reciprocal
Extremely preferred	9	1/9
Very strongly to extremely preferred	8	1/8
Very strongly preferred	7	1/7
Strongly to very strongly preferred	6	1/6
Strongly preferred	5	1/5
Moderately to strongly preferred	4	1/4
Moderately preferred	3	1/3
Equally to moderately preferred	2	1/2
Equally preferred	1	1

*Proposed by Saaty, R.W. 1987.

Analytic Hierarchy Process

The AHP is a suitable technique for identifying and mapping erosion-prone areas (Belkendil, A. *et al.* 2018; Belloula, M. *et al.* 2020; Aslam, B. *et al.* 2021; Sinshaw, B.G. *et al.* 2021; Ebhuoma, O. *et al.* 2022). AHP is a method that compares qualitative factors and expresses them as numerical values. This research used AHP due to its advantages, such as the availability of input factors, the capability of comparing multiple parameters, and ease of use (Rajesh, C. *et al.* 2016; Belkendil, A. *et al.* 2018; Tairi, A. *et al.* 2019). *Table 1* shows the numerical scale (by Saaty, R.W. 1987) proposed to be used as a source for the pairwise comparison. Depending on the importance of the selected factors, AHP assigns a value of 1 to 9 to each factor to decide the significance of the factor in association with the objective.

The AHP method comprises three primary steps. The initial step involves selecting the pertinent criteria for erosion. Criterion selection is contingent upon the impact of each factor on the occurrence of the phenomenon, our knowledge about the study area, insights gleaned from related researches, and crucially, the availability of data for each region (Arabameri, A. *et al.* 2018; Azareh, A. *et al.* 2019; Neji, N. *et al.* 2021; Kucuker, D.M. and Giraldo, D.C. 2022). Considering these critical considerations, we selected 7 factors including slope, aspect, elevation, drainage density, lithology, normalized difference vegetation index (NDVI), and precipitation. The flowchart and factors utilized in the AHP method for our study are depicted in *Figure 2.* Maps corresponding to each factor were generated using ArcMap and QGIS software *(Figure 3).*

One of the key geomorphological parameters influencing erosion is topography (Rahmati, O. *et al.* 2016). Topographic factors, including slope, aspect, and elevation, were derived from the SRTM (1 Arc sec) Digital Elevation Model. The substantial influence of slope gradient on soil erosion is widely acknowledged (Saini, S.S. *et al.* 2015; Meshram, S.G. *et al.* 2022; Olii, M.R. *et al.* 2023). Hence, it is imperative to recognize slope as a pivotal factor in studies pertaining to soil erosion, given its profound impact on the phenomenon (Aslam, B. *et al.* 2021).

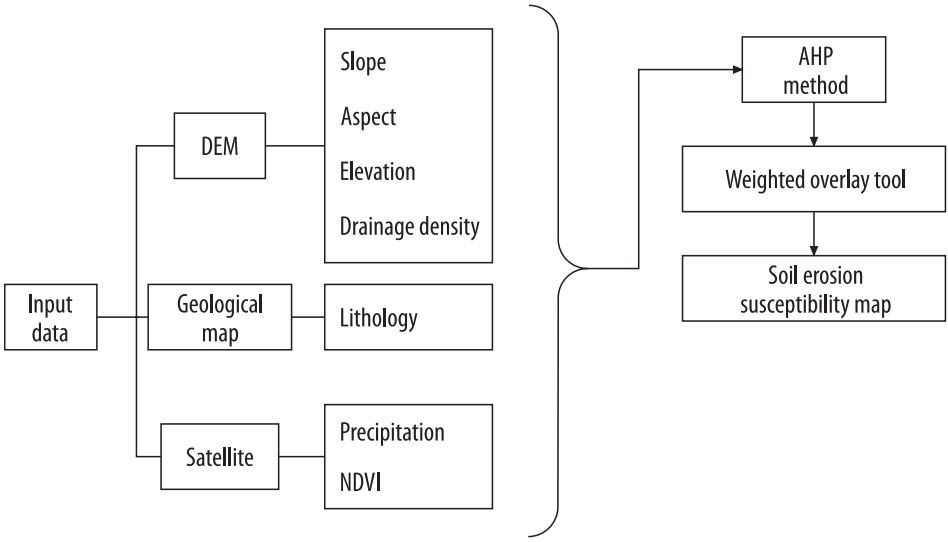

Fig. 2. The flowchart depicting the AHP method and the input data utilized for soil erosion susceptibility mapping. *Source:* Authors' own elaboration.

The slope map in our study was categorized into nine classes: 0°–5°, 5°–10°, 10°–15°, 15°–20°, 20°–25°, 25°–30°, 30°–35°, 35°–40°, and > 40° (see *Figure 3*, a). Considering the impracticality of agricultural expansion on steep slopes, the effective slope limit for erosion was set at 40°. Aspect influences erosion by regulating vegetation type, moisture, evaporation and transpiration, and sunlight exposure duration (Jaafari, A. *et al.* 2014).

The aspect map encompasses ten directional classes: flat (–1°), north (0°–22.5°), northeast (22.5°–67.5°), east (67.5°–112.5°), southeast (112.5°–157.5°), south (157.5°–202.5°), southwest (202.5°–247.5°), west (247.5°–292.5°), northwest (292.5°–337.5°), and north (337.5°–360°) (see *Figure 3*, b).

Elevation, by impacting vegetation type and precipitation, can affect erosion and gully development (Gómez-Gutiérrez, Á. *et al.* 2015). Given the mountainous nature of the area, this study adopted an eight-category elevation map with 290-metre elevation intervals to allow for more precise weight assignments for each category. The elevation categories include 460–750 m, 750–1,040 m, 1,040–1,330 m, 1,330–1,620 m, 1,620–1,910 m, 1,910–2,200 m, 2,200–2,490 m, and 2,490–2,780 m (see *Figure 3*, c).

The drainage density map, extracted from SRTM-DEM using the line density tool in ArcGIS 10.3, was divided into seven classes to construct the AHP comparison matrix with higher precision. The drainage density classes include 0.02–0.52, 0.52–1.02, 1.02–1.52, 1.52–2.02, 2.02–2.52, 2.52–3.02, and 3.02–3.70 (see *Figure 3*, d).

The lithology raster layer was prepared based on the 1:250,000 scale geologic map of the study area (see *Figure 3*, e). The study area, including 16 major lithological units, was divided into two categories, namely loess and solid rocks, given the focus on loess and erosion in loess-covered regions. It is important to note that the number of classes for factors such as slope, elevation, and drainage density may vary depending on the specific characteristics and conditions of each study area.

Numerous studies have highlighted the significance of precipitation and NDVI as influential factors in erosion susceptibility mapping using AHP (Alexakis, D.D. *et al.*

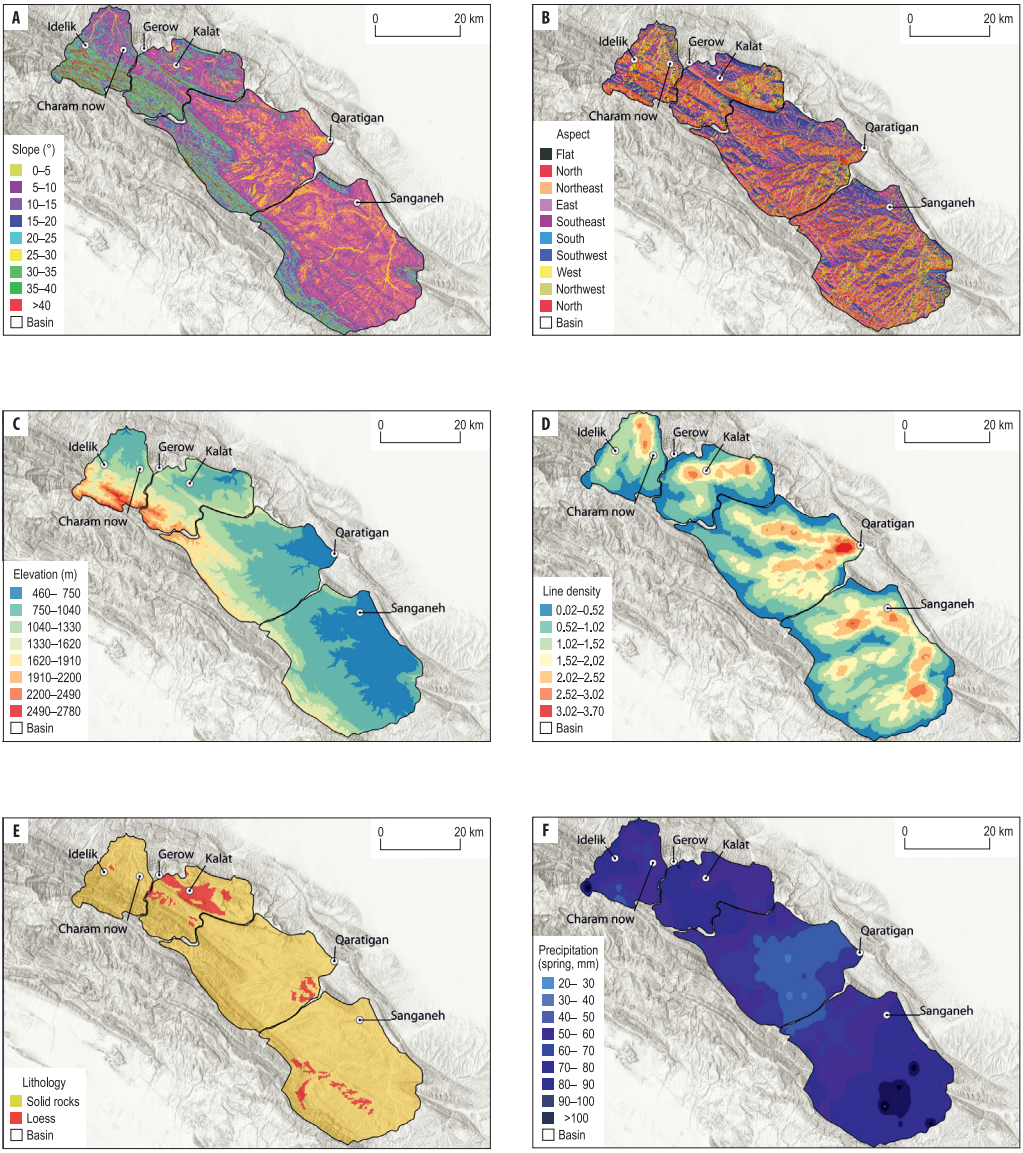

Fig. 3. Erosion contributing factor layers of the study area: slope (a), aspect (b), elevation (c), line density (d), lithology (e), and precipitation for spring (f). *Source:* Authors' own elaboration.

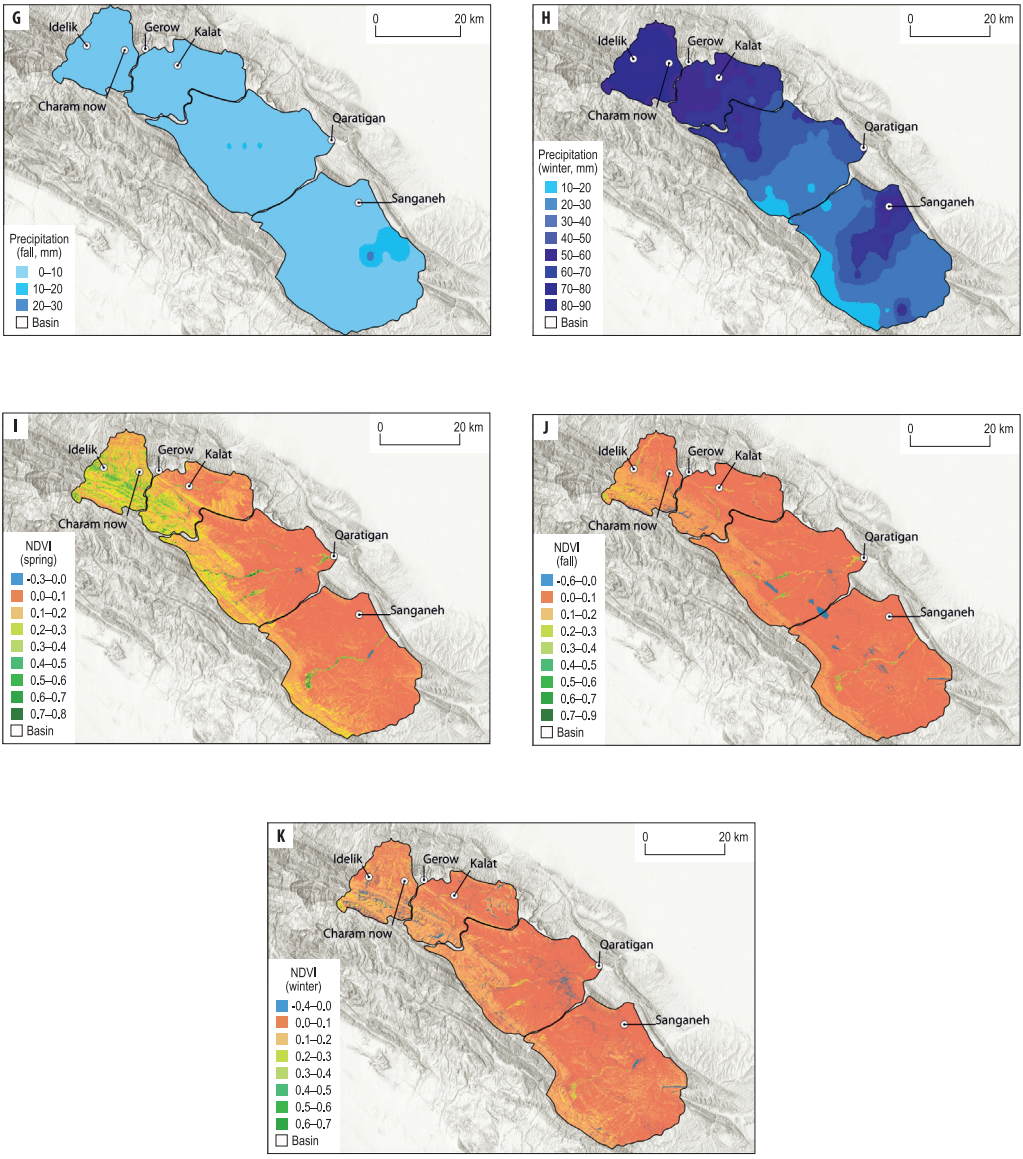

Fig. 3. Continued – Erosion contributing factor layers of the study area: precipitation for autumn, and winter (g, h), and NDVI for spring, autumn, and winter (i, j, k). *Source*: Authors' own elaboration.

2013; Kachouri, S. *et al.* 2015; Tairi, A. *et al.* 2019; Aslam, B. *et al.* 2021; Bouamrane, A. *et al.* 2021; Sandeep, P. *et al.* 2021; Mushtaq, F. *et al.* 2023). However, it has been observed that many researchers have relied on mean annual precipitation data (Kachouri, S. *et al.* 2015; Boufeldja, S. *et al.* 2020; Neji, N. *et al.* 2021), disregarding the uneven distribution of precipitation across different seasons. To overcome this limitation and improve the accuracy of the erosion susceptibility maps, it is essential to consider seasonal precipitation data. This is crucial because varying precipitation values have an impact on other factors and, more broadly, on erosional processes. By incorporating seasonal variability, our study can provide more accurate and nuanced insights into the spatiotemporal dynamics of soil erosion and inform more effective soil conservation strategies, particularly given the significance of agricultural activities in the study area.

In our study, we encountered the unavailability of meteorological station data for the study area. As a solution, we obtained precipitation data from the Center of Hydrometeorology and Remote Sensing (CHRS), University of California, Irvine, data portal (https://chrsdata.eng.uci.edu). To generate a comprehensive precipitation map for the year 2021, we utilized ArcMap and employed the Inverse Distance Weighted (IDW) interpolation method specifically for the spring, autumn, and winter seasons (see *Figure 3*, f, g, h). It is worth noting that since there was no recorded precipitation during the summer of 2021, the summer map depicting precipitation and NDVI was excluded from our analysis.

The NDVI maps were extracted from Sentinel-2 images using ArcMap. NDVI values range from -1 to +1 and are calculated using the following equation (Farah, A. *et al.* 2021; Parsian, S. *et al.* 2021; Durlević, U. *et al.* 2022):

$$NDVI = (NIR–RED)/(NIR+RED) \quad (1)$$

In Equation (1) *NIR* represents the near-infrared (band 8), and *RED* corresponds to the red band (band 4) of the Sentinel-2 imagery. *NDVI* values less than zero indicate the presence of water bodies and moisture, while values near zero (0–0.2) signify bare surfaces, rocks, sand, and snow. Values from 0.2 to 0.4 indicate areas covered by shrubs, grassland, and crops, while values exceeding 0.4 signify the presence of dense vegetation, such as orchards and, in certain regions, rice fields (see *Figure 3*, f, g, h).

The second step in the AHP involves assigning weights to the chosen criteria and conducting pairwise comparisons, a process that must also be extended to the sub-classes of each criterion. As presented in *Table 1*, each factor is assigned a value ranging from 1 to 9 based on its perceived importance or impact on erosion. The final step entails constructing a pairwise comparison matrix using the values assigned to the factors in the previous step. In AHP, the acceptable limit for the consistency ratio is equal to or less than 10 percent (Saaty, T.L. 1988; Alonso, J.A. and Lamata, M.T. 2006). The consistency ratio (*CR*) and consistency index (*CI*) are determined using the following equations:

$$CR = \frac{CI}{RI}, \quad (2)$$

where *CI* is the consistency index, and *RI* is the random consistency index that is obtained from *Table 2* (Saaty, T.L. and Vargas, L.G. 2001). *CI* is calculated using the following equation:

$$CI = \frac{(\beta_{max} - n)}{n - 1}, \quad (3)$$

where β_{max} is the largest eigenvalue of the comparison matrix, and n is the comparison matrix size. The process of determining the priority or weight for each factor involves calculating the eigenvalue (Costa, C.A.B. and Vansnick, J.-C. 2008). The eigenvalue is obtained by summing the products of each element in the eigenvector and the sum of the reciprocal matrix. To affirm the consistency of the given values, the consistency ratio (*CR*) must be calculated for each factor's pairwise comparison, as well as for the pairwise comparison of each factor's subclasses.

Table 2. Random consistency index (RI) values

n	RI	n	RI	n	RI
1	0.00	4	0.90	7	1.32
2	0.00	5	1.12	8	1.41
3	0.58	6	1.24	9	1.45

The erosion susceptibility maps for the study area were generated using the weighted overlay tool in ArcMap. The values assigned in the tool were selected based on the weight or importance of each class. Subsequently, the validation process was conducted through field surveys on visiting sites (see *Figure 1*). Field surveys allowed us to assess the model's success in identifying susceptible areas.

Results

As mentioned earlier, AHP pairwise comparison was drawn during the AHP preparation stages. Subsequently, the pairwise comparison tables and erosion susceptibility maps for each season are presented.

The spring season

In pairwise comparison, a score of 1 indicates equal importance, while a score of 9 signifies very high importance of one factor over the other (Saaty, T.L. 1980) (see *Table 1*). The pairwise comparison table for the spring season *(Table 3)* reveals that precipitation, lithology, slope, and drainage density carry the highest weights among the factors, with values of 0.34, 0.22, 0.13, and 0.10, respectively. Conversely, elevation (0.06), aspect (0.07), and NDVI (0.08) have the least impact on erosion in the spring season.

Slope, with a score value of 3, is moderately preferred over aspect and elevation. Over 716 km^2 of the area falls within slope categories between 15° and 40°. Field observations highlighted that these slopes, due to the presence of soil and agricultural development, are particularly prone to erosion. Consequently, a value of 8 is assigned to these sub-criteria in the weighted overlay tool. Lithology is moderately preferred over all factors except precipitation. Field observations confirmed various forms of erosion on loess-covered surfaces, indicating that loess is highly susceptible to erosion even with minimal rainfall. Thus, loess is assigned a value of 8 as a sub-criterion of lithology. In the spring season, precipitation is moderately to strongly preferred over aspect, NDVI, and drainage density (see *Table 3*). The highest precipitation values in the spring season (90–100 mm, and >100 mm) receive a score value of 9 in the weighted overlay tool, indicating the highest importance in erosion. To validate the assigned values, the consistency ratio was computed, yielding a spring season consistency ratio of 0.06, affirming the correct assignment of weights to the factors.

The autumn season

According to *Table 4*, precipitation (0.26), lithology (0.23), and slope (0.14) emerge as the most influential factors contributing to erosion in the autumn season. Conversely, NDVI

Table 3. Pairwise comparison table of the spring season

Pairwise comparison	Slope	Aspect	Lithology	Elevation	NDVI	Precipitation	Drainage density	Weight
Slope	1	3	1/3	3	1	1/3	2	0.13
Aspect	1/3	1	1/3	1	2	1/4	1/2	0.07
Lithology	3	3	1	3	3	1/3	3	0.22
Elevation	1/3	1	1/3	1	1/2	1/3	1/2	0.06
NDVI	1	1/2	1/3	2	1	1/4	1/2	0.08
Precipitation	3	4	3	3	4	1	4	0.34
Drainage density	1/2	2	1/3	2	2	1/4	1	0.10
CR: 0.06								

Table 4. Pairwise comparison table of the autumn season

Pairwise comparison	Slope	Aspect	Lithology	Elevation	NDVI	Precipitation	Drainage density	Weight
Slope	1	1/2	1/2	2	2	1/2	3	0.14
Aspect	2	1	1/3	1	2	1/3	1	0.12
Lithology	2	3	1	3	3	1/2	3	0.23
Elevation	1/2	1	1/3	1	2	1/2	2	0.10
NDVI	1/2	1/2	1/3	1/2	1	1/3	1	0.07
Precipitation	2	3	2	2	3	1	2	0.26
Drainage density	1/3	1	1/3	1/2	1	1/2	1	0.08
CR: 0.05								

and drainage density, with weight values of 0.07 and 0.08, respectively, exhibit the least influence on erosion during the autumn season. Aspect and elevation, carrying weight values of 0.12 and 0.10, prove to be more impactful than NDVI and drainage density, yet less significant than precipitation, lithology, and slope. In terms of preference, lithology and precipitation are moderately favoured over aspect and NDVI. Notably, slope, with a score value of 3, is moderately preferred in comparison to drainage density. Given the semi-arid climate of Kalat-e-Naderi region, the erosion in the region can be influenced even by minimal rainfall. The primary agents of erosion during the autumn season are the areas covered by loess, coupled with precipitation and steep slopes. The consistency ratio for the autumn season (0.05) assures the reliability of the assigned weights.

The winter season

Precipitation, lithology, slope, and drainage density emerge as the most impactful factors on erosion during the winter season, with respective weight values of 0.33, 0.23, 0.14, and 0.10 *(Table 5).* Elevation, aspect, and NDVI carry lower weights of 0.07, 0.07, and 0.06, indicating their relatively lesser influence on erosion. Precipitation, with score values of 3 and 4, is moderately to strongly preferred over aspect and NDVI, and moderately preferred over slope, lithology, elevation, and drainage density. As depicted previously, the Archangan and Kalat basins receive the highest amount of precipitation during the winter season (see *Figure 3*, h), while the spring season precipitation is distributed almost evenly across the four basins (see *Figure 3*, f), with Archangan, Kalat, and Chahchaheh being more prominent. For the weighted overlay tool, the assigned value for the highest amount of precipitation (80–90 mm) is 8 *(Table 6).* Furthermore, lithology, scoring 3, is moderately preferred over slope, aspect, elevation, NDVI, and drainage density. Recognizing the susceptibility of loess to erosion, it is assigned a value of 8 in the weighted overlay tool (see *Table 6*). The winter season's consistency ratio of 0.04 falls within an acceptable range, affirming the reliability of the assigned weights.

The calculated consistency ratio for each factor's sub-classes, as presented in *Table 6*, is below 10 percent (< 0.1), meeting the acceptable threshold. Subsequently, erosion susceptibility maps were generated in ArcGIS 10.3 using the weighted overlay tool. Values ranging from 1 to 9 were assigned in the tool based on the weight assigned to each subclass. The Weighted Overlay Tool operates according to Equation (4) (Feizizadeh, B. *et al.* 2014; Arabameri, A. *et al.* 2018; Kahsay, A. *et al.* 2018; Tairi, A. *et al.* 2019; Boufeldja, S. *et al.* 2020; Aslam, B. *et al.* 2021), wherein the dataset is multiplied by its weight, and the sum of all results yields the erosion susceptibility (*ES*) value for each pixel.

$$ES = [(Sl \cdot W) + (As \cdot W) + (Li \cdot W) + (El \cdot W) + (NDVI \cdot W) + (Pr \cdot W) + (Drd \cdot W)], \quad (4)$$

where *Sl* is the slope, *As* is the aspect, *Li* is the lithology, *El* is the elevation, *Pr* is the precipitation, *Drd* is the drainage density, and *W*

Table 5. Pairwise comparison table of the winter season

Pairwise comparison	Slope	Aspect	Lithology	Elevation	NDVI	Precipitation	Drainage density	Weight
Slope	1	3	1/3	3	2	1/3	2	0.14
Aspect	1/3	1	1/3	1	2	1/4	1/2	0.07
Lithology	3	3	1	3	3	1/3	3	0.23
Elevation	1/3	1	1/3	1	1	1/3	1/2	0.07
NDVI	1/2	1/2	1/3	1	1	1/4	1/2	0.06
Precipitation	3	4	3	3	4	1	3	0.33
Drainage density	1/2	2	1/3	2	2	1/3	1	0.10
CR: 0.04								

Table 6. Weight, consistency ratio (CR), and assigned values to the weighted overlay tool of all sub-classes of each factor

Criteria	CR	Sub-criteria	Weights	Assigned values to weighted overlay tool
Slope	0.007	0–5°	0.020	1
		5–10°	0.031	2
		10–15°	0.044	3
		15–20°	0.177	8
		20–25°	0.177	8
		25–30°	0.177	8
		30–35°	0.177	8
		35–40°	0.177	8
		>40°	0.020	1
Aspect	0.030	Flat	0.021	1
		North	0.074	5
		Northeast	0.074	5
		East	0.035	2
		Southeast	0.222	7
		South	0.222	7
		Southwest	0.222	7
		West	0.035	2
		Northwest	0.095	5
Lithology	0.000	Solid rocks	0.111	4
		Loess	0.889	8
Elevation	0.006	460–750	0.030	1
		750–1,040	0.135	5
		1,040–1,330	0.135	5
		1,330–1,620	0.135	5
		1,620–1,910	0.231	6
		1,910–2,200	0.231	6
		2,200–2,490	0.051	2
		2,490–2,780	0.051	2
Drainage density	0.010	0.02–0.52	0.041	1
		0.52–1.02	0.061	2
		1.02–1.52	0.101	3
		1.52–2.02	0.113	3
		2.02–2.52	0.169	4
		2.52–3.02	0.258	5
		3.02–3.70	0.258	5

Table 6. Continued

Criteria	CR	Sub-criteria	Weights	Assigned values to weighted overlay tool
NDVI (spring)	0.003	-0.31–0.0	0.043	1
		0.0–0.1	0.223	4
		0.1–0.2	0.223	4
		0.2–0.3	0.137	3
		0.3–0.4	0.075	2
		0.4–0.5	0.075	2
		0.5–0.6	0.075	2
		0.6–0.7	0.075	2
		0.7–0.83	0.075	2
NDVI (autumn)	0.006	-0.56–0.0	0.075	1
		0.0–0.1	0.140	2
		0.1–0.2	0.140	2
		0.2–0.3	0.271	3
		0.3–0.4	0.075	1
		0.4–0.5	0.075	1
		0.5–0.6	0.075	1
		0.6–0.7	0.075	1
		0.7–0.86	0.075	1
NDVI (winter)	0.004	-0.37–0.0	0.047	1
		0.0–0.1	0.241	4
		0.1–0.2	0.241	4
		0.2–0.3	0.146	3
		0.3–0.4	0.081	2
		0.4–0.5	0.081	2
		0.5–0.6	0.081	2
		0.6–0.7	0.081	2
Precipitation (spring)	0.090	20–30	0.015	2
		30–40	0.021	3
		40–50	0.031	4
		50–60	0.047	5
		60–70	0.071	6
		70–80	0.107	7
		80–90	0.162	8
		90–100	0.239	9
		>100	0.307	9
Precipitation (autumn)	0.000	0–10	0.250	1
		10–20	0.250	1
		20–30	0.500	2
Precipitation (winter)	0.030	10–20	0.024	1
		20–30	0.033	2
		30–40	0.048	3
		40–50	0.071	4
		50–60	0.106	5
		60–70	0.157	6
		70–80	0.231	7
		80–90	0.331	8

represents the weight value of each factor. In this study, Equation 4 is applied three times as each factor's weight has three different values associated with three distinct seasons.

Figures 4, *5*, and *6* depict the final erosion susceptibility maps for each season. Employing the natural break method (Shahabi, H. and Hashim, M. 2015; Saha, S. *et al.* 2019), the maps

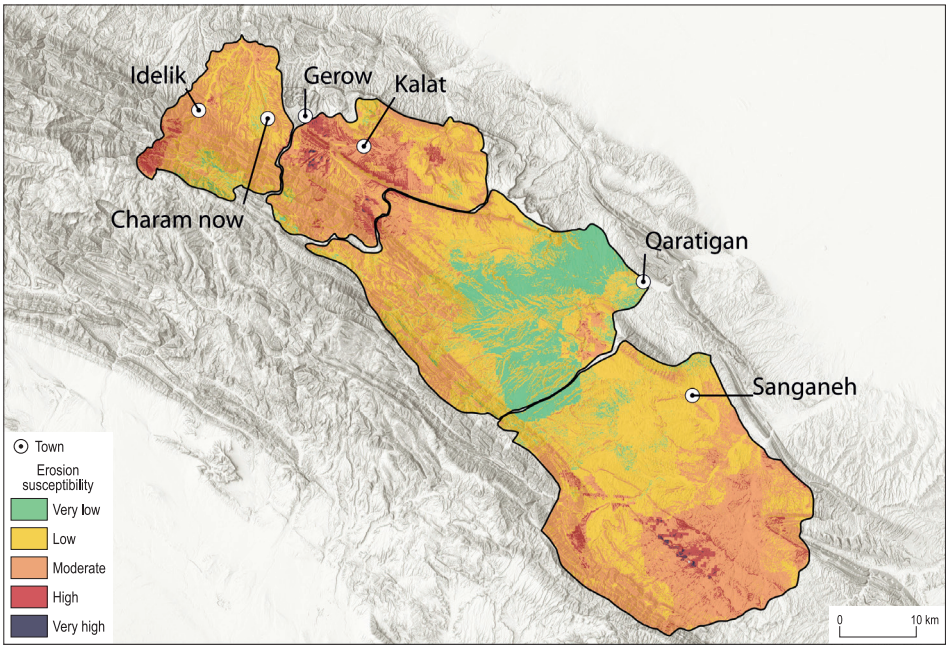

Fig. 4. AHP-based erosion susceptibility map of the spring season. *Source:* Authors' own elaboration.

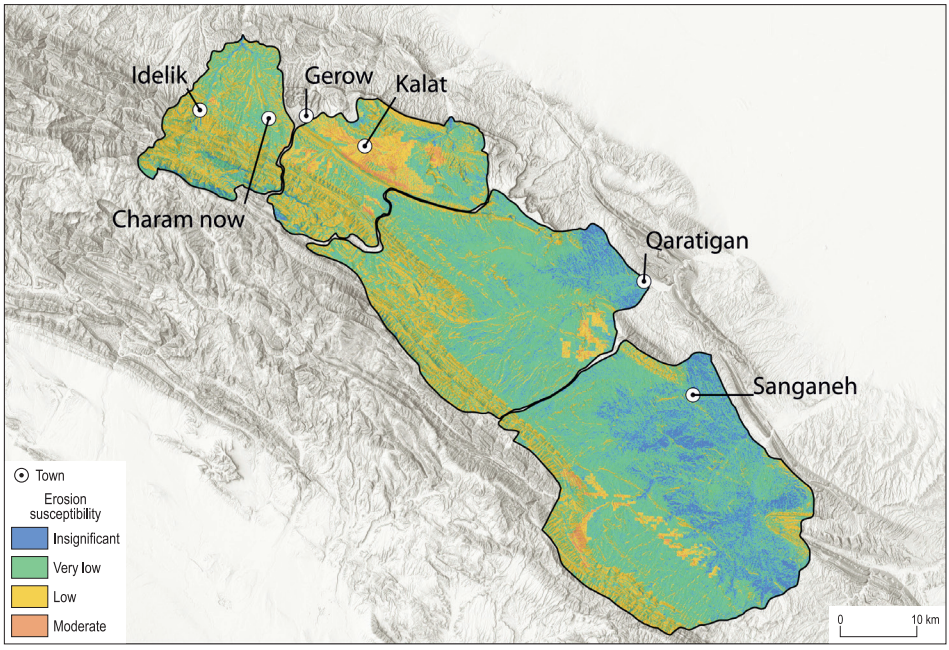

Fig. 5. AHP-based erosion susceptibility map of the autumn season. *Source:* Authors' own elaboration.

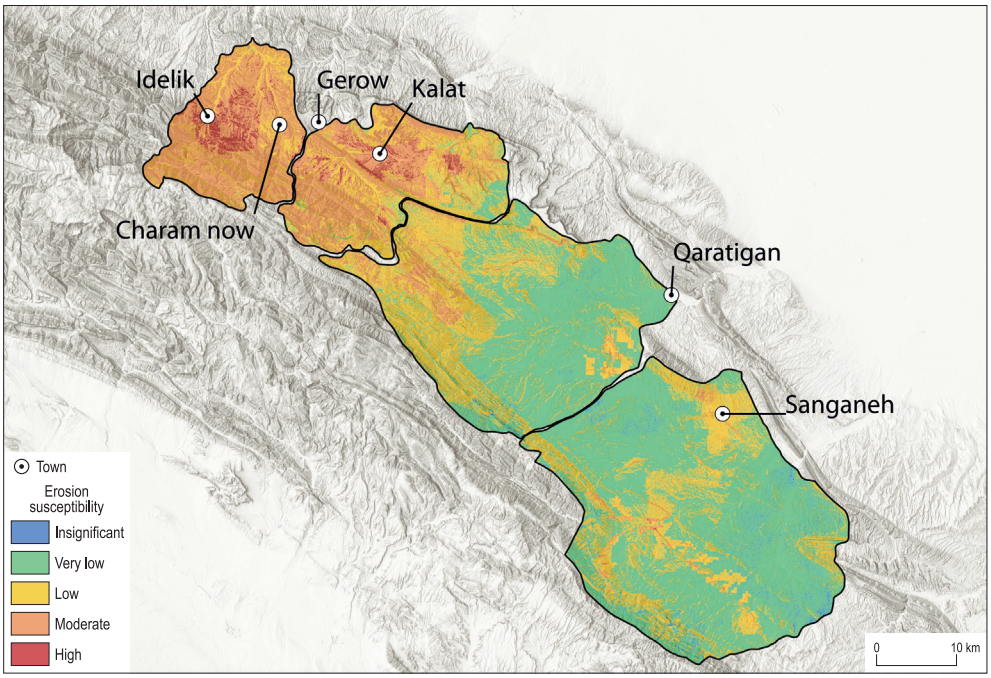

Fig. 6. AHP-based erosion susceptibility map of the winter season. *Source:* Authors' own elaboration.

were reclassified into six categories: insignificant, very low, low, moderate, high, and very high (Ebhuoma, O. *et al.* 2022). It is noteworthy that, owing to the seasonal variation in the impact of each factor, the erosion susceptibility maps encompass different categories.

The very high susceptibility class in the spring map (see *Figure 4*) is predominantly distributed in Chahchaheh and Kalat basins, covering an area of 2.511 km^2 in the study area. In contrast, the areas with very low erosion levels (259.59 km^2) are mainly located in the central and north-eastern parts of the Qaratigan basin. The distribution of each erosion susceptibility class in the spring season is detailed in *Table 6*. The low (1,023.09 km^2), and moderate (869.37 km^2) erosion susceptibility classes cover the majority of the studied basins in the spring season. High erosion susceptibility areas are minor in the Qaratigan basin during the spring season. In Kalat and Chahchaheh basins, the high erosion susceptibility area is primarily in the central section, while in the Archangan basin, the south-western part is mainly in the high erosion susceptibility class. Overall, 105.615 km^2 of the study area is classified as having high erosion susceptibility in the spring season.

The spring season erosion susceptibility map highlights that regions with the highest susceptibility to erosion are mainly associated with high precipitation values, loess cover, and steep slopes. Conversely, regions with the lowest susceptibility to erosion correspond to gentle slopes and lower precipitation values.

The winter season's erosion susceptibility map (see *Figure 6*) was categorized into five classes, ranging from insignificant to a high level. The Chahchaheh and Qaratigan basins are primarily covered with the very low (1,077.80 km^2) and low (743.38 km^2) classes, while the other two basins (Kalat and Archangan) are dominated by moderate (382.28 km^2) and high (36.73 km^2) classes (see *Table 7*). As shown in *Figure 6*, the areas

Table 7. Area and percentage of each class of erosion

Season	Insignificant		Very low		Low		Moderate		High		Very high	
	km²	%	km²	%	km²	%	km²	%	km²	%	km²	%
Spring	–	259.59	259.59	11.48	1,023.09	45.27	869.37	38.47	105.61	4.67	2.51	0.11
Autumn	12.00	1,370.45	1,370.45	60.65	591.79	26.19	26.29	1.16	–	–	–	–
Winter	0.88	1,077.80	1,077.80	47.69	743.38	32.90	382.28	16.91	36.73	1.62	–	–

with moderate and high erosion potential in winter coincide with the region covered by loess, which is very sensitive to water erosion. Thus, precipitation and lithology can be considered as the most dominant factors in the overall erosion process.

Discussion

Based on the pairwise comparisons (see *Tables 3*, *4*, and *5*), erosion has been more significantly influenced by precipitation and lithology than any other factors, as they consistently exhibit higher weights in all three pairwise comparison tables for each studied season. The increased impact of precipitation and lithology can be attributed to the relatively intense yet short downpours in the study area, leading to flash floods, rill and sheet erosion, especially on unresistant and unvegetated surfaces such as loess. Ghahraman, K. and Nagy, B. (2023) have also reported intense rainfall in short time periods in arid and semi-arid regions of northeast Iran.

Field observations indicated that both active and inactive agricultural lands have been undergoing erosion (*Photo 1*, a, b). This observation aligns with our soil erosion maps, where high-susceptibility areas correspond to the location of agricultural lands. The increased vulnerability of agricultural lands to erosion can be attributed to their location on loess deposits, as well as human activities like cultivation and plowing, making the surface more prone to erosion (Beniston, J.W. *et al.* 2015; Zhang, J. *et al.* 2019).

According to the erosion susceptibility maps, the region around Gerow village falls into the high erosion susceptibility category in winter and spring seasons, and the moderate category in the autumn season (see *Figures 4*, *5*, and *6*). Field observations confirm the presence of significant erosional features near Gerow village, including loess sinkholes, gully erosion, and suffusion (*Photo 1*, a, d, and e). The occurrence of sinkholes, even in agricultural lands, can be primarily attributed to the presence of water, especially in the form of precipitation, and lithology. In loess-covered regions, subsurface cracks allow rainfall to penetrate, extending existing fissures and washing away material, leading to the formation of sinkholes, gullies, and suffusion. It is noteworthy that field observations indicate the presence of small and occasionally large pebbles in the loess around Gerow. The existence of these materials in the loess suggests that, in this area, sediment/material transportation is not solely occurring through wind processes; water transportation has also been active in these areas.

In other areas classified as moderately to highly erosion-susceptible, such as the mountain slopes upstream of the abandoned agricultural lands near Gerow village, erosion has led to the exposure of bedrock (*Photo 1*, c). The presence of exposed bedrock highlights the significance of erosion in the study area. Large-scale erosional processes, including landslides, were also observed during field surveys (not in loess-covered sections) (*Photo 1*, b), underscoring the importance of mass movements in the area. Authorities and planners need to take these factors into consideration when planning in these areas.

Another visited site was Idelik village (see *Figure 1*), also classified in high and moderate erosion-susceptible classes on our maps. The predominant form of erosion in this area is the selective erosion of the folded structure

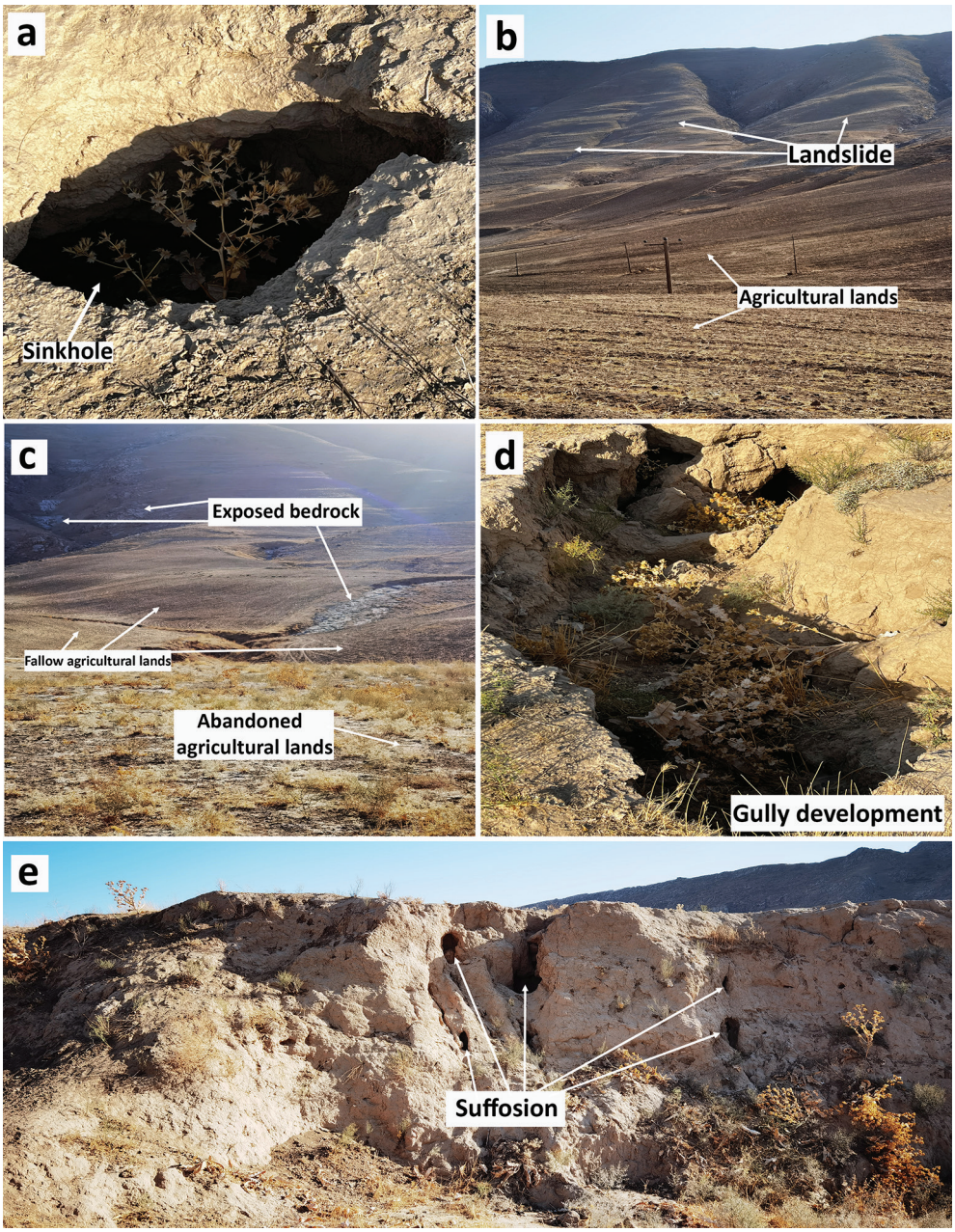

Photo 1. Validation sites around Gerow village. Sinkhole in an abandoned agricultural land (a), landslides in the vicinity of active agricultural fields (b), exposed bedrock on the slopes and in fallow agricultural fields (c), gully development on the abandoned agricultural fields (d), and suffusion on loess walls caused by $CaCO_3$ dissolution (e). Photos taken by the authors.

of the mountains by water and mass movements, resulting in steep walls from the more resistant layers and less steep slopes on the less resistant layers (*Photo 2*, a). Although this type of erosion does not directly impact farmlands in the study area, it holds significance from a hazard perspective. Our field observations revealed gully erosion, as well as topples and slides, especially around the rice fields located on loess-covered lands (*Photo 2*, b). Additional erosional processes, such as solifluction and landslides, were observed on the slopes, exposing the underlying materials by removing the topsoil. This type of erosion resembles a minor mass movement, evident on the slopes.

According to our maps, the regions around the "Charam now" village are classified as

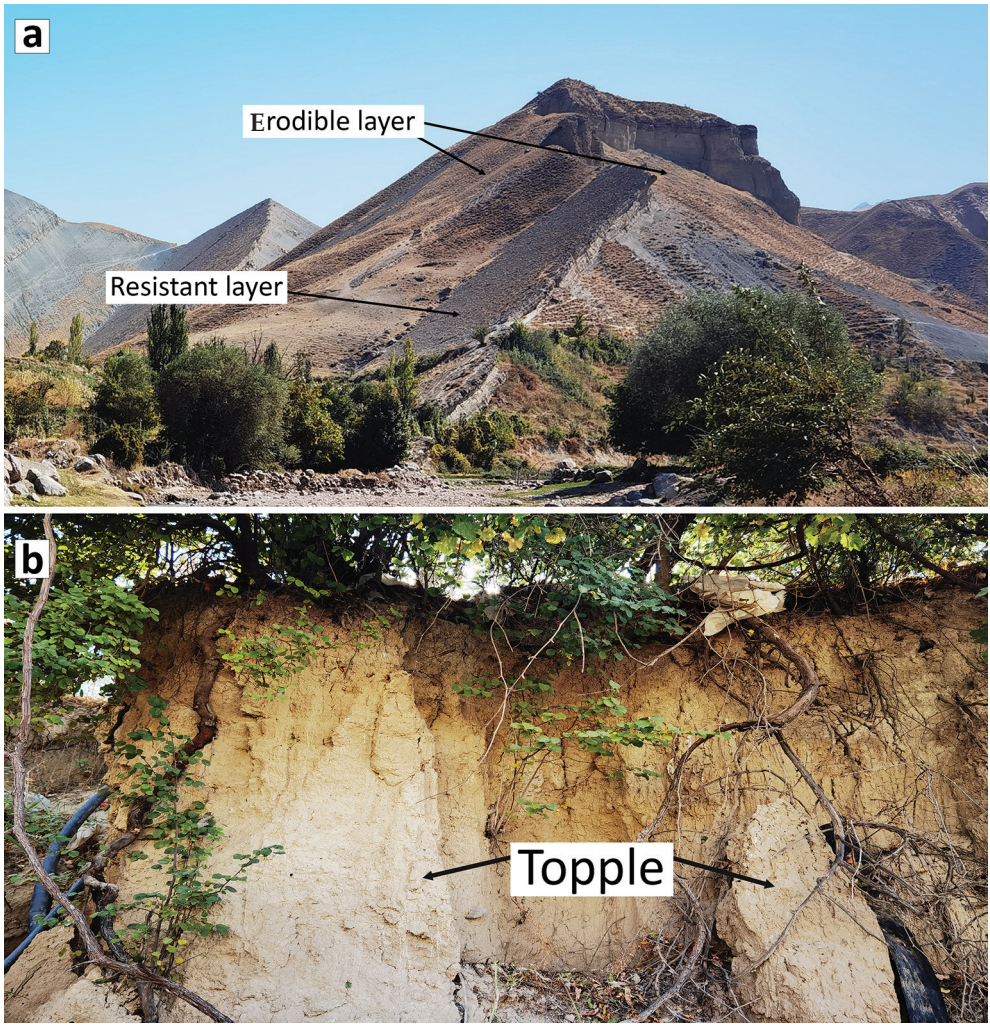

Photo 2. Validation sites around the Idelik village showing erodible layers on the erosion resistant underlying layer on the slopes (a), and columnar blocks being detached from the loess mass (topples) on the loess walls (b). Photos taken by the authors.

very low and low classes, while field observations reveal substantial soil erosion in this area. This discrepancy can be primarily attributed to the scale of the lithological map, as some parts of this area were not classified as loess. However, field observations showed strong erosion on the loess near this village. According to the lithological input, the model considered the lithology as resistant, classifying this area in very low and low soil erosion susceptible classes. It is noteworthy that we have systematically checked the entire basins for this issue, and the "Charam now" village and its surrounding area were the only instances where the lithological map did not accurately indicate the units. In general, fallen loess walls, gully development, fallen riverbanks, and small-scale landslides were observed in this area.

To examine remote or inaccessible areas of the "Charam now" village, we utilized Google Earth satellite imagery. Erosional features such as landslides and gullies near the village are illustrated in *Photo 3.* Local roads have been constructed to facilitate access to agricultural lands situated on the top of the hills. Instability of the slopes and increased chance of landslides in this area can also be related to anthropogenic activities such as road construction.

The majority of agricultural lands in the Kalat basin are located on slopes, with some fields occupying less inclined gradients. Ploughing these agricultural fields, in conjunction with the loess composition of the land and steeper slopes, has exacerbated erosion in this region, as evidenced by our soil erosion maps. With respect to cultivation, erosional processes in these loess-covered areas have the potential to adversely impact crop production. Harris, H.L. and Drew, W.B. (1943) have demonstrated that uneroded loess fields provide an environment that is 50–100 percent more favourable for plant growth than eroded loess fields. Observations of gully and sheet erosion, subsurface erosional features, and landslides in the Kalat basin indicate the prevalence of strong erosional processes in this area *(Photo 4).*

Considering the inherent limitations of the availability of relevant lithological map, namely its 1:250,000 scale and lack of detailed information and given our research focus on loess-covered regions, we opted to categorize the lithological map into two classes: loess and solid rocks. Solid rocks encompass both erodible and resistant rocks, such as limestone, shale, sandstone, and marl. Consequently, in the weighted overlay tool, loess was assigned a score of 8 due to its erosivity and prevalence in the study area, while solid rocks were assigned a score of 4, reflecting their lower susceptibility to erosion owing to the presence of resistant rocks (~ 740 km^2). This approach aligns with other studies that have employed different weights for resistant and erodible rocks in their AHP models (Arabameri, A. *et al.* 2018; El Jazouli, A. *et al.* 2019; Bozali, N. 2020).

In addition to precipitation and lithology, the influence of slope on soil erosion is significant. This is primarily attributed to the impact of slope on flow accumulation, runoff velocity, and surface instability (Rahmati, O. *et al.* 2017). Multiple studies have demonstrated that even gentle slopes can be vulnerable to erosion and gully development (Le Roux, J.J. and Sumner, P. 2012; Lukić, T. *et al.* 2018; Arabameri, A. *et al.* 2019; Phinzi, K. *et al.* 2021).

Vegetation cover in the study area has been subjected to overgrazing by livestock, such as goats and sheep, which can exacerbate soil erosion by removing protective vegetation cover. However, in our study area, we observed that animal footpaths have created micro-terrace structures on the slopes, while other slopes have remained intact from this process *(Photo 5).* This observation is consistent with the findings of Afrah, H. *et al.* (2010), who reported that micro-terraces in the Golestan Province loesses have remained unchanged in terms of morphological structure for an extended period. This preservation is primarily attributed to the fact that animals have consistently used the old paths for grazing, leaving the vegetation cover intact in other parts of the rangeland.

Photo 3. The Google Earth image showing erosional features such as gullies and landslides as well as anthropogenic features such as agricultural lands and a road in the vicinity of the "Charam now" village. Authors' own elaboration based on the Google Earth image.

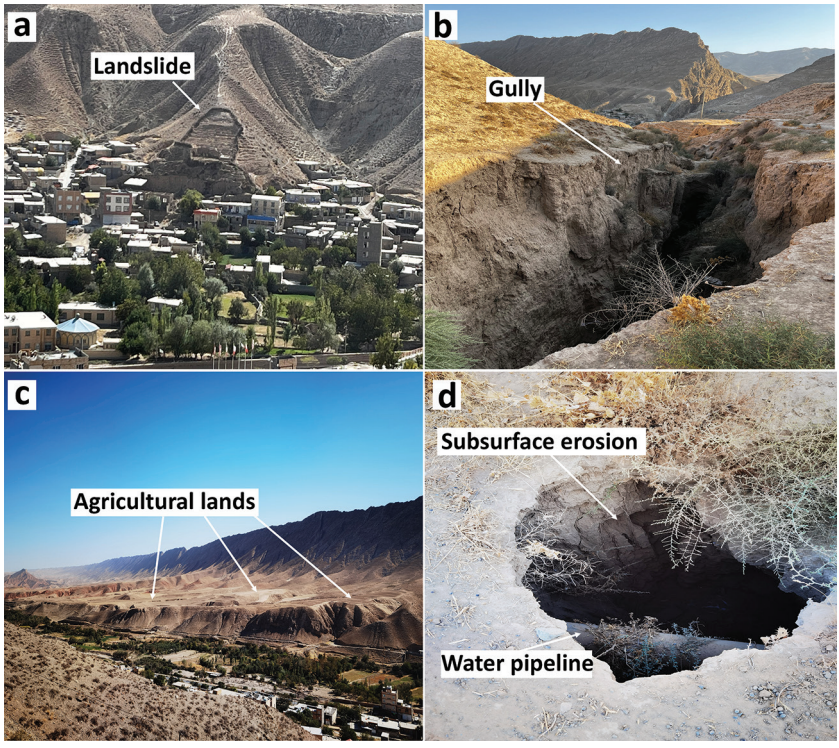

Photo 4. Validation sites in the vicinity of the Kalat city showing landslide (a), deep gully erosion (b), agricultural lands developed on loess-covered areas (c), and sinkholes created by the subsurface erosion on loess-covered areas impacting urban infrastructure (d). Photos taken by the authors.

Photo 5. Micro-terraces created by livestocks on the slopes of the study area.
Photo taken by Nooshin Nokhandan, F.

Conclusions

This research comprehensively investigated erosion-susceptible areas within the major basins of Kalat-e-Naderi county, situated in northeast Iran. The study's focal point was the dual nature of loess, serving as fertile ground for agriculture while presenting vulnerability to erosion. Leveraging the AHP method with 7 key parameters, including slope, aspect, elevation, lithology, NDVI, drainage density, and precipitation, we successfully delineated the spatial distribution of erosion-susceptible regions. The integration of seasonal data, accounting for variations in precipitation and vegetation cover, allowed for the creation of detailed erosion susceptibility maps. Key factors influencing water erosion, as identified through pairwise comparison tables, include precipitation, lithology, and slope. These findings have been visually represented on erosion susceptibility maps, highlighting areas prone to erosion during different seasons. Notably, these vulnerable regions exhibit a discernible correlation with the three primary factors – precipitation, lithology, and slope – while the convergence of the additional four factors amplifies erosion.

Given the semi-arid climate of the region and the loess's heightened erodibility in wet seasons with higher precipitation, the research focused specifically on water erosion. Validation through field observations affirmed the accuracy of the erosion susceptibility maps where erosion-susceptible areas in the map correspond to the observed areas in the field. Despite limitations, such as the absence of comparable studies in neighbouring areas for validation, challenges in reaching erosion sites, and data constraints, the results of this method are invaluable. They offer actionable insights for policymakers and planners, facilitating effective damage mitigation and the formulation of preventative strategies.

Acknowledgements: We express our gratitude to the Stipendium Hungaricom program for their support. Additionally, we extend our thanks to the Erasmus + 20% project (2021-1-HU01-KA131-HED-000003804) for their financial assistance towards our fieldwork expenses. We would also like to acknowledge Professor Farhad Khormali for his invaluable scientific support and his dedication in facilitating our field observations. We also would like to thank the reviewers for their comments, which improved the quality of our work.

REFERENCES

Abbas, S., Dastgeer, G., Yaseen, M. and Latif, Y. 2022. Land-use change impacts on soil and vegetation attributes in the Kanshi River basin, Potohar Plateau, Pakistan. *Land Degradation & Development* 33. (15): 2649–2662. Available at https://doi.org/10.1002/ldr.4252

Afrah, H., Barani, H., Bahremand, A. and Sheikh, V. 2010. Comparison of soil physical properties in micro terraces and inters micro terraces on rangelands. Case study: Baba Shamlak Ranch. *WJournal of Water and Soil Conservation* 17. (2): 141–153.

Ahmadi, M., Minaei, M., Ebrahimi, O. and Nikseresht, M. 2020. Evaluation of WEPP and EPM for improved predictions of soil erosion in mountainous watersheds: A case study of Kangir River basin, Iran. *Modelling Earth Systems and Environment* 6. (4): 2303–2315. Available at https://doi.org/10.1007/s40808-020-00814-w

Alam, N.M., Jana, C., Mandal, D., Meena, S.K., Shrimali, S.S., Mandal, U., Mitra, S. and Kar, G. 2022. Applying Analytic Hierarchy Process for identifying best management practices in erosion risk areas of northwestern Himalayas. *Land* 11. (6): 1–18.

Aleksova, B., Lukić, T., Milevski, I., Spalević, V. and Marković, S.B. 2023. Modelling water erosion and mass movements (Wet) by using GIS-based multihazard susceptibility assessment approaches: A case study – Kratovska Reka catchment (North Macedonia). *Atmosphere* 14. (7): 1–28.

Alexakis, D.D., Hadjimitsis, D.G. and Agapiou, A. 2013. Integrated use of remote sensing, GIS and precipitation data for the assessment of soil erosion rate in the catchment area of "Yialias" in Cyprus. *Atmospheric Research* 131. 108–124. Available at https://doi.org/10.1016/j.atmosres.2013.02.013

Alizadeh, M., Zabihi, H., Wolf, I.D., Langat, P.K., Pour, A.B. and Ahmad, A. 2022. Remote sensing technique and ICONA based-GIS mapping for assessing the risk of soil erosion: A case of the Rudbar Basin, Iran. *Environmental Earth Sciences* 81. (21): 512. Available at https://doi.org/10.1007/s12665-022-10634-z

Alonso, J.A. and Lamata, M.T. 2006. Consistency in the analytic hierarchy process: A new approach. *International Journal of Uncertainty, Fuzziness and Knowledge-based Systems* 14. (04): 445–459.

Amini, A. 1995. *Study of loess provenance and mechanisms of loess formation in Gharatikan watershed, Northeast Iran.* MSC thesis, Tehran, Tehran University. (in Persian)

Arabameri, A., Rezaei, K., Pourghasemi, H.R., Lee, S. and Yamani, M. 2018. GIS-based gully erosion susceptibility mapping: a comparison among three data-driven models and AHP knowledge-based technique. *Environmental Earth Sciences* 77. (17): 1–22.

Arabameri, A., Cerda, A., Rodrigo-Comino, J., Pradhan, B., Sohrabi, M., Blaschke, T. and Tien Bui, D. 2019. Proposing a novel predictive technique for gully erosion susceptibility mapping in arid and semi-arid regions (Iran). *Remote Sensing* 11. (21): 2577.

Asadi, S., Moore, F. and Keshavarzi, B. 2013. The nature and provenance of Golestan loess deposits in northeast Iran. *Geological Journal* 48. (6): 646–660. Available at https://doi.org/10.1002/gj.2466

Aslam, B., Maqsoom, A., Alaloul, W.S., Musarat, M.A., Jabbar, T. and Zafar, A. 2021. Soil erosion susceptibility mapping using a GIS-based multicriteria decision approach: Case of district Chitral, Pakistan. *Ain Shams Engineering Journal* 12. (2): 1637–1649.

Aswathi, J., Sajinkumar, K.S., Rajaneesh, A., Oommen, T., Bouali, E.H., Binoj Kumar, R.B., Rani, V.R., Thomas, J., Thrivikramji, K.P., Ajin, R.S. and Abioui, M. 2022. Furthering the precision of RUSLE soil erosion with PSInSAR data: An innovative model. *Geocarto International* 37. (27): 16108–16131. Available at https://doi.org/10.1080/10106049.2022.2105407

Azareh, A., Rahmati, O., Rafiei-Sardooi, E., Sankey, J.B., Lee, S., Shahabi, H. and Ahmad, B.B. 2019. Modelling gully-erosion susceptibility in a semi-arid region, Iran: Investigation of applicability of certainty factor and maximum entropy models. *Science of the Total Environment* 655. 684–696.

Barbera, V., Poma, I., Gristina, L., Novara, A. and Egli, M. 2012. Long-term cropping systems and tillage management effects on soil organic carbon stock and steady state level of C sequestration rates in a semiarid environment. *Land Degradation & Development* 23. (1): 82–91. Available at https://doi.org/10.1002/ldr.1055

Belkendil, A., Habi, M., Boutkhil, M., Bouzouina, O. and Boufeldja, S. 2018. Using multi–criteria evaluation (MCE): Analytical Hierarchy Process (AHP) in investigation of erosion phenomenon in arid zones. (Case study: Watershed of Bechar, southwest of Algeria). *Commission Scientifique / Scientific Commitee* 18. 99–117.

Belloula, M., Dridi, H. and Kalla, M. 2020. Spatialization of water erosion using analytic hierarchy process (AHP) method in the high valley of the Medjerda, eastern Algeria. *Journal of Water and Land Development* 44. 19–25. Available at https://doi.org/10.24425/jwld.2019.127041

Beniston, J.W., Shipitalo, M.J., Lal, R., Dayton, E.A., Hopkins, D.W., Jones, F., Joynes, A. and Dungait, J.A.J. 2015. Carbon and macronutrient losses during accelerated erosion under different tillage and residue management. *European Journal of Soil Science* 66. (1): 218–225. Available at https://doi.org/10.1111/ejss.12205

Bhattacharya, R.K., Chatterjee, N.D. and Das, K. 2020. Sub-basin prioritization for assessment of soil erosion susceptibility in Kangsabati, a plateau basin: A comparison between MCDM and SWAT models. *Science of the Total Environment* 734. 139474. Available at https://doi.org/10.1016/j.scitotenv.2020.139474

Bouamrane, A., Bouamrane, A. and Abida, H. 2021. Water erosion hazard distribution under a semi-arid climate condition: Case of Mellah watershed, north-eastern Algeria. *Geoderma* 403. 115381. Available at https://doi.org/10.1016/j.geoderma.2021.115381

Boufeldja, S., Baba Hamed, K., Bouanani, A. and Belkendil, A. 2020. Identification of zones at risk of erosion by the combination of a digital model and the method of multi-criteria analysis in the arid regions: case of the Bechar Wadi watershed. *Applied Water Science* 10. (5): 121. Available at https://doi.org/10.1007/s13201-020-01191-6

Bozali, N. 2020. Assessment of the soil protection function of forest ecosystems using GIS-based Multi-Criteria Decision Analysis: A case study in Adıyaman, Turkey. *Global Ecology and Conservation* 24. e01271. Available at https://doi.org/10.1016/j.gecco.2020.e01271

Cen, Y., Zhang, B., Luo, J., Deng, Q., Liu, H. and Wang, L. 2022. Influence of topographic factors on the characteristics of gully systems in mountainous areas of Ningnan Dry-Hot Valley, SW China. *International Journal of Environmental Research and Public Health* 19. (14): 8784. Available at https://doi.org/10.3390/ijerph19148784

Costa, C.A.B. and Vansnick, J.-C. 2008. A critical analysis of the eigenvalue method used to derive priorities in AHP. *European Journal of Operational Research* 187. (3): 1422–1428. Available at https://doi.org/10.1016/j.ejor.2006.09.022

Das, B., Bordoloi, R., Thungon, L.T., Paul, A., Pandey, P.K., Mishra, M. and Tripathi, O.P. 2020. An integrated approach of GIS, RUSLE and AHP to model soil erosion in West Kameng watershed, Arunachal Pradesh. *Journal of Earth System Science* 129. (1): 94. Available at https://doi.org/10.1007/s12040-020-1356-6

Durlević, U., Valjarević, A., Novković, I., Ćurčić, N.B., Smiljić, M., Morar, C., Stoica, A., Barišić, D. and Lukić, T. 2022. GIS-based spatial modelling of snow avalanches using analytic hierarchy process: A case study of the Šar Mountains, Serbia. *Atmosphere* 13. (8): 1229. Available at https://doi.org/10.3390/atmos13081229

Ebhuoma, O., Gebreslasie, M., Ngetar, N.S., Phinzi, K. and Bhattacharjee, S. 2022. Soil erosion vulnerability mapping in selected rural communities of u'Thukela catchment, South Africa, using the analytic hierarchy process. *Earth Systems and Environment* 6. (4): 851–864.

Echogdali, F.Z., Boutaleb, S., Taia, S., Ouchchen, M., Id-Belqas, M., Kpan, R.B., Abioui, M., Aswathi, J. and Sajinkumar, K.S. 2022. Assessment of soil erosion risk in a semi-arid climate watershed using SWAT model: Case of Tata basin, South-East of Morocco. *Applied Water Science* 12. (6): 137. Available at https://doi.org/10.1007/s13201-022-01664-w

El Jazouli, A., Barakat, A. and Khellouk, R. 2019. GIS-multicriteria evaluation using AHP for landslide susceptibility mapping in Oum Er Rbia high basin (Morocco). *Geoenvironmental Disasters* 6. (3): 1–12. Available at https://doi.org/10.1186/s40677-019-0119-7

Emerson, W.W. and McGarry, D. 2003. Organic carbon and soil porosity. *Soil Research* 41. (1): 107–118. Available at https://doi.org/10.1071/SR01064

Ennaji, N., Ouakhir, H., Halouan, S. and Abahrour, M. 2022. Assessment of soil erosion rate using the EPM model: Case of Ouaoumana basin, Middle Atlas, Morocco. *IOP Conference Series: Earth and Environmental Science* 1090. (1): 012004. Available at https://doi.org/10.1088/1755-1315/1090/1/012004

Farah, A., Algouti, A., Algouti, A., Ifkirne, M. and Ezziyani, A. 2021. Mapping of soil degradation in semi-arid environments in the ouarzazate basin in the south of the central High Atlas, Morocco, using sentinel 2A data. *Remote Sensing Applications: Society and Environment* 23. 100548. Available at https://doi.org/10.1016/j.rsase.2021.100548

Feizi, V., Azizi, G., Alimohammadian, H. and Mollashahi, M. 2023. Magnetic properties and geochemistry of loess/paleosol sequences at Nowdeh section northeastern of Iran. *Climate of the Past, Discuss.* 2023-56. 1–14. Available at https://doi.org/10.5194/cp-2023-56

Feizizadeh, B., Shadman Roodposhti, M., Jankowski, P. and Blaschke, T. 2014. A GIS-based extended fuzzy multi-criteria evaluation for landslide susceptibility mapping. *Computers & Geosciences* 73. 208–221. Available at https://doi.org/10.1016/j.cageo.2014.08.001

Fenn, K., Millar, I.L., Durcan, J.A., Thomas, D.S.G., Banak, A., Marković, S.B., Veres, D. and Stevens, T. 2022. The provenance of Danubian loess. *Earth-Science Reviews* 226. 103920. Available at https://doi.org/10.1016/j.earscirev.2022.103920

Frechen, M., Kehl, M., Rolf, C., Sarvati, R. and Skowronek, A. 2009. Loess chronology of the Caspian Lowland in Northern Iran. *Quaternary International* 198. (1): 220–233. Available at https://doi.org/10.1016/j.quaint.2008.12.012

Ghafarpour, A., Khormali, F., Balsam, W., Karimi, A. and Ayoubi, S. 2016. Climatic interpretation of loess-paleosol sequences at Mobarakabad and Aghband, Northern Iran. *Quaternary Research* 86. (1): 95–109. Available at https://doi.org/10.1016/j.yqres.2016.05.004

Ghafarpour, A., Khormali, F., Tazikeh, H., Kehl, M., Rolf, C., Frechen, M. and Zeeden, C. 2023. Geophysical sediment properties of a late Pleistocene loess–paleosol sequence, Chenarli, northeastern Iran. *Quaternary Research* 114. 114–129. Available at https://doi.org/10.1017/qua.2023.5

Ghahraman, K. and Nagy, B. 2023. Flood risk on arid alluvial fans: a case study in the Joghatay Mountains, northeast Iran. *Journal of Mountain Science* 20. (5): 1183–1200. Available at https://doi.org/10.1007/s11629-022-7635-8

Gharibreza, M., Zaman, M., Porto, P., Fulajtar, E., Parsaei, L. and Eisaei, H. 2020. Assessment of deforestation impact on soil erosion in loess formation using 137Cs method (case study: Golestan Province, Iran). *International Soil and Water Conservation Research* 8. (4): 393–405. Available at https://doi.org/10.1016/j.iswcr.2020.07.006

Gómez-Gutiérrez, Á., Conoscenti, C., Angileri, S.E., Rotigliano, E. and Schnabel, S. 2015. Using topographical attributes to evaluate gully erosion proneness (susceptibility) in two mediterranean basins: Advantages and limitations. *Natural Hazards* 79. (1): 291–314.

Harris, H.L. and Drew, W.B. 1943. On the establishment and growth of certain legumes on eroded and uneroded sites. *Ecology* 24. (2): 135–148.

Hayatzadeh, M., Moosavi, V. and Aliramaee, R. 2023. Assessment and prioritization of soil erosion triggering factors using analytical hierarchy process and Taguchi method. *International Journal of Sediment Research* 38. (3): 396–404. Available at https://doi.org/10.1016/j.ijsrc.2022.11.002

Huang, C., Hou, X. and Li, H. 2022. An improved minimum cumulative resistance model for risk assessment of agricultural non-point source pollution in the coastal zone. *Environmental Pollution* 312. 120036. Available at https://doi.org/10.1016/j.envpol.2022.120036

Jaafari, A., Najafi, A., Pourghasemi, H., Rezaeian, J. and Sattarian, A. 2014. GIS-based frequency ratio and index of entropy models for landslide susceptibility assessment in the Caspian forest, northern Iran. *International Journal of Environmental Science and Technology* 11. (4): 909–926.

Jebur, M.N., Pradhan, B. and Tehrany, M.S. 2014. Optimization of landslide conditioning factors using very high-resolution airborne laser scanning (LIDAR) data at catchment scale. *Remote Sensing of Environment* 152. 150–165.

Kachouri, S., Achour, H., Abida, H. and Bouaziz, S. 2015. Soil erosion hazard mapping using Analytic Hierarchy Process and logistic regression: A case study of Haffouz watershed, central Tunisia. *Arabian Journal of Geosciences* 8. (6): 4257–4268.

Kahsay, A., Haile, M., Gebresamuel, G. and Mohammed, M. 2018. Land suitability analysis for sorghum crop production in northern semi-arid Ethiopia: Application of GIS-based fuzzy AHP approach. *Cogent Food & Agriculture* 4. (1): 1507184. Available at https://doi.org/10.1080/23311932.2018.1507184

Karimi, A., Frechen, M., Khademi, H., Kehl, M. and Jalalian, A. 2011. Chronostratigraphy of loess deposits in northeast Iran. *Quaternary International* 234. (1–2): 124–132.

Kebede, Y.S., Endalamaw, N.T., Sinshaw, B.G. and Atinkut, H.B. 2021. Modelling soil erosion using RUSLE and GIS at watershed level in the Upper Beles, Ethiopia. *Environmental Challenges* 2. 100009. Available at https://doi.org/10.1016/j.envc.2020.100009

Kehl, M., Vlaminck, S., Köhler, T., Laag, C., Rolf, C., Tsukamoto, S., Frechen, M., Sumita, M., Schmincke, H.-U. and Khormali, F. 2021. Pleistocene dynamics of dust accumulation and soil formation in the southern Caspian Lowlands – New insights from the loess-paleosol sequence at Neka-Abelou, northern Iran. *Quaternary Science Reviews* 253. 106774. Available at https://doi.org/10.1016/j.quascirev.2020.106774

Khormali, F., Ajami, M., Ayoubi, S., Srinivasarao, C. and Wani, S.P. 2009. Role of deforestation and hillslope position on soil quality attributes of loess-derived soils in Golestan province, Iran. *Agriculture, Ecosystems & Environment* 134. (3): 178–189. Available at https://doi.org/10.1016/j.agee.2009.06.017

Köppen, W. 1900. Versuch einer Klassifikation der Klimate, vorzugsweise nach ihren Beziehungen zur Pflanzenwelt. (Schluss). *Geographische Zeitschrift* 6. (12): 657–679. Available at http://www.jstor.org/stable/27803939

Kucuker, D.M. and Giraldo, D.C. 2022. Assessment of soil erosion risk using an integrated approach of GIS and Analytic Hierarchy Process (AHP) in Erzurum, Turkiye. *Ecological Informatics* 71. 101788.

Le Roux, J.J. and Sumner, P. 2012. Factors controlling gully development: comparing continuous and discontinuous gullies. *Land Degradation & Development* 23. (5): 440–449.

Li, Y., Jiang, Z., Chen, Z., Yu, Y., Lan, F., Shan, Z., Sun, Y., Liu, P., Tang, X. and Rodrigo-Comino, J. 2020. Anthropogenic disturbances and precipitation affect karst sediment discharge in the Nandong

underground river system in Yunnan, Southwest China. *Sustainability* 12. (7). 3006. Available at https://doi.org/10.3390/su12073006

Lukić, T., Leščešen, I., Sakulski, D., Basarin, B. and Jordaan, A. 2016. Rainfall erosivity as an indicator of sliding occurrence along the southern slopes of the Bačka loess plateau: a case study of the Kula settlement, Vojvodina (North Serbia). *Carpathian Journal of Earth and Environmental Sciences* 11. (2): 303-318.

Lukić, T., Bjelajac, D., Fitzsimmons, K.E., Markovic, S.B., Basarin, B., Mladan, D., Micic, T., Schaetzl, R.J., Gavrilov, M.B. and Milanovic, M. 2018. Factors triggering landslide occurrence on the Zemun loess plateau, Belgrade area, Serbia. *Environmental Earth Sciences* 77. 13. Available at https://doi.org/10.1007/s12665-018-7712-z

Lukić, T., Lukić, A., Basarin, B., Ponjiger, T.M., Blagojević, D., Mesaroš, M., Milanović, M., Gavrilov, M., Pavić, D., Zorn, M., Komac, B., Miljković, Đ., Sakulski, D., Babić-Kekez, S., Morar, C. and Janićević, S. 2019. Rainfall erosivity and extreme precipitation in the Pannonian basin. *Open Geosciences* 11. (1): 664–681. Available at https://doi.org/doi:10.1515/geo-2019-0053 (Open Geosciences)

Marković, S.B., Timar-Gabor, A., Stevens, T., Hambach, U., Popov, D., Tomić, N., Obreht, I., Jovanović, M., Lehmkuhl, F., Kels, H., Marković, R. and Gavrilov, M.B. 2014. Environmental dynamics and luminescence chronology from the Orlovat loess–palaeosol sequence (Vojvodina, northern Serbia). *Journal of Quaternary Science* 29. (2): 189–199. Available at https://doi.org/10.1002/jqs.2693

Meshram, S.G., Singh, V.P., Kahya, E., Sepehri, M., Meshram, C., Hasan, M.A., Islam, S. and Duc, P.A. 2022. Assessing erosion prone areas in a watershed using interval rough-analytical hierarchy process (IR-AHP) and fuzzy logic (FL). *Stochastic Environmental Research and Risk Assessment* 36. (2): 297–312. Available at https://doi.org/10.1007/s00477-021-02134-6

Micić Ponjiger, T., Lukić, T., Wilby, R.L., Marković, S.B., Valjarević, A., Dragićević, S., Gavrilov, M.B., Ponjiger, I., Durlević, U., Milanović, M.M., Basarin, B., Mlađan, D., Mitrović, N., Grama, V. and Morar, C. 2023. Evaluation of rainfall erosivity in the Western Balkans by mapping and clustering ERA5 reanalysis data. *Atmosphere* 14. (1): 104. Available at https://doi.org/10.3390/atmos14010104

Morgan, R. 1995. *Soil Erosion and Conservation*. London, Longman.

Morgan, R., Quinton, J., Smith, R., Govers, G., Poesen, J., Auerswald, K., Chisci, G., Torri, D. and Styczen, M. 1998. The European Soil Erosion Model (EUROSEM): A dynamic approach for predicting sediment transport from fields and small catchments. *Earth Surface Processes and Landforms: The Journal of the British Geomorphological Group* 23. (6): 527–544.

Muhs, D.R. 2007. Loess deposits, origins and properties. In *Encyclopedia of Quaternary Science*. Eds.: Scott, E.A. and Mock, C.J., Elsevier, 1405–1418. Available at https://doi.org/10.1016/B0-44-452747-8/00158-7

Mushtaq, F., Farooq, M., Tirkey, A.S. and Sheikh, B.A. 2023. Analytic hierarchy process (AHP) based soil erosion susceptibility mapping in northwestern Himalayas: A case study of Central Kashmir province. *Conservation* 3. (1): 32–52. Available at https://doi.org/10.3390/conservation3010003

Neitsch, S.L., Arnold, J.G., Kiniry, J.R. and Williams, J.R. 2011. *Soil and water assessment tool theoretical documentation.* Version 2009. Temple, TX, USA, Blackland Research Center.

Neji, N., Ayed, R.B. and Abida, H. 2021. Water erosion hazard mapping using analytic hierarchy process (AHP) and fuzzy logic modeling: a case study of the Chaffar Watershed (Southeastern Tunisia). *Arabian Journal of Geosciences* 14. (13): 1–15.

Okhravi, R. and Amini, A. 2001. Characteristics and provenance of the loess deposits of the Gharatikan watershed in northeast Iran. *Global and Planetary Change* 28. (1–4): 11–22.

Olii, M.R., Olii, A., Pakaya, R. and Olii, M.Y.U.P. 2023. GIS-based analytic hierarchy process (AHP) for soil erosion-prone areas mapping in the Bone Watershed, Gorontalo, Indonesia. *Environmental Earth Sciences* 82. (9): 225. Available at https://doi.org/10.1007/s12665-023-10913-3

Pandey, S., Kumar, P., Zlatic, M., Nautiyal, R. and Panwar, V.P. 2021. Recent advances in assessment of soil erosion vulnerability in a watershed. *International Soil and Water Conservation Research* 9. (3): 305–318. Available at https://doi.org/10.1016/j.iswcr.2021.03.001

Parsian, S., Amani, M., Moghimi, A., Ghorbanian, A. and Mahdavi, S. 2021. Flood hazard mapping using fuzzy logic, analytical hierarchy process, and multi-source geospatial datasets. *Remote Sensing* 13. (23): 4761. Available at https://doi.org/10.3390/rs13234761

Pécsi, M. 1990. Loess is not just the accumulation of dust. *Quaternary International* 7. 1–21.

Phinzi, K., Ngetar, N.S. and Ebhuoma, O. 2021. Soil erosion risk assessment in the Umzintlava catchment (T32E), Eastern Cape, South Africa, using RUSLE and random forest algorithm. *South African Geographical Journal* 103. (2): 139–162.

Pye, K. and Tsoar, H. 1987. The mechanics and geological implications of dust transport and deposition in deserts with particular reference to loess formation and dune sand diagenesis in the northern Negev, Israel. *Geological Society, London, Special Publications* 35. (1): 139–156.

Rahmati, O., Haghizadeh, A., Pourghasemi, H.R. and Noormohamadi, F. 2016. Gully erosion susceptibility mapping: The role of GIS-based bivariate

statistical models and their comparison. Natural hazards 82. (2): 1231–1258.

Rahmati, O., Tahmasebipour, N., Haghizadeh, A., Pourghasemi, H.R. and Feizizadeh, B. 2017. Evaluating the influence of geo-environmental factors on gully erosion in a semi-arid region of Iran: An integrated framework. *Science of the Total Environment* 579. 913–927.

Rajesh, C., Dibyendu, D., Rabindra, N.B. and Uttam, K.M. 2016. Analytic hierarchy process and multi-criteria decision-making approach for selecting the most effective soil erosion zone in Gomati river basin. *International Journal of Engineering Research & Technolgy* 5. (1): 595–600. Available at https://doi.org/10.17577/IJERTV5IS010474

Raza, A., Ahrends, H., Habib-Ur-Rahman, M. and Gaiser, T. 2021. Modeling approaches to assess soil erosion by water at the field scale with special emphasis on heterogeneity of soils and crops. *Land* 10. (4): 422. Available at https://doi.org/10.3390/land10040422

Richthofen, F. 1872. Reisen im nördlichen China: Ueber den chinesischen Löss. *Verhandlungen der Kaiserlich-Königlichen geologischen Reichsanstalt* 8. 153–160.

Saaty, R.W. 1987. The analytic hierarchy process – what it is and how it is used? *Mathematical Modelling* 9. (3–5): 161–176.

Saaty, T.L. 1980. *The Analytic Hierarchy Process.* New York, Mcgraw Hill.

Saaty, T.L. 1988. What is the analytic hierarchy process? In *Mathematical Models for Decision Support.* Eds.: Mitra, G., Greenberg, H.J., Lootsma, F.A., Rijkaert, M.J. and Zimmermann, H.J., Cham, Springer, 109–121.

Saaty, T.L. and Vargas, L.G. 2001. How to make a decision. In *Models, Methods, Concepts & Applications of the Analytic Hierarchy Process.* New York, Springer, 1–25.

Saha, S., Gayen, A., Pourghasemi, H.R. and Tiefenbacher, J.P. 2019. Identification of soil erosion-susceptible areas using fuzzy logic and analytical hierarchy process modeling in an agricultural watershed of Burdwan district, India. *Environmental Earth Sciences* 78. (23): 1–18.

Saini, S.S., Jangra, R. and Kaushik, S. 2015. Vulnerability assessment of soil erosion using geospatial techniques: A pilot study of upper catchment of Markanda river. *International Journal of Advancement in Remote Sensing, GIS and Geography* 2. (1): 9–21.

Sandeep, P., Reddy, G.P.O., Jegankumar, R. and Arun Kumar, K.C. 2021. Modeling and assessment of land degradation vulnerability in semi-arid ecosystem of southern India using temporal satellite data, AHP and GIS. *Environmental Modeling & Assessment* 26. (2): 143–154. Available at https://doi.org/10.1007/s10666-020-09739-1

Shahabi, H. and Hashim, M. 2015. Landslide susceptibility mapping using GIS-based statistical models and remote sensing data in tropical environment. *Scientific Reports* 5. (1): 9899.

Sharifigarmdareh, J., Khormali, F., Scheidt, S., Rolf, C., Kehl, M. and Frechen, M. 2020. Investigating soil magnetic properties with pedogenic variation along a precipitation gradient in loess-derived soils of the Golestan province, northern Iran. *Quaternary International* 552. 100–110. Available at https://doi.org/10.1016/j.quaint.2019.11.022

Shen, N., Wang, Z., Zhang, F. and Zhou, C. 2023. Response of soil detachment rate to sediment load and model examination: A key process simulation of rill erosion on steep loessial hillslopes. *International Journal of Environmental Research and Public Health* 20. (4): 2839. Available at https://doi.org/10.3390/ijerph20042839

Sinshaw, B.G., Belete, A.M., Tefera, A.K., Dessie, A.B., Bizuneh, B.B., Alem, H.T., Atanaw, S.B., Eshete, D.G., Wubetu, T.G., Atinkut, H.B. and Moges, M.A. 2021. Prioritization of potential soil erosion susceptibility region using fuzzy logic and analytical hierarchy process, upper Blue Nile Basin, Ethiopia. *Water-Energy Nexus* 4. 10–24. Available at https://doi.org/10.1016/j.wen.2021.01.001

Smalley, I., Marković, S.B. and Svirčev, Z. 2011. Loess is [almost totally formed by] the accumulation of dust. *Quaternary International* 240. (1–2): 4–11.

Tairi, A., Elmouden, A. and Aboulouafa, M. 2019. Soil erosion risk mapping using the analytical hierarchy process (AHP) and geographic information system in the tifnout-askaoun watershed, southern Morocco. *European Scientific Journal* 15. (30): 1857–1743.

Thomas, J., Joseph, S. and Thrivikramji, K. 2018. Assessment of soil erosion in a tropical mountain river basin of the southern Western Ghats, India using RUSLE and GIS. *Geoscience Frontiers* 9. (3): 893–906.

Vanmaercke, M., Panagos, P., Vanwalleghem, T., Hayas, A., Foerster, S., Borrelli, P., Rossi, M., Torri, D., Casali, J., Borselli, L., Vigiak, O., Maerker, M., Haregeweyn, N., De Geeter, S., Zgłobicki, W., Bielders, C., Cerdà, A., Conoscenti, C., de Figueiredo, T., Evans, B., Golosov, V., Ionita, I., Karydas, C.G., Kertész, Á., Krasa, J., Le Bouteiller, C., Radoane, M., Ristic, R., Rousseva, S., Stankoviansky, M., Stolte, J., Stolz, C., Bartley, R., Wilkinson, S., Jaribahi, B. and Poesen, J. 2021. Measuring, modelling and managing gully erosion at large scales: A state of the art. *Earth-Science Reviews* 218. 103637. Available at https://doi.org/10.1016/j.earscirev.2021.103637

Wang, X., Jiao, F., Li, X. and An, S. 2017. The Loess Plateau. In *Multifunctional Land-Use Systems for Managing the Nexus of Environmental Resources.* Eds.: Zhang, L. and Schwärzel, K., Cham, Springer, 11–27. Available at https://doi.org/10.1007/978-3-319-54957-6_2

Wu, Q., Jia, C., Chen, S. and Li, H. 2019. SBAS-InSAR based deformation detection of urban land, created from mega-scale mountain excavating and valley filling in the Loess Plateau: The case study of Yan'an city. *Remote Sensing* 11. (14): 1673. Available https://doi.org/10.3390/rs11141673

Xu, J., Wu, Z., Chen, H., Shao, L., Zhou, X. and Wang, S. 2022. Influence of dry-wet cycles on the strength behavior of basalt-fiber reinforced loess. *Engineering Geology* 302. 106645. Available at https://doi.org/10.1016/j.enggeo.2022.106645

Young, R., Onstad, C., Bosch, D. and Anderson, W. 1989. AGNPS: A nonpoint-source pollution model for evaluating agricultural watersheds. *Journal of Soil and Water Conservation* 44. (2): 168–173.

Zhang, J., Yang, M., Deng, X., Liu, Z., and Zhang, F. 2019. The effects of tillage on sheet erosion on sloping fields in the wind-water erosion crisscross region of the Chinese Loess Plateau. *Soil and Tillage Research* 187. 235–245. Available at https://doi.org/10.1016/j.still.2018.12.014

Zhao, J., Vanmaercke, M., Chen, L. and Govers, G. 2016. Vegetation cover and topography rather than human disturbance control gully density and sediment production on the Chinese Loess Plateau. *Geomorphology* 274. 92–105.

Zhu, K.-W., Chen, Y.-C., Zhang, S., Yang, Z.-M., Huang, L., Li, L., Lei, B., Zhou, Z.-B., Xiong, H.-L., Li, X.-X., Li, Y.-C. and Islam, S. 2020. Output risk evolution analysis of agricultural non-point source pollution under different scenarios based on multi-model. *Global Ecology and Conservation* 23. e01144. Available at https://doi.org/10.1016/j.gecco.2020.e01144

Zou, L., Liu, Y., Wang, Y. and Hu, X. 2020. Assessment and analysis of agricultural non-point source pollution loads in China: 1978–2017. *Journal of Environmental Management* 263. 110400. Available at https://doi.org/10.1016/j.jenvman.2020.110400

DOI: 10.15201/hungeobull.72.4.3 Hungarian Geographical Bulletin **72** 2023 (4) 365–381.

Channel-reach morphometric analysis on a headwater stream in a low-mountainous region: A case study from Mecsek Hills

Balázs VÍG[1], Gábor VARGA[2], Richárd BALOGH[3], Dénes LÓCZY[2], László NAGYVÁRADI[2] and Szabolcs Ákos FÁBIÁN[2]

Abstract

Small catchments in mountainous regions affect downstream rivers as a primary source of sediment supply and also generate flash swasfloods, especially during extreme events. These floods have significantly shaped the catchments of small streams in the Mecsek Hills and some rural areas over the past two decades. However, there has been no previous study examining the hydromorphology of headwater catchments in low mountain environments in Hungary. The present study was meant to investigate the fundamental hydrogeomorphological properties of a first-order catchment. A customary and detailed GIS survey of 50-metre sections was aimed at deciphering flash flood vulnerability and geomorphic interrelations within a micro-watershed. We found moderate susceptibility to flash floods compared to the whole Mecsek Hills. Stable large woody debris jams were identified during the field survey as major geomorphic channel features functioning as natural barriers which drive channel evolution and reduce flood hazards.

Keywords: hydromorphometry, large woody debris, semi-natural, stream reach, field survey, Öreg-patak stream

Introduction

An important aspect of fluvial landscape evolution research involves streams and their channel characterisation from various perspectives. This topic is widespread and has an extensive global scientific literature, dating back to the late 19th century and continuing to the present day, evidenced by the numerous papers published on the description and systematic classification of streams (Leopold, L.B. and Markley, G.W. 1957; Kaszowski, L. and Krzemien, K. 1999; Lóczy, D. 2012; Buffington, J.M. and Montgomery, D.R. 2013; Bisson, P.A. *et al*. 2017, and references therein).

The streams and their immediate environment (floodplains and valleys) are often described by their hydrogeomorphological characteristics. In addition, essential parameters can be derived from the geological, hydrological, land cover, land use, and ecological features of the catchment (Rosgen, D.L. 1994; Fryirs, K.A. and Brierley, G.J. 2001; Fryirs, K.A. *et al*. 2007; Gurnell, A.M. and Grabowski, R.C. 2016; Grabowski, R.C. *et al*. 2019, and references therein). At present, anthropogenic influences such as flood control measures, channelisation, and forestry are increasing in frequency and intensity. The literature overview demonstrates the lack of a uni-

[1] Doctoral School of Earth Sciences, Institute of Geography and Earth Sciences, University of Pécs, Pécs, Hungary. Ifjúság útja 6. H-7624 Pécs, Hungary. E-mail: vbalazs90@hotmail.com

[2] Institute of Geography and Earth Sciences, University of Pécs, Pécs, Hungary. Ifjúság útja 6. H-7624 Pécs, Hungary. E-mails: gazi@gamma.ttk.pte.hu, loczyd@gamma.ttk.pte.hu, nagyvarl@gamma.ttk.pte.hu, smafu@gamma.ttk.pte.hu

[3] Doctoral School of Earth Sciences, Institute of Geography and Earth Sciences, University of Pécs, Pécs, Hungary. Ifjúság útja 6. H-7624 Pécs, Hungary. E-mail: brichard@gamma.ttk.pte.hu

versal classification system valid across all geographical locations. Nonetheless, the available classification techniques enable the adoption of a suitable survey approach that considers all the relevant attributes of the area under study.

The hierarchical classification system is well suited to streams with various features. A clear advantage is that the units within a given catchment are split along the scale into smaller and more interpretable segments. These units, such as valley segment (100–10,000 m), stream reach (10–1,000 m), and channel unit (1–10 m) make the investigations of headwater streams possible. Thus, even for small streams, as well as larger rivers, qualitative and quantitative parameters can be assessed both along the longitudinal profile and at cross-sections (Płaczkowska, E. 2016; Bisson, P.A. *et al*. 2017).

The longitudinal profile allows differentiation of segments according to stream power, incision rate, accumulation zones, and sediment load in terms of quantity, composition, and particle size (Buffington, J.M. and Montgomery, D.R. 2013). The sections offer key information on changes in channel shape and sinuosity (such as straight, meandering, and braided). These processes significantly affect cross-section parameters (for example, bankfull width and/or depth, channel shape index) and channel forms (including cutbanks, steps, alluvial bars, potholes, riffles, and pools) (Kamykowska, M. *et al*. 1999).

Organic material accumulation also significantly affects bed morphology. This effect is especially noticeable in headwater areas covered by mountain forests, where organic matter is abundant, ranging from tiny seeds, leaves, twigs (Jeffries, R. *et al*. 2003) to branches and woody debris of much larger size (Galia, T. *et al*. 2018; Thompson, M.S.A. *et al*. 2018). Its impact on the channel and processes is diversified and complex. Woody debris accumulation can transform the flow conditions and thalweg of the channel. Therefore, it cannot be neglected in bank evolution either since it can accelerate streambank erosion or protect streambanks (Bilby, R.E. and Ward, J.W. 1991; Abbe, T.B. and Montgomery, D.R. 2003; Comiti, F. *et al*. 2006; Ruiz Villanueva, V. *et al*. 2014; Short, L.E. *et al*. 2015; Wohl, E. *et al*. 2017, and references therein). It is important to note that the organic materials in channels also contribute to trapping sediment. This can have spectacular consequences in the formation of impoundments and steps in the channel, whereby the morphological conditions and processes can change (e.g., erosion potholes can be created) (Galia, T. *et al*. 2017; Zhang, N. *et al*. 2020). Furthermore, these accumulations promote the precipitation of travertine, which can enhance the stability of natural dams (Carter, C.D. and Marks, J.C. 2007; Compson, Z.G. *et al*. 2009; Fuller, B. *et al*. 2011).

A comprehensive understanding of their features can be achieved through examining the aforementioned forms, factors and impacts along the longitudinal profile of streams. The distinction between segments is aided by the detailed field survey protocols developed for this purpose (Myers, T.J. and Swanson, S. 1997; Kamykowska, M. *et al*. 1999; Galia, T. *et al*. 2018). Numerous studies using a similar approach have been completed over the last decade, but typically conducted in high and mid-mountain watersheds and streams (Galia, T. and Hradecký, J. 2011; Galia, T. and Škarpich, V. 2013; Płaczkowska, E. *et al*. 2015; Płaczkowska, E. and Krzemień, K. 2018; Ondráčková, L. and Máčka, Z. 2019; Prokop, P. *et al*. 2020).

Nonetheless, many field methods can be adapted for small watercourses with lower relief, even in hilly regions. Comparable studies have already been carried out in Hungary (Kalmár, P. *et al*. 2013; Fábián, Sz.Á. *et al*. 2016), but they are few in number at the national level.

The objective of this paper was twofold. Firstly, it aimed to describe and analyse the trunk channel of the micro-catchment for bed types, shapes, and evolution, based on a comprehensive field survey. Particular emphasis was placed on the formation and evolution of natural log jams affecting sediment transport. Secondly, it was meant to estimate the flash flood susceptibility (FFS) value for the selected micro-catchment since flash floods have increased in frequency in Hungary due to recent extreme weather events.

Study area

This study focused on the southern branch of the Öreg-patak (Öreg Stream) Mecseknádasd, which originates from a spring in eastern Mecsek. It runs in a north-easterly direction for just over seven and a half kilometres, where it joins the Puszta-árok (Óbányai-patak) between the villages Mecseknádasd and Óbánya. The studied watercourse and its associated permanent and ephemeral streams have a catchment area of 9.75 km^2, which just falls into the micro-watershed category (Daipan, B.P.O. 2020). The highest point of the catchment is the Zengő (682 m), the lowest near the confluence is at 224 m *(Figure 1)*. Relative relief ranges from 123 to 247 m/km^2. Although the studied stream may be considered relatively natural, intensive forest management by the Mecsekerdő Zrt. (Mecsek Forestry Co. Ltd.) and the popularity of the marked hiking trails indicate significant anthropogenic impact.

Sedimentary rocks dominate the geological setting. The Lower Jurassic Pliensbachian and Toarcian beds of limestone, chalk marl and siltstone (Óbánya Aleurolite Formation), locally intercalated by Lower Cretaceous (Valanginian) alkaline basalts (Mecsekjános Basalt Formation), are the most widespread formations. They are mostly covered by young Quaternary sediments, including slope deposits, loess, and its derivates. Sporadically, sedimentary and sub-volcanic rocks are exposed (Raucsik, B. and Varga, A. 2008; Haas, J. 2013).

The studied catchment and its immediate surroundings display the characteristic subdued, denuded shape of the Eastern Mecsek

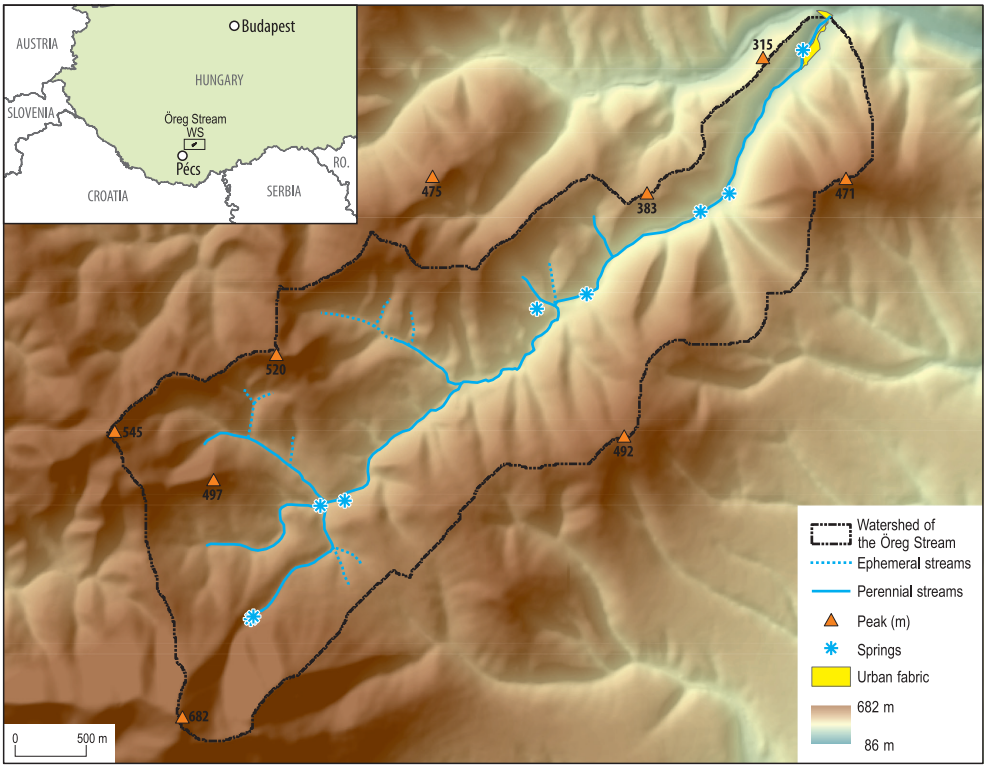

Fig. 1. Map of the study area.

region. Main features of the topography are the radially spreading horsts and connecting ridges on which the boundary of the watershed (divide) runs. The valley shoulders are described in several places in the valleys and the higher hilly surfaces are dissected by erosional-derasional valleys (Ádám, L. *et al*. 1981; Kocsis, K. 2018). Slope angles range from 0 to 35 degrees. The majority of the study area is represented by the range from 7 to 25 degrees (mean 15.47; Std. dev. 6.24; 8.31 km^2; 85.2%) *(Figure 2).*

The climate is notably influenced by the north-northeast orientation of the catchment and its main valley. Mean annual air temperatures (MAAT) vary between 7 and 9 °C; mean annual precipitation (MAP) totals are 750–850 mm. However, in certain years the MAP reaches very extreme values, for example, in exceptionally wet 2010 and 2014 years and in the arid year 2011 (Czigány, Sz. *et al*. 2010; Hungarian Meteorological Service, n.d.).

The Öreg-patak (second-order stream at the mouth) and a few short, perennial and ephemeral streams are all part of the Danube water system, reaching the Danube via the Völgységi-patak (Völgységi Stream) and the Sió canal (Kocsis, K. 2018). The length of streams which are considered permanent is 9.9 km.

The watershed is almost entirely covered with forests managed by the Mecsekerdő Zrt. The vast majority of tree species are European beech (*Fagus sylvatica*), sessile oak (*Quercus patraea)*, Turkey oak (*Quercus cerris)*, downy oak (*Quercus pubescens)* and hornbeam (*Carpinus betulus*), which are often mixed. Indeed, in more limited spots in the upper reaches of the main streams, planted spruce (*Picea abies*) is also found (Kevey B. 2008). The closed forests are only occasionally dissected by small clearings or seedling orchards, and more significantly, by gaps between forest stands (data from Mecsekerdő

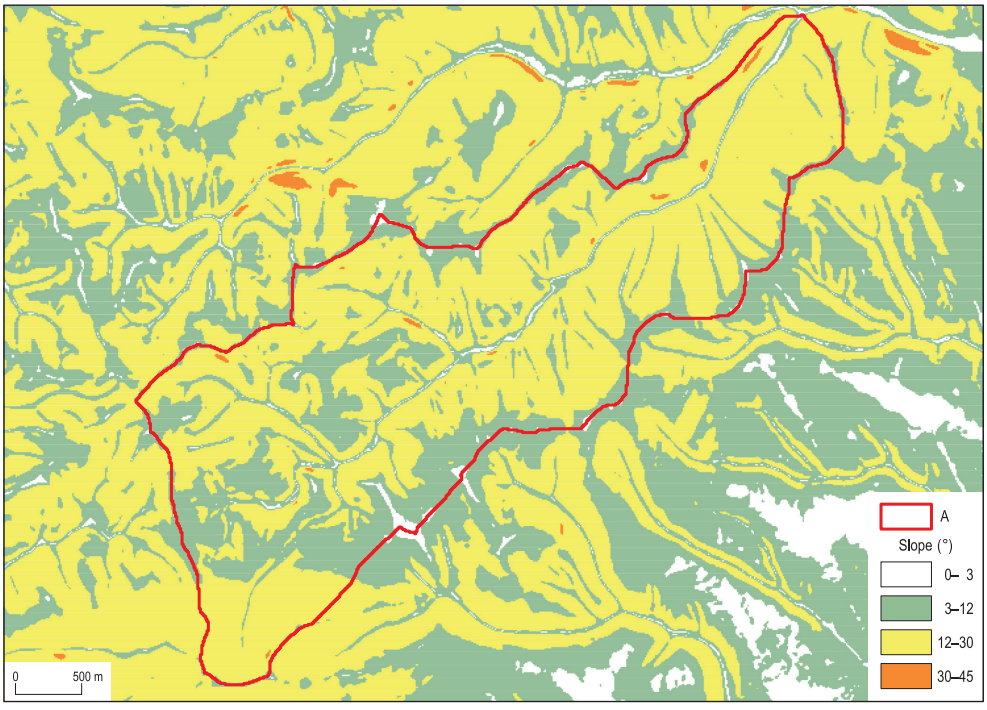

Fig. 2. Slope map of the study area with its border line (A)

Zrt. and Ministry of Agriculture, 2019). Highly acidic Luvisols and Alisols predominate with only small patches of Regosols (Kocsis, K. 2018).

The study area covers parts of the administrative areas of five settlements (Hosszúhetény, Mecseknádasd, Óbánya, Pécsvárad and Zengővárkony). However, only a minute portion of inhabited land is affected, near the mouth of the Óbányai-patak stream (Mecseknádasd Resort Area). Human activities significantly affected the morphology of the riverbed in these areas and near the forest tracks and logging stations of permanent use.

Materials and methods

For the present study, two methodological procedures were applied. Firstly, 25 catchment parameters (e.g., area, perimeter, drainage density, Gravelius coefficient, number of streams, total stream length, max stream order, max and min height, basin relief, forested area) derived from a hydrologically correct digital elevation model (DEM) with 10 m resolution were identified (Schumm, S.A. 1956; Strahler, A.N. 1957; Sassolas-Serrayet, T. *et al*. 2018; Daipan, B.P.O. 2020; Víg, B. *et al*. 2022). For detailed GIS analyses, we also applied the South-Transdanubian Water Management Directorate (STWMD) vector surface water database, the Corine Land Cover 2012 (CLC2012) dataset, the closed sources forestry data of Mecsek Forestry Company (MF), and the ecosystem map of Hungary by Ministry of Agriculture (2019). For the spatial analyses, we used ArcGIS 10.4 (ESRI, 2016) and open-source ArcHydro Toolbox v2.0 (ESRI, 2011).

Relying on previous FFS studies (Esper Angillieri, M.Y. 2008; Singh, P. *et al*. 2013; Abdel-Fattah, M. *et al*. 2017; Puno, G.R. and Puno, R.C.C. 2019; Alam, A. *et al*. 2020; Obeidat, M. *et al*. 2021), the following morphometric parameters had been selected for examination: area (*A*), drainage texture (*Rt*), drainage density (*Dd*), elongation ratio (*Re*), form factor (*Ff*), lemniscate index (*k*), Gravelius coefficient (*GC*), forested area (*Fa*), relief ratio (*Rr*). Among them, *A*, *Dd* and *Rr* were assumed as directly related to the probability of flash flood generation, while *Rt*, *Re*, *Fa*, *Ff*, *k*, and *GC* were inversely related to flash floods. All selected factors are related to runoff intensity and flash flood generation; therefore, they could be applied, using the approach of Víg, B. *et al*. (2022), for assessing FFS at the watershed level. Thus, the currently studied watershed parameters were compared with previously published data for the Mecsek Hills region.

Secondly, a comprehensive field survey was conducted to record in detail geology, bed morphometry, geomorphology and land cover of the Öreg-patak catchment. The field survey was essentially carried out following the paper of Kamykowska, M. *et al*. (1999), from the source to the mouth, over a length of more than 7,700 m, divided into 155 fifty-metre-long sections. The protocol developed in Polish Carpathian Mountains was applied to low-mountainous environments and low-discharge streams (Kalmár, P. *et al*. 2013; Kalmár, P. 2015; Fábián, Sz.Á. *et al*. 2016). About four-fifths of the original protocol has been used, supplemented by measuring woody debris jams (WDJ) in the channel, which strongly influence hydromorphological features (Bilby, R.E. and Likens, G.E. 1980; Dahlström, N. and Nilsson, C. 2004; Galia, T. and Hradecky, J. 2014). Following the original protocol's logic, the WDJ parameters survey was structured to collect the data detailed below.

We used a laser rangefinder (Hecht 2006 laser distance meter) to record the relative position of the WDJ in the channel and their basic physical parameters including the predominant and maximum height, width, and length. Furthermore, the WDJ's orientation to the flow direction and the effect of organic matter (such as leaf litter, green leaves, senescent leaves, and small wood fragments) accumulation in the channel was also recorded, as they can influence flow conditions independently of log jams (Přibyla, Z. *et al*. 2016).

Using a portable GPS device (Garmin 60 CSx), we recorded all the features (including bedrock steps, anthropogenic elements, and WDJ) that impact the hydromorphological processes in the riverbed according to the HD72/EOV reference system (EPSG:23700). In addition, springs, tributaries, and even short ephemeral or perennial watercourses were surveyed to augment our primary database.

Mean stream gradient was measured using a digital level (SOKKIA SDL50). The limiting factor was the dense vegetation in the incised stream bed and the steep valley side. Sinuosity was calculated as a ratio between the unit (50 m) curvilinear length of the channel centreline and the straight distance of each unit endpoint. Data could not be obtained in 67 out of the 155 surveyed sections, mainly in the upstream segment with a steep slope and incision. There was also sporadic data loss downstream due to dense vegetation hindering the survey even in winter.

The extent of the bedrock outcrop (estimated proportion) was recorded in the surveyed sections. The rock types identified in the field were checked with the help of the detailed geological maps (scale 1:10,000) available for the Mecsek Hills area. The genetic types of any riverbed sediments and their grain size categories were also documented.

Cross-sections and longitudinal profiles were classified according to the protocol categories (Kamykowska, M. *et al*. 1999) by channel section. Where applicable, qualitative data were recoded (e.g., cross sections of channel types). Among the quantitative characteristics, we measured the channel gradient (∑m/50m), the bank height and the total bankfull depth and width. These measurements yielded the channel shape index (bankfull width/maximum bankfull depth) for each channel section. We collected over 2,000 data points, which were then recorded in a Microsoft Excel spreadsheet, also used to perform the necessary statistical analysis to interpret and evaluate data. Eleven campaigns were conducted between March 2019 and May 2020, primarily during low water stages.

Results and discussion

Watershed morphometric analysis and flash flood susceptibility

A complex hydrological, relief and land use analysis of the Öreg-patak catchment provided valuable information on the FFS of the region. The relatively small area and the associated maximum catchment basin length (*L*) imply a high flash flood sensitivity due to the low accumulation time. However, this is offset by low (≤ 2) drainage texture and drainage density, which decreases the likelihood of flash floods occurrence. Among the areal parameters, low (highly elongated, ≤ 0.5, or elongated, 0.5–0.7) values of elongation ratio, form factor and circularity ratio also reduce FFS due to the highly elongated shape. High values of the Lemniscate index and Gravelius coefficient, as well as the high degree of forest cover, were also interpreted as moderating effects on the studied catchment. Comparing the presented values in this paper with the former general FFS analysis of the Mecsek region by Sarkadi, N. *et al*. (2022), and Víg, B. *et al*. (2022), FFS in the catchment was estimated to be moderate or medium. Based on the flash flood events observed in the past decade, mud and woody debris 'floods' can only be caused by extreme precipitation at the confluence of headwater branches *(Table 1, Photo 1).*

Channel reach analysis

The field survey was carried out on 155 channel sections with a length of 50 m from the source of the southern headwater of the Öreg-patak to the mouth of the watercourse. Of these, 30 sections are located upstream the confluence of the three headwaters.

Early Jurassic (Pliensbachian and Toarcian) sediments dominate the examined sections (n = 144). Further eleven sections overlie thin alkali basalt, trachybasalt, and phonolite dykes of Early Cretaceous (Valanginian) age. We estimated the percentage of bedrock

Table 1. Fundamental morphometric parameters of the studied catchment with the highlighted FFS relevant data

Parameters	Formula	Value	References
FFS parameters			
Area (A), km²	–	9.75	–
Max. basin length (L), km	–	6.80	Kamykowska, M. *et al.* 1999
Drainage texture (Rt)	$Rt = Nu/P$	0.31	Horton, R.E. 1945
Drainage density (Dd), km/km²	$Dd = \sum L/A$	1.01	Strahler, A.N. 1957
Elongation ratio (Re)	$Re = D$	0.52	Schumm, S.A. 1956
Form factor (Ff)	$Ff = A/L^2$	0.21	Mesa, L.M. 2006
Circularity ratio (Rc)	$Rc = 4\pi A/P^2$	0.24	Mesa, L.M. 2006
Lemniscate index (k)	$k = L^2\pi/4A$	3.69	Moores, E.A. 1966
Gravelius coefficient (GC)	$GC = P/2\sqrt{\pi A}$	2.03	Sassolas-Serrayet, T. *et al.* 2018
Forested area (Fa), %	–	100.00	Kamykowska, M. *et al.* 1999
Traditional further parameters			
Perimeter (P), km	–	22.5	–
Fitness ratio (Rf)	$Rf = Cl/P$	0.29	Pareta, K. and Pareta, U. 2011
Number of streams (Nu)	–	7	–
Integration index (C), km²/km	$C = A/L$	1.40	Kamykowska, M. *et al.* 1999
Total stream length (ΣL), km	–	9.90	–
Max stream order (u max)	–	2	Morisawa, M.E. 1962
Total length of stream order (∑u), km	–	4.44 (u1); 5.46 (u2)	–
Mean stream length (Lu), km	$Lu = SL/Nu$	1.40	Biswas, S.S. 2016
Length of main channel (Cl), km	–	6.50	–
Maximum height (H), m	–	680	–
Minimum height (h), m	–	224	–
Basin relief (r), m	$r = H - h$	456	–
Relief ratio (Rr)	$Rr = H - h\text{-}L$	67.28	Schumm, S.A. 1956
Grassland area (Ga), %	–	0	Kamykowska, M. *et al.* 1999
Arable land area (Aa), %	–	0	Kamykowska, M. *et al.* 1999

Photo 1. Woody debris 'flood' after an extreme precipitation event at the end of May, 2019. (Photo taken by Attila Szalay, Mecsek Forestry Co. Ltd, 2019).

outcrops exposed in each section and classified the sections into four categories. Some bedrock was found in 58 percent (n = 90) of the surveyed sections. The lowest proportion of bedrock (< 10%) was found in 66 sections. It was measured between 10–50 percent in 21 sections, and the highest outcrop rate was between 50–90 percent in only three sections. In the remaining 65 sections (42% of the total surveyed), no bedrock could be detected. No definite pattern or regularity of the bedrock distribution can be discerned along the longitudinal profile. However, rocks could be traced in all sections from 39 to 59, and from 67 to 90. Furthermore, the 10 to 50 percent occurrence was dominant in sections from 86 to 94 (n = 7). In all the sections where volcanic or subvolcanic rocks were present, bedrock also occurred in the stream bed. In addition, the 11 sections mentioned above alternated between the 10–50 percent, and 50–90 percent categories. A decrease in rock occurrence was observed downstream section 100, justified by the thickness and accumulation of younger cover sediments. The low proportion of the bedrock outcrops (only 24 sections have >10% outcrop ratio) is typical of the low-mountain region in the Pannonian Basin (i.e., low altitude, relief, channel gradient, water discharge and bedload transport intensity, and high portion of alluvial fans) (Mezősi, G. 2015; Kocsis, K. 2018). Furthermore, this feature is reinforced by the laws governing catchments and stream channel conditions (i.e., low gradient, stream power, sinuosity), which inhibit the evolution of bedrock and colluvial channels (Bisson, P.A. *et al*. 2017).

Slope (waste mantle) and alluvial sediments could be observed in channel deposits for most of the sections (n = 151; 91%). In the remaining minority of sections (n = 4), the same could be assumed but could not be assessed adequately due to thick leaf litter cover. Sediment grain size showed slight variation. The upstream sections (5–15) were characterised by clay and silt, while the remaining sections contained all grain sizes from clay (< 0.004 mm) to small boulders (> 256 mm) in varying amounts. Similar sediment size distributions have been reported in the streambed for small headwater streams (Galia, T. *et al*. 2015). Estimating the number of different grain sizes over such a long reach would be difficult, imprecise, and impossible in the field. According to Russel, R.J. (1954) and Charlton, R. (2008), alluvial channels can contain a mixture of grain sizes from boulders to clay. The variable grain size may also be explained by the low channel gradient and the 'semi-alluvial' nature of the stream. The relatively low sediment transport capacity only changes during extreme debris floods (Bywater-Reyes, S. *et al*. 2017).

In the longitudinal profile four types were identified, such as stepped, irregular, levelled and undulating. The fifth possible type (toothed) was not observed. The occurrence of the observed types did not show a clear regularity along the stream. The four types being quite similar, only 60 of the measured sections the reaches could be classified unequivocally. The vast majority of them (n = 49) were either irregular or levelled. However, the entire longitudinal profile of the studied stream displayed a concave curvature with a steep upper course (0–1,500 m) and a gentle lower course downstream (1,500–7,700 m) (see upper part of *Photo 1*), a typical longitudinal profile for alluvial streams (Rice, S.P. and Church, M. 2001). Earlier research also confirmed that natural alluvial streams usually have an irregular longitudinal profile (Western, A.W. *et al*. 1997; Schumm, S.A. 2005).

The width/depth ratio, measured in a total of 120 sections, characterises cross-section geometry. The upstream segment (0–1,500 m) of the watercourse had a narrow and relatively deep valley floor with a low discharge (estimated mean annual discharge at the confluence < 0.015 m^3/s), resulting in an ill-defined stream channel. In the sections spanning from 30 to 155, the dominant types of beds were those whose width was much greater than depth. From 1,500 to 3,000 m, the width of the bed varied between 0.3 and 0.8 m (average 0.54 m). Then, the width increased significantly. Up to the confluence, the width

varied between 1.26 and 12.05 m (average 4.33 m). Channel depth was only measured from section 30 onwards. The 125 sections from here up to the confluence ranged from 0.05 to 1.2 m in depth (average is only 0.3 m). Deeper channels were often linked to anthropogenic influence. Moreover, the pools due to organic dams or bedrock steps induced higher-than-average values. The width/depth ratio (W/D) ranged from 2.5 to 143.2, with an average of 21.67 and was used for the fundamental Rosgen's classification (Rosgen, D.L. 1994). The first group consisted of forty-four sections with low values (W/D < 12; mean 8.56), which were dominated by alluvial deposits with floodplain and riffle/pool bed morphology. The next class (moderate W/D values between 12 and 40) characterised 69 sections (mean 21.24) with moderate or low channel gradient, riffle/pool bed morphology, and high bank-erosion anastomosed channel. In the third class (high W/D values > 40), 12 sections were included (mean 72.17) with broad valleys and considerable amounts of alluvial deposits. The channel types and bed morphology defined by the W/D values (Buffington, J.M. and Montgomery, D.R. 2013) can also be identified in the current study area.

The slope, stability and maximum height of the natural banks were also surveyed since they significantly affect bank erosion and sediment transport (Sass, C.K. and Keane, T.D. 2012; Willett, C.D. *et al*. 2012; Buffington, J.M. and Montgomery, D.R. 2013). Banks were classified as very gentle, gentle, steep, vertical or overhanging along the stream. Establishing any regularity was not possible, as the pattern was found to be highly variable even within sections. The valley side characteristics were estimated in the upstream segment (3–29) due to the lack of definite banks. Here the steep class predominated. With few exceptions, the downstream segment (30–155) was dominated by stable and semi-stable banks. The maximum relative height of the banks ranged from 0.2 to 3 m (average 1.06 m). It is important to note that in sections with vertical or overhanging bank types, the banks were still considered semi-stable due to anthropogenic influences (i.e., gabion walls) or to stabilising vegetation *(Photo 2).*

The segment upstream had a steeper gradient (average 8.3%), whilst the downstream segment had only 2 percent. The downstream segment showed a consistently higher ratio (≥ 4%, n = 4) in sites where both bedrock outcrops and woody debris with a step system were present. Sections with a gradient of 2–4 percent (n = 48), either bedrock steps or woody debris, were reported in 39 cases. The entire longitudinal profile exhibited slope values ranging from 0.44–16.9 percent. Bed slopes (0.2–1%), typical according to Bisson, P.A. *et al*. (2017), dominated on the pool-riffle reaches (n = 3 all downstream), 1–3 percent on the plane-bed reaches (n = 118 dominated downstream), 3–8 percent on the step-pool reaches (n = 21) and 8–26 percent on the cascade stream reaches (n = 13 all upstream but not cascade types).

Sinuosity ranged from 1 to 2.31 (mean: 1.12, standard deviation: 0.19). The sinuosity ratio (*SR*) of the whole valley (6,310 m) was also estimated as 1.22. Traditionally, channels are classified into three categories: straight (SR < 1.1), sinuous (1.1–1.5) and meandering (> 1.5) (Leopold, L.B. and Markley, G.W. 1957). In the sections we surveyed, straight type occurred in 63, sinuous in 21 and meandering only in 4 cases (see *Figure 3*). We agreed with Charlton's notes that the SR descriptions are confused in the literature, thus, making it hard to compare and interpret recent results (Charlton, R. 2008).

The total number of large woody debris sites obstructing the riverbed was 48, located in 25 percent of the sections (n = 39). In most cases (79%), only one log jam per section was documented (n = 31 sections). The maximum number of dams observed in a section was three, which occurred in only one case (section 109). The overall average was c. 0.62 WDJs per 100 m *(Figure 4).*

The interpretation of our results is difficult since no similar survey has been conducted in the Pannonian Basin yet. However, the

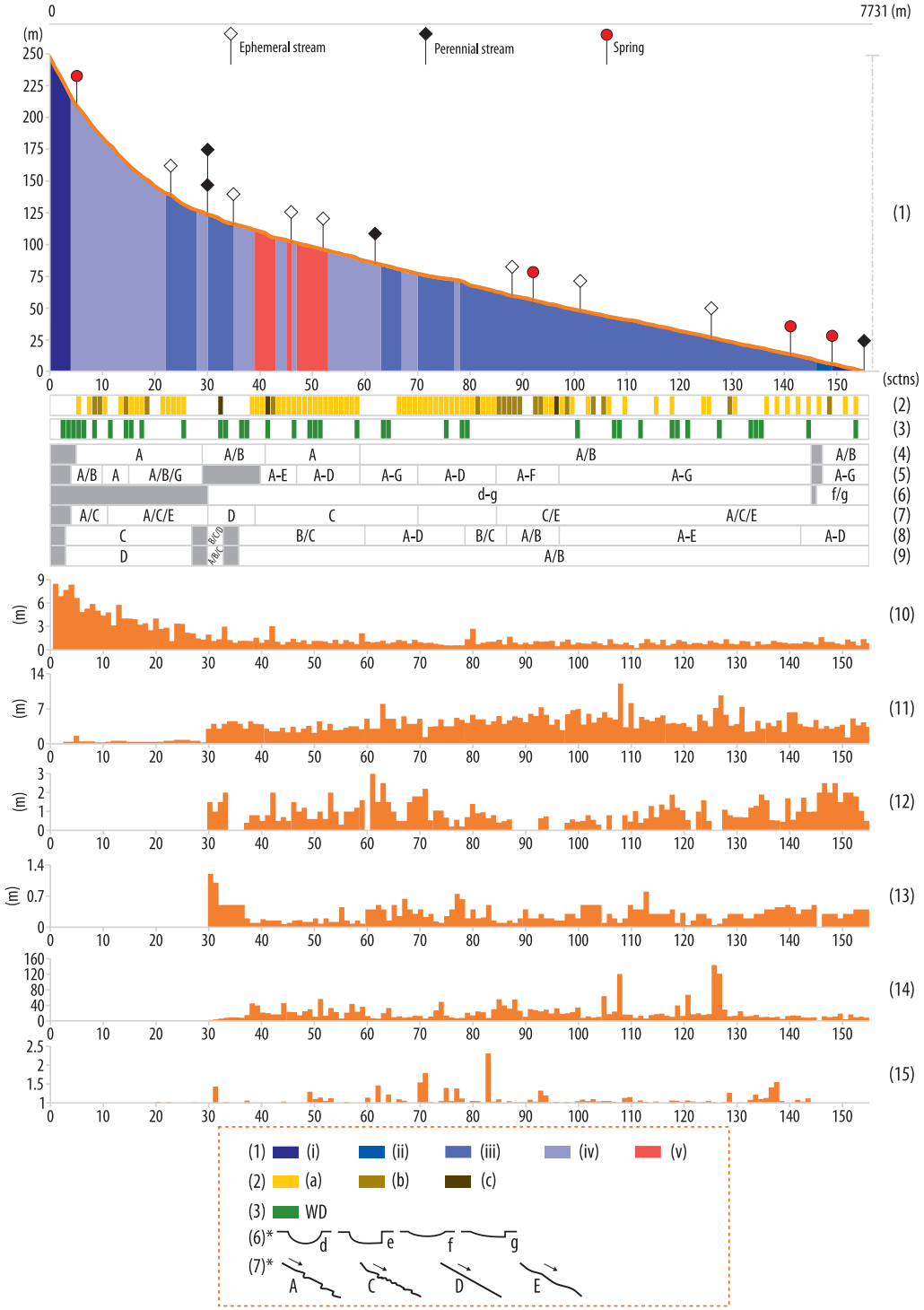
0
7731 (m)
(m)
Ephemeral stream
Perennial stream
Spring
(1)
(sctns)
(2)
(3)
(4)
(5)
(6)
(7)
(8)
(9)
(10)
(11)
(12)
(13)
(14)
(15)
(1) (i) (ii) (iii) (iv) (v)
(2) (a) (b) (c)
(3) WD
(6)* d e f g
(7)* A C D E

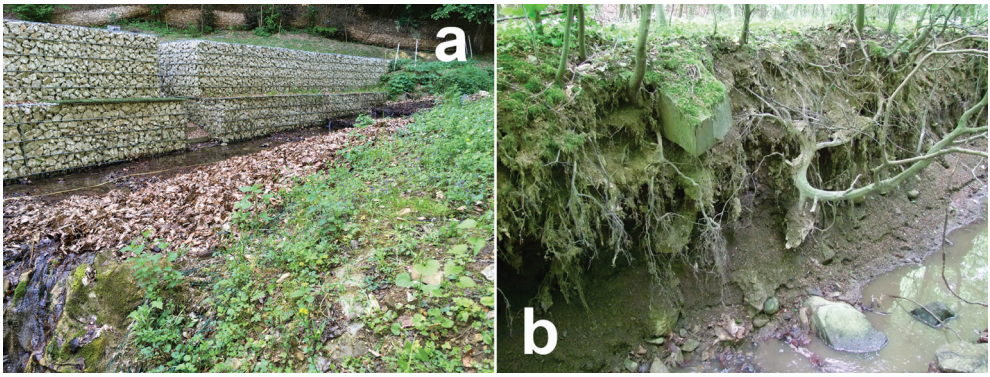

Photo 2. Examples of semi-stable stream banks: Technically fixed by retaining gabion walls (a), naturally semi-fixed by roots (b). (Photos taken by the authors.)

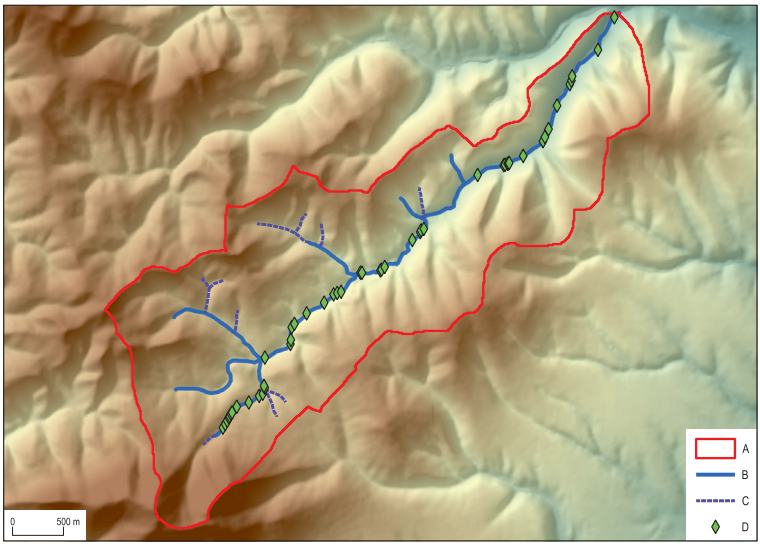

Fig. 4. Map of the woody debris along the Öreg-patak (Öreg Stream): Borderline of the study area (A), perennial/ephemeral stream (B/C), woody debris (D).

←

Fig. 3. Longitudinal profile of Öreg-patak (Öreg Stream) with the main measured stream channel characteristics (on the right side axis, 1–15). *Geology* (1) = Lower Jurassic Pliensbachian marl (i); Lower Jurassic Pliensbachian marl and marlstone (ii); Lower Jurassic Pliensbachian marl and siltstone (iii); Lower Jurassic Toarcian marl and silt (iv); Lower Cretaceous (Valanginian) alkaline basalts (v). *Surface of outcrops* (2) = <10% (a); 10–50% (b); 50–90% (c). *Woody debris* (3). *Genetic type of sediment* (4) = slope origin (A); alluvial (B). *Size composition of sediments* (5) = clay (A); silt (B); sand (C); granules, 2–8 mm (D); pebbles, 8–64 mm (E); cobbles, 64–256 mm (F); boulders, > 256 mm (G). *Cross-section of the channel* (6) = triangular, depth > width (d); trapezoidal, depth = width (e); (f) elliptical, depth < width (f); parabolic, depth < width (g). *Longitudinal profile* (7) = atepped (A); irregular (C); levelled (D); undulating(E). *Bank slope* (8) = very gentle banks (A); gentle banks (B); steep banks (C); vertical banks (D); overhanging banks (E). *River bank fixation* (9) = naturally fixed (A); artificially fixed – biologically (B); artificially fixed – technically (C); unfixed (E). *Stream gradient* (10). *Max bankfull width* (1). *Max height of the natural banks* (12). *Max bankfull depth* (all in metre) (13). *Channel shape index* (14). *Sinuosity* (15).

frequency of WDJ is considered extremely low. Previous studies measured significantly higher values (range 2.4 to 8.6) with matching catchment areas (≤ 10 km^2) and comparable reach lengths (≤ 50 m) (Jackson, K.J. and Wohl, E. 2015.). A higher value (1.2–1.4) with similar catchment parameters (channel length approx. 8 km, stream order HS ≥ 2, forested ratio close to 100%) was also reported (Comiti, F. *et al*. 2006). We assumed that low WDJ frequency is predominantly related to regular forest management, as the managed forest provides less wood than the old-growth forest to develop jams (Dahlström, N. and Nilsson, C. 2004; Motta, R. *et al*. 2006; Wohl, E. *et al*. 2017). The composition of debris jams (grain size, length, and diameter) varied along the stream. All surveyed WDJ contained organic material of the smallest dimension (leaves, seeds, and twigs) as well as elements classified in the literature as coarse woody debris (CWD) and large woody debris (LWD). This hybrid structure and grain size are consistent with most WDJ in the forest-covered headwater channels in low-mountainous regions (Manners, R.B. *et al*. 2007; Přibyla, Z. *et al*. 2016). The CWD and LWD consisted of pieces from deciduous trees dominated by *agus sylvatica* and *Carpinus betulus.* The increased ratio of *Fagus sylvatica* in the WDJ and other in-stream wood material has also been observed in the Czech Carpathians when this species is mixed with conifers to a much greater extent (Galia, T. *et al*., 2017). It may be assumed that *Fagus sylvatica* has a unique role in WDJ generation in Central European low- and mid-mountainous mixed forests.

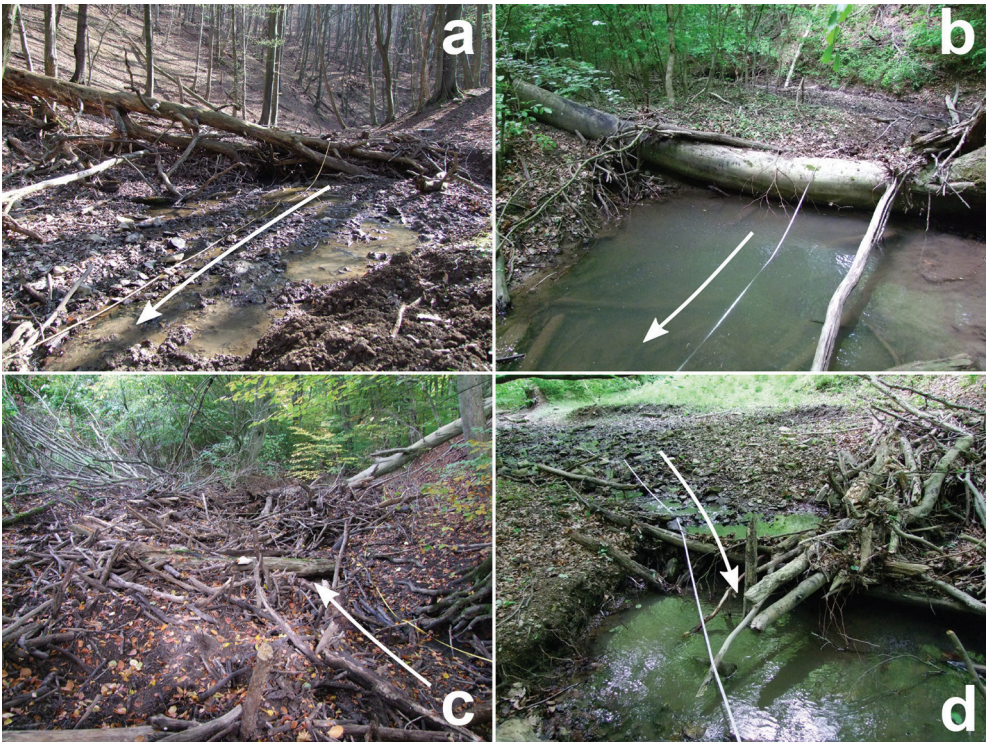

Photo 3. Examples of woody debris jams (arrows show the flow direction): Log jam in juvenile phase (a), log jam with massive trunk and soil ball (b), typical log jam in mature phase (c), log jam with steps and pothole (d). (Photos taken by the authors.)

A separate group is formed by types that usually contain massive trunks (≥ 25–30 cm diameter, ≥ 2 m length) typically found in the bed with soil ball (n = 3), all of them *Fagus sylvatica*. These are referred to as stable types in this study, as their potential for displacement is relatively small, mainly due to their large mass and low average discharge of the trunk stream. They form a step in the bed, enhance the accumulation of sediment and the upwelling of wood, and promote the creation of erosional depressions after blockage. This way, they also have a complex and essential influence on bed morphology *(Photo 3).* Our findings on this issue are the same as Ondráčková and Máčka's results on the role of in-stream wood and rootball accumulations (Ondráčková, L. and Máčka, Z. 2019). Geomorphic (dis)connectivity in a middle-mountain context: Human interventions in the landscape. Furthermore, we consider the type we defined as stable WDJ comparable to the "active jam" type published by Cashman, M.J. *et al*. (2021), which increases the jam's structural complexity and hydromorphological diversity.

Conclusions

This study delineated the Öreg-patak watershed using standard GIS processes on a 10 m DEM. To estimate FFS for the catchment, we evaluated the computed parameters of the basin and the modelled data for this area. The FFS of the studied watershed can be assessed as medium to moderate. However, extreme meteorological events can generate severe sediment and woody debris 'floods', easily observed during the fieldwork, especially in the upstream segment. With slight modifications and additions, the method we developed and utilised for the field survey of stream morphology was successfully applied in the Mecsek Hills and low-mountainous relief.

Channel types and reaches were surveyed based on measured and estimated streambed morphological properties and classified according to a currently accepted geomorphological system (Buffington, J.M. and Montgomery, D.R. 2013). The upstream part was identified as a colluvial channel of 0 or 1 stream order and low streamflow discharge, incised into a colluvial valley. On the downstream segment, step-pool (steps formed by woody debris and bedrock), pool-riffle (moderate or low gradient) and braided channel (large W/D ratio) types dominated without any regularity. The bedrock channel reach occurred in less than 2 percent of all measured sections; the typical cascade, plane-bed and dune-ripple stream reaches could not be observed in the study area.

The measured and estimated sporadic data of the natural streambanks (e.g. height, stability, and slope) may be suitable to determine the potential stages of bank erosion activity (Rosgen's BEHI Index) at different levels.

In this study, we recorded all woody debris jams in the channel, built up of either CWD or LWD. We focused on the 'stable' type of these log jams because they significantly affect streambed morphology. Forming natural barriers in the channel, wood jams can block or reduce sediment and organic material transport. Furthermore, their stability can be increased by travertine formation.

Analysis of small headwater streams is lacking in Hungary as fluvial geomorphological studies focus mainly on larger rivers and their floods. However, increasingly frequent extreme rainfall events and flash floods justify complex morphological studies of small catchments and headwater streams.

***Acknowledgement*:** We sincerely thank the anonymous Reviewers for their useful and comprehensive comments on the manuscript, and we greatly appreciate their time and effort spent in this paper. This research was funded by the Higher Education Institutional Excellence Program of Ministry of Human Capacities (Hungary), grant number "20765-3/2018/FEKUTSTRAT" at the University of Pécs and the Hungarian National Office for Research and Innovation (project GINOP-2.3.2-15-2016-00055). The authors also grateful to the Mecsek Forestry Co. Ltd. (Mecsekerdő Zrt.) and the South-Transdanubian Water Management Directorate (Dél-Dunántúli Vízügyi Igazgatóság, DDVIZIG) for providing data for the current research. The authors sincerely thank graduate students (Beáta Farkas, Máté Kiss, Frida Király, Emese Soltész) and Gábor Víg for their assistance during the fieldwork.

REFERENCES

Abbe, T.B. and Montgomery, D.R. 2003. Patterns and processes of wood debris accumulation in the Queets river basin, Washington. *Geomorphology* 51. (1–3): 81–107. Available at https://doi.org/10.1016/S0169-555X(02)00326-4

Abdel-Fattah, M., Saber, M., Kantoush, S.A., Khalil, M.F., Sumi, T. and Sefelnasr, A. M. 2017. A hydrological and geomorphometric approach to understanding the generation of wadi flash floods. *Water* 9. (7): 553. Available at https://doi.org/10.3390/w9070553

Ádám, L., Marosi, S. and Szilárd, J. (eds.). 1981. *Magyarország tájföldrajza 4. A Dunántúli-dombság – Dél-Dunántúl* (Landscape geography of Hungary 4. Transdanubian Hills – South Transdanubia). Budapest, Akadémiai Kiadó.

Alam, A., Ahmed, B. and Sammonds, P. 2020. Flash flood susceptibility assessment using the parameters of drainage basin morphometry in SE Bangladesh. *Quaternary International* 575–576. 295–307. Available at https://doi.org/10.1016/j.quaint.2020.04.047

Bilby, R.E. and Likens, G.E. 1980. Importance of organic debris dams in the structure and function of stream ecosystems. *Ecology* 61. (5): 1107–1113. Available at https://doi.org/10.2307/1936830

Bilby, R.E. and Ward, J.W. 1991. Characteristics and function of large woody debris in streams draining old-growth, clear-cut, and second-growth forests in southwestern Washington. *Canadian Journal of Fisheries and Aquatic Sciences* 48. (12): 2499–2508. Available at https://doi.org/10.1139/f91-291

Bisson, P.A., Montgomery, D.R. and Buffington, J.M. 2017. Valley segments, stream reaches, and channel units. In *Methods in Stream Ecology*. Vol. 1. Eds.: Hauer, F.R. and Lamberti, G.A., Elsevier, 21–47. Available at https://doi.org/10.1016/B978-0-12-416558-8.00002-0

Biswas, S.S. 2016. Analysis of GIS based morphometric parameters and hydrological changes in Parbati river basin, Himachal Pradesh, India. *Journal of Geography & Natural Disasters* 6. (2): 1000175. Available at https://doi.org/10.4172/2167-0587.1000175

Buffington, J.M. and Montgomery, D.R. 2013. Geomorphic classification of rivers. In *Treatise on Geomorphology*. Ed.-in-Chief: Shroder, J.F. Elsevier, 730–767. Available at https://doi.org/10.1016/B978-0-12-374739-6.00263-3

Bywater-Reyes, S., Segura, C. and Bladon, K.D. 2017. Geology and geomorphology control suspended sediment yield and modulate increases following timber harvest in temperate headwater streams. *Journal of Hydrology* 548. 754–769. Available at https://doi.org/10.1016/j.jhydrol.2017.03.048

Carter, C.D. and Marks, J.C. 2007. Influences of travertine dam formation on leaf litter decomposition and algal accrual. *Hydrobiologia* 575. (1): 329–341. Available at https://doi.org/10.1007/s10750-006-0379-6

Cashman, M.J., Harvey, G.L. and Wharton, G. 2021. Structural complexity influences the ecosystem engineering effects of in-stream large wood. *Earth Surface Processes and Landforms* 46. (10): 2079–2091. Available at https://doi.org/10.1002/esp.5145

Charlton, R. 2008. *Fundamentals of Fluvial Geomorphology*. London, Routledge, Taylor and Francis Group.

Comiti, F., Andreoli, A., Lenzi, M.A. and Mao, L. 2006. Spatial density and charactereistic of woody debris in five mountain rivers of the Dolomites (Italian Alps). *Geomorphology* 78. (1–2): 44–63. Available at https://doi.org/10.1016/j.geomorph.2006.01.021

Compson, Z.G., Mier, M.Z. and Marks, J.C. 2009. Effects of travertine and flow on leaf retention in Fossil Creek, Arizona. *Hydrobiologia* 630. (1): 187–197. Available at https://doi.org/10.1007/s10750-009-9791-z

Czigány, Sz., Pirkhoffer, E. and Geresdi, I. 2010. Impact of extreme rainfall and soil moisture on flash flood generetion. *Időjárás* 114. (1–2): 79–110.

Dahlström, N. and Nilsson, C. 2004. Influence of woody debris on channel structure in old growth and managed forest streams in Central Sweden. *Environmental Management* 33. (3): 376–384. Available at https://doi.org/10.1007/s00267-003-3042-2

Daipan, B.P.O. 2020. Geomorphometric characterization and analysis of the Bued Watershed using advanced spaceborne thermal emission and reflection radiometer – Global Digital Elevation Model V3 through geospatial techniques. *Philippine Journal of Science* 149. (3a): 955–967.

Esper Angillieri, M.Y. 2008. Morphometric analysis of Colangüil river basin and flash flood hazard, San Juan, Argentina. *Environmental Geology* 55. (1): 107–111. Available at https://doi.org/10.1007/s00254-007-0969-2

ESRI 2011. *ArcHydro Toolbox v2.0*. Environmental Systems Research Institute.

ESRI 2016. *ArcGIS 10.4*. Environmental Systems Research Institute.

Fábián, Sz.Á., Kalmár, P., Józsa, E. and Sobucki, M. 2016. Hydrogeomorphic exploration of a local headwater stream in low mountainous environment following detailed field survey protocol (Mecsek Mountains, Hungary). *Revista de Geomorfologie* 18. 78–82.

Fryirs, K.A. and Brierley, G.J. 2001. Variability in sediment delivery and storage along river courses in Bega catchment, NSW, Australia: implications for geomorphic river recovery. *Geomorphology* 38. (3–4): 237–265. Available at https://doi.org/10.1016/S0169-555X(00)00093-3

Fryirs, K.A., Brierley, G.J., Preston, N.J. and Spencer, J. 2007. Catchment-scale (dis)connectivity in sediment flux in the upper Hunter catchment, New South Wales, Australia. *Geomorphology* 84. (3–4): 297–316. Available at https://doi.org/10.1016/j.geomorph.2006.01.044

Fuller, B., Sklar, L., Compson, Z., Adams, K., Marks, J. and Wilcox, A. 2011. Ecogeomorphic feedbacks in regrowth of travertine step-pool morphology after dam decommissioning, Fossil Creek, Arizona. *Geomorphology* 126. (3–4): 314–332. Available at https://doi.org/10.1016/j.geomorph.2010.05.010

Galia, T. and Hradecký, J. 2011. Bedload transport and morphological effects of high-magnitude floods in small headwater streams – Moravskoslezské Beskydy Mts. (Czech Republic). *Journal of Hydrology and Hydromechanics* 59. (4): Available at https://doi.org/10.2478/v10098-011-0020-x

Galia, T. and Škarpich, V. 2013. Coarse bed sediments in a headwater channel as indicators of fluvial process and slope-channel coupling: A case study from the Carpathian Mountains (Czech Republic). *Moravian Geographical Reports* 21. 2–11. Available at https://doi.org/10.2478/mgr-2013-0012

Galia, T. and Hradecky, J. 2014. Channel-reach morphology controls of headwater streams based in flysch geologic structures: An example from the Outer Western Carpathians, Czech Republic. *Geomorphology* 216. 1–12. Available at https://doi.org/10.1016/j.geomorph.2014.03.026

Galia, T., Hradecký, J. and Škarpich, V. 2015. Sediment transport in headwater streams of the Carpathian Flysch Belt: Its nature and recent effects of human interventions. In *Sediment Matters.* Eds.: Heininger, P. and Cullmann, J., Springer International Publishing, 13–26. Available at https://doi.org/10.1007/978-3-319-14696-6_2

Galia, T., Šilhán, K., Ruiz-Villanueva, V., Tichavský, R. and Stoffel, M. 2017. Temporal dynamics of instream wood in headwater streams draining mixed Carpathian forests. *Geomorphology* 292. 35–46. Available at https://doi.org/10.1016/j.geomorph.2017.04.041

Galia, T., Ruiz-Villanueva, V., Tichavský, R., Šilhán, K., Horáček, M. and Stoffel, M. 2018. Characteristics and abundance of large and small instream wood in a Carpathian mixed-forest headwater basin. *Forest Ecology and Management* 424. 468–482. Available at https://doi.org/10.1016/j.foreco.2018.05.031

Grabowski, R.C., Gurnell, A.M., Burgess-Gamble, L., England, J., Holland, D., Klaar, M.J., Morrissey, I., Uttley, C. and Wharton, G. 2019. The current state of the use of large wood in river restoration and management. *Water and Environment Journal* 33. (3): 366–377. Available at https://doi.org/10.1111/wej.12465

Gurnell, A.M. and Grabowski, R.C. 2016. Vegetation-hydrogeomorphology interactions in a low-energy, human-impacted river. *River Research and Applications* 32. (2): 202–215. Available at https://doi.org/10.1002/rra.2922

Haas, J. (ed.). 2013. *Geology of Hungary*. Berlin–Heidelberg, Springer. Available at https://doi.org/10.1007/978-3-642-21910-8

Horton, R.E. 1945. Erosional development of streams and their draniage basins; Hydrophysical approach to quantiative morphology. *Geologocal Society of America Bulletin* 56. (3): 275.

Hungarian Meteorological Service (n.d.) *Climate of Hungary – general characteristics*. Budapest, OMSZ. Retrieved 10 October 2021 from https://www.met.hu/en/eghajlat/magyarorszag_eghajlata/altalanos_eghajlati_jellemzes/altalanos_leiras/

Jackson, K.J. and Wohl, E. 2015. Instream wood loads in montane forest streams of the Colorado Front Range, USA. *Geomorphology* 234. 161–170. Available at https://doi.org/10.1016/j.geomorph.2015.01.022

Jeffries, R., Darby, S.E. and Sear, D.A. 2003. The influence of vegetation and organic debris on flood-plain sediment dynamics: case study of a low-order stream in the New Forest, England. *Geomorphology* 51. (1–3: 61–80. Available at https://doi.org/10.1016/S0169-555X(02)00325-2

Kalmár, P., Fábián, Sz.Á. and Sobucki, M. 2013. Esettanulmány a természetes vízfolyások felszínformálásáról: A Váraljai-árok északi forrásága a Mecsekben (A case study about the surface shaping of natural waterflows: The northern springbranch of Váralja Trench in the Mecsek Hills). *Természetföldrajzi Közlemények a Pécsi Tudományegyetem Földrajzi Intézetéből 2*. Pécs, PTE.

Kalmár, P. 2015. *Terepi morfometriai és -dinamikai vizsgálatok a Váraljai-völgy vízgyűjtőjén* (Morphometric and morphodinamic measures on the Váralja Valley catchment). Pécs, PTE-TTK, Földrajzi Intézet.

Kamykowska, M., Kaszowski, L. and Krzemien, K. 1999. River channel mapping instruction. Key to the river bed descreption. In *River Channels. Pattern, Structure and Dynamics.* Ed.: Krzemien, K., Cracow, Poland, Institute of Geography of the Jagiellonian University, 9–25).

Kaszowski, L. and Krzemien, K. 1999. Classification systems of mountain river channel. *Prace Geograficzne IG UJ* 104. 27–40.

Kevey B. 2008. *Magyarország erdőtársulásai. XIV. kötet* (Forest associations of Hungary. Vol. XIV). Ed.: Bartha, D., Sopron, NYME Erdőmérnöki kar.

Kocsis, K. (ed.-in-chief). 2018. *National Atlas of Hungary, 2. Natural Environment*. Budapest, MTA Research Centre of Astronomy and Earh Sciences, Geographical Institute.

Leopold, L.B. and Markley, G.W. 1957. *River Channel Patterns: Braided, Meandering, and Straight*. Washington, D.C., USGS Publications Warehouse. Doi 10.3133/pp282B

Lóczy, D. 2012. A folyómedrek morfológiai tipizálásának hierarchiája a nemzetközi irodalomban (Hierarchical presentation of typologies of river channel morphology in international literature). *Földrajzi Közlemények 136.* (2): 124–137.

Manners, R.B., Doyle, M.W. and Small, M.J. 2007. Structure and hydraulics of natural woody debris jams. *Water Resources Research* 43. (6): 1–16. Available at https://doi.org/10.1029/2006WR004910

Mesa, L.M. 2006. Morphometric analysis of a subtropical Andean basin (Tucumán, Argentina). *Environmental Geology 50.* (8): 1235–1242. Available at https://doi.org/10.1007/s00254-006-0297-y

Mezősi, G. 2015. *Magyarország természetföldrajza* (Physical geography of Hungary). Budapest, Akadémiai Kiadó. Available at https://doi.org/10.1556/9789630589765

Moores, E.A. 1966. *Regional Drainage Basin Morphometry.* Ames, Iowa State University, Digital Repository. Available at https://doi.org/10.31274/rtd-180814-1017

Morisawa, M.E. 1962. Quantitative geomorphology of some watersheds in the Appalachian Plateau. *GSA Bulletin* 73. (9): 1025–1046. Available at https://doi.org/10.1130/0016-7606(1962)73[1025:QGOSWI]2.0.CO;2

Motta, R., Berretti, R., Lingua, E. and Piussi, P. 2006. Coarse woody debris, forest structure and regeneration in the Valbona Forest Reserve, Paneveggio, Italian Alps. *Forest Ecology and Management* 235. (1–3): 155–163. Available at https://doi.org/10.1016/j.foreco.2006.08.007

Myers, T.J. and Swanson, S. 1997. Precision of channel width and pool area measurments. *Journal of the American Water Resources Association* 33. (3): 647–659. Available at https://doi.org/10.1111/j.1752-1688.1997.tb03539.x

Obeidat, M., Awawdeh, M. and Al-Hantouli, F. 2021. Morphometric analysis and prioritisation of watersheds for flood risk management in Wadi Easal Basin (WEB), Jordan, using geospatial technologies. *Journal of Flood Risk Management* 14. (2): e12711. Available at https://doi.org/10.1111/jfr3.12711

Ondráčková, L. and Máčka, Z. 2019. Geomorphic (dis)connectivity in a middle-mountain context: Human interventions in the landscape modify catchment-scale sediment cascades. *Area* 51. (1): 113–125. Available at https://doi.org/10.1111/area.12424

Pareta, K. and Pareta, U. 2011. Quantitative morphometric analysis of a watershed of Yamuna Basin, India using ASTER (DEM) data and GIS. *International Journal of Geomatics and Geosciences* 2. (1): 248–269.

Płaczkowska, E., Górnik, M., Mocior, E., Peek, B., Potoniec, P., Rzonca, B. and Siwek, J. 2015. Spatial distribution of channel heads in the Polish Flysch Carpathians. *CATENA* 127. 240–249. Available at https://doi.org/10.1016/j.catena.2014.12.033

Płaczkowska, E. 2016. Structure of the headwater valley segment in the Western Tatras. *Studia Geomorphologica Carpatho-Balcanica* 50. 89–103.

Płaczkowska, E. and Krzemień, K. 2018. Natural conditions of coarse bedload transport in headwater catchments (Western Tatras, Poland). *Geografiska Annaler: Series A, Physical Geography* 100. (4): 370–387. Available at https://doi.org/10.1080/04353676.2018.1522957

Přibyla, Z., Galia, T. and Hradecký, J. 2016. Biogeomorphological effects of leaf accumulations in stepped-bed channels: Exploratory study, Moravskoslezské Beskydy Mountains, Czech Republic. *Moravian Geographical Reports* 24. (3): 13–23. Available at https://doi.org/10.1515/mgr-2016-0013

Prokop, P., Wiejaczka, Ł., Sarkar, S., Bryndal, T., Bucała-Hrabia, A., Kroczak, R., Soja, R. and Płaczkowska, E. 2020. Morphological and sedimentological responses of small stream channels to extreme rainfall and land use in the Darjeeling Himalayas. *CATENA* 188. 104444. Available at https://doi.org/10.1016/j.catena.2019.104444

Puno, G.R. and Puno, R.C.C. 2019. Watershed conservation prioritization using geomorphometric and land use-land cover parameters. *Global Journal of Environmental Science and Management* 5. (3): 279–294. Available at https://doi.org/10.22034/GJESM.2019.03.02

Raucsik, B. and Varga, A. 2008. Az alsó-toarci feketepala Réka-völgyi szelvényének ásványtani jellemzése (Óbányai Alurolit Formáció, Mecsek hegység): őséghajlattani következtetések (Mineralogy of the Lower Toarcian black shale section from the Réka Valley [Óbánya Siltstone Formation, Mecsek Mountains, Hungary]: implications for palaeoclimate). *Földtani Közlöny* 138. (2): 133–146.

Rice, S.P. and Church, M. 2001. Longitudinal profiles in simple alluvial systems. *Water Resources Research* 37. (2): 417–426. Available at https://doi.org/10.1029/2000WR900266

Rosgen, D.L. 1994. A classification of natural rivers. *CATENA* 22. (3): 169–199. Available at https://doi.org/10.1016/0341-8162(94)90001-9

Ruiz Villanueva, V., Bladé Castellet, E., Díez-Herrero, A., Bodoque, J. M. and Sánchez-Juny, M. 2014. Two-dimensional modelling of large wood transport during flash floods. *Earth Surface Processes and Landforms* 39. (4): 438–449. Available at https://doi.org/10.1002/esp.3456

Russel, R.J. 1954. Alluvial morphology of Anatolian rivers. *Annals of the Association of American Geographers* 55. (4): 363–391.

Sarkadi, N., Pirkhoffer, E., Lóczy, D., Balatonyi, L., Geresdi, I., Fábián, Sz., Varga, G., Balogh, R., Gradwohl-Valkay, A., Halmai, Á. and Czigány, Sz. 2022. Generation of a flood susceptibility map of evenly weighted conditioning factors for Hungary. *Geographica Pannonica* 26. (3): 200–214. Available at https://doi.org/10.5937/gp26-38969

Sass, C.K. and Keane, T.D. 2012. Application of Rosgen's BANCS model for NE Kansas and the development of predictive streambank erosion curves. *Journal of the American Water Resources Association* 48. (4): 774–787.

Sassolas-Serrayet, T., Cattin, R. and Ferry, M. 2018. The shape of watersheds. *Nature Communications* 9. (1): 3791. Available at https://doi.org/10.1038/s41467-018-06210-4

Schumm, S.A. 1956. Evolution of drainage systems and slopes in badlands at Perth Amboy, New Jersey. *Bulletin of the Geological Society of America* 67. 597–646.

Schumm, S.A. 2005. *River Variability and Complexity*. Cambridge, Cambridge University Press. Available at https://doi.org/10.1017/CBO9781139165440

Short, L.E., Gabet, E.J. and Hoffman, D.F. 2015. The role of large woody debris in modulating the dispersal of a post-fire sediment pulse. *Geomorphology* 246. 351–358. Available at https://doi.org/10.1016/j.geomorph.2015.06.031

Singh, P., Thakur, J.K. and Singh, U.C. 2013. Morphometric analysis of Morar River Basin, Madhya Pradesh, India, using remote sensing and GIS techniques. *Environmental Earth Sciences* 68. (7): 1967–1977. Available at https://doi.org/10.1007/s12665-012-1884-8

Strahler, A.N. 1957. Quantitative analysis of watershed geomorphology. *Transactions, American Geophysical Union* 38. (6): 913. Available at https://doi.org/10.1029/TR038i006p00913

Thompson, M.S.A., Brooks, S.J., Sayer, C.D., Woodward, G., Axmacher, J.C., Perkins, D.M. and Gray, C. 2018. Large woody debris "rewilding" rapidly restores biodiversity in riverine food webs. *Journal of Applied Ecology* 55. (2): 895–904. Available at https://doi.org/10.1111/1365-2664.13013

Víg, B., Fábian, Sz.Á., Czigány, Sz., Pirkhoffer, E., Halmai, Á., Kovács, I.P., Varga, G., Dezső, J., Nagy, G. and Lóczy, D. 2022. Morphometric analysis of low mountains for mapping flash flood susceptibility in headwaters. *Natural Hazards* 114. (3): 3235–3254. Available at https://doi.org/10.1007/s11069-022-05513-6

Western, A.W., Finlayson, B.L., McMahon, T.A. and O'Neill, I.C. 1997. A method for characterising longitudinal irregularity in river channels. *Geomorphology* 21. (1): 39–51. Available at https://doi.org/10.1016/S0169-555X(97)00023-8

Willett, C.D., Lerch, R.N., Schultz, R.C., Berges, S.A., Peacher, R.D. and Isenhart, T.M. 2012. Streambank erosion in two watersheds of the Central Claypan Region of Missouri, United States. *Journal of Soil and Water Conservation* 67. (4): 249–263. Available at https://doi.org/10.2489/jswc.67.4.249

Wohl, E., Lininger, K.B., Fox, M., Baillie, B.R. and Erskine, W.D. 2017. Instream large wood loads across bioclimatic regions. *Forest Ecology and Management* 404. 370–380. Available at https://doi.org/10.1016/j.foreco.2017.09.013

Zhang, N., Rutherfurd, I. and Ghisalberti, M. 2020. Effect of instream logs on bank erosion potential: a flume study with a single log. *Journal of Ecohydraulics* 5. (1): 43–56. Available at https://doi.org/10.1080/24705357.2019.1634499

DOI: 10.15201/hungeobull.72.4.4 Hungarian Geographical Bulletin **72** 2023 (4) 383–398.

Effectiveness of machine learning and deep learning models at county-level soybean yield forecasting

Nizom FARMONOV[1], Khilola AMANKULOVA[1], Shahid Nawaz KHAN[2], Mokhigul ABDURAKHIMOVA[3], József SZATMÁRI[1], Tukhtaeva KHABIBA[4], Radjabova MAKHLIYO[4], Meiliyeva KHODICHA[5] and László MUCSI[1]

Abstract

Crop yield forecasting is critical in modern agriculture to ensure food security, economic stability, and effective resource management. The main goal of this study was to combine historical multisource satellite and environmental datasets with a deep learning (DL) model for soybean yield forecasting in the United States' Corn Belt. The following Moderate Resolution Imaging Spectroradiometer (MODIS) products were aggregated at the county level. The crop data layer (CDL) in Google Earth Engine (GEE) was used to mask the data so that only soybean pixels were selected. Several machine learning (ML) models were trained by using 5 years of data from 2012 to 2016: random forest (RF), least absolute shrinkable and selection operator (LASSO) regression, extreme gradient boosting (XGBoost), and decision tree regression (DTR) as well as DL-based one-dimensional convolutional neural network (1D-CNN). The best model was determined by comparing their performances at forecasting the soybean yield in 2017–2021 at the county scale. The RF model outperformed all other ML models with the lowest RMSE of 0.342 t/ha, followed by XGBoost (0.373 t/ha), DTR (0.437 t/ha), and LASSO (0.452 t/ha) regression. However, the 1D-CNN model showed the highest forecasting accuracy for the 2018 growing season with RMSE of 0.280 t/ha. The developed 1D-CNN model has great potential for crop yield forecasting because it effectively captures temporal dependencies and extracts meaningful input features from sequential data.

Keywords: agriculture, remote sensing, farmers, random forest, soybean, machine learning

Received September 2023, accepted October 2023.

Introduction

Crop yield forecasting is crucial in agricultural decision-making for food security, crop insurance, and improving overall food production (Tantalaki, N. *et al.* 2019). Traditionally, farmers relied on their personal experience and incorporated weather and other relevant data to forecast their individual crop yields and make informed decisions (Liakos, K. *et al.* 2018). However, this traditional approach is associated with inherent uncertainties, particularly when extrapolated to large-scale scenarios, because of influencing factors that differ depending on the region and crop type (Shahhosseini, M. *et al.* 2020). Crop yield forecasting and prediction are distinct approaches that differ in methodology and

[1] Department of Geoinformatics, Physical and Environmental Geography, University of Szeged, Egyetem utca 2, 6722 Szeged, Hungary. Corresponding author's e-mail: farmonov.nizom@stud.u-szeged.hu

[2] Geospatial Sciences Center of Excellence, Department of Geography and Geospatial Sciences, South Dakota State University, Brookings, SD 57007, USA.

[3] Department of State Cadastre, Tashkent Institute of Irrigation and Agricultural Mechanization Engineers, National Research University, Tashkent, Uzbekistan

[4] Department of Hydrology and Ecology, "TIIAME" NRU Bukhara Institute of Natural Resources Management, Gazli Avenue 32, Bukhara, Uzbekistan.

[5] Department of Land Resources, Cadastre and Geoinformatics, Karshi Institute of Irrigation and Agrotechnology, "TIIAME" National Research University, Karshi, Uzbekistan.

data utilization (Shahhosseini, M. *et al.* 2020). Forecasting entails using historical observations to train a model and subsequently generating forecasts by employing input features specific to the future (Paudel, D. *et al.* 2021). The forecasting process acknowledges the influence of various biotic and abiotic factors on crop yield and necessitates a comprehensive understanding and management of these elements for a full grasp of the yield dynamics. A critical issue is the scarcity of extensive data encompassing all pertinent factors on a large scale.

Crop yield prediction differs from crop yield forecasting in that the former can utilize the target variable of the current year in the training phase (Shahhosseini, M. *et al.* 2020). Current crop yield prediction approaches can be divided into two main categories: physical models and statistical models (Tripathy, R. *et al.* 2022). Physical models simulate crop-growing conditions in combination with parameters that affect crop yield. Representative physical models include the Agricultural Production Simulator (Keating, B.A. *et al.* 2003) and Decision Support System for Agrotechnology Transfer (Jones, J.W. *et al.* 2003). Physical models are widely used, but they require extensive data for calibration, which limits their capabilities for large-scale crop monitoring. In contrast, statistical models are simpler with fewer input requirements, which make them very convenient for large-scale studies. Machine learning (ML) models use historical data to characterize the relationship between input variables and crop yield (Ma, Y. *et al.* 2021). A major advantage of ML models is that they can be used even when some specific crop parameters are not available. With the increased availability of data and computing power, robust ML methods have been developed and applied to crop yield prediction.

The increased availability of extensive remote sensing data has greatly facilitated their utilization in various agricultural applications, including crop classification, identification, and drought characterization (Sun, J. *et al.* 2019; Khan, S.N. *et al.* 2023), which has opened new avenues for extracting meaningful input features from remote sensing data for crop yield prediction. Vegetation indices (VIs) include factors such as greenness, vegetation health, and stress, and they have received substantial interest for research in vegetation dynamics (Panda, S.S. *et al.* 2010; Khan, K. *et al.* 2020). The normalized difference vegetation index (NDVI) is widely used for crop health characterization and yield prediction (Fernandes, J.L. *et al.* 2017). The NDVI measures the difference in reflectance of near-infrared (Nir) and red light to capture variations in plant biomass and photosynthetic activity, which makes it very useful for assessing crop productivity. Other VIs that have been employed for crop yield prediction include the enhanced vegetation index (EVI), soil-adjusted vegetation index, and normalized difference water index. In addition to remote sensing data, some studies have utilized climatic variables and soil data for crop yield prediction.

Recent studies have combined remote sensing data with ML models for crop yield prediction (Shahhosseini, M. *et al.* 2020). For example, Piekutowska, M. *et al.* (2021) used multiple linear regression on phenological and meteorological data to predict the potato yield and obtained a mean absolute percentage error of < 15 percent. Zeng, W. *et al.* (2018) used partial least-squares regression on weather data to predict the sunflower yield with an accuracy of $R^2 = 0.69$. Other ML models, including random forest (RF) (Khan, S.N. *et al.* 2022), support vector regression (Khosla, E. *et al.* 2020), and decision tree regression (Khan, S.N. *et al.* 2022) have been used for crop yield prediction at different scales and with different variables. In addition to conventional ML models, several deep learning (DL) models have recently been applied to crop yield prediction (Kang, Y. *et al.* 2020). Sun, J. *et al.* (2019) used a convolutional neural network and long short-term memory (CNN-LSTM) model with Moderate Resolution Imaging Spectroradiometer (MODIS) data to predict the soybean yield at the county level.

They classified data into different stages of the crop-growing season and evaluated the model performance in the stages. The end-of-season models outperformed the in-season models. (Ma, Y. *et al.* 2021) used a Bayesian neural network (BNN) with VI, climate, and soil data to predict the corn yield at the county level. They compared the performances of several models and found that the BNN outperformed other ML models such as RF, support vector regression, and LSTM. Although Earth Observation Systems (EOS) play a crucial role in monitoring crop yield through satellite data, there exists a significant research gap in enhancing the integration of multiplatform data, including data processing techniques, and the effective application of this technology in precision agricultural management. Novel research efforts are needed to bridge this gap and further optimize the utilization of EOS for informed decision-making in agriculture.

In this study, we applied several ML and DL models to forecast the soybean yield of the United States (US) at the county level and evaluated their performances. The spatial patterns between the observed and forecasted yields were also analysed. To address the above tasks, the following research questions were selected:

1. What are the most significant input features to predict the crop yield at the county scale?

2. How does the deep learning-based 1D-CNN model compare to traditional ML models for forecasting soybean yield in the US Corn Belt using historical satellite and environmental data?

Data

Study area

The study area comprised fourteen soybean-producing states: North Dakota (ND), South Dakota (SD), Nebraska (NE), Kansas (KS), Minnesota (MN), Iowa (IA), Missouri (MO), Arkansas (AR), Wisconsin (WI), Illinois (IL), Mississippi (MS), Michigan (MI), Indiana (IN), and Ohio (OH) *(Figure 1).* Most of the study area is in the Midwest, also known as the Corn Belt (Green, T.R. *et al.* 2018), and it is responsible for producing most of the corn

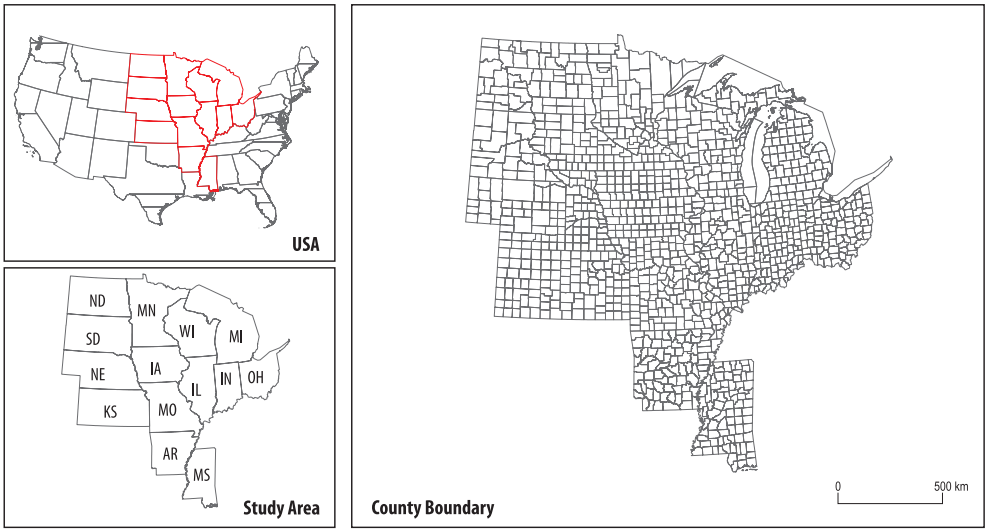

Fig. 1. Map of the study area. For state codes see the text.

and soybean in the US. Corn and soybean are often grown in rotation. The study area is primarily rainfed, and only a very small part is irrigated.

Crop yield data

County-level soybean yield data were obtained from the United States Department of Agriculture (USDA) for 2012–2021 (USDA/NASS 2021). The data were originally in bushels per acre, but we converted the values to tons per hectare (t/ha). The crop yield data were used for training, testing, and validating the models considered in this study. Annual soybean yields at a county level were different in the years from 2012 to 2021 *(Figure 2).*

Cropland data layer

The cropland data layer (CDL) is a crop-specific land-cover data layer created for the continental US that is generated each year by using MODIS and ground truth data at a resolution of 30 m (Boryan, C. *et al.* 2011). The CDL was developed by the Geospatial Information Branch, Spatial Analysis Research Section of the Research and Development Division at the National Agricultural Statistics Service (NASS), which is part of the USDA. In this study, we utilized the CDL to create a mask that identifies soybean pixels while excluding other data. We also used the CDL to derive statistics that helped identify counties with zero soybean pixels, which aided in the selection and exclusion of counties for further analysis.

County boundaries

The geographic boundaries of the counties in the study area were derived from the US Census Topologically Integrated Geographic Encoding and Referencing project, which provides accurate and comprehensive spatial data on county boundaries in the US (https://www.census.gov/geographies/mapping-files/time-series/geo/tiger-line-file.html). The geographic boundaries were used to collect and represent county-level data each year within the specified period.

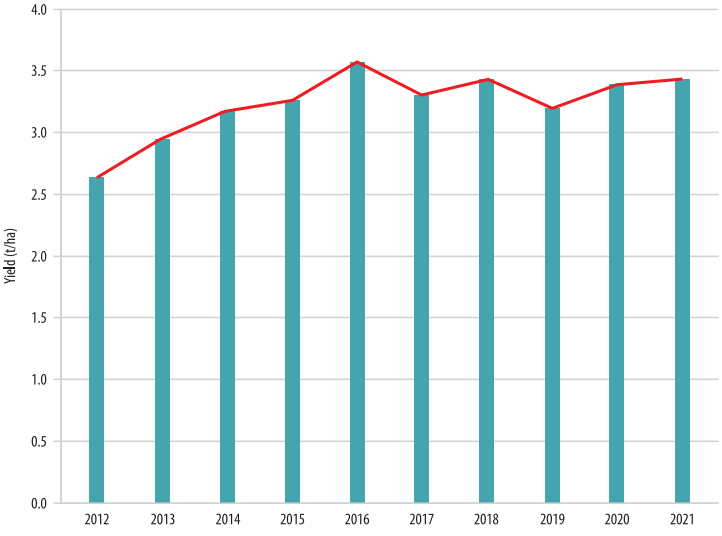

Fig. 2. Average soybean yield at the county level for 2012–2021.

Remote sensing and weather data

We employed MODIS data from the NASA Earth Observing System Data and Information System (https://search.earthdata.nasa.gov/), which are collected at regular intervals of 16 days and are available at spatial resolutions of 250, 500, and 1,000 m. We utilized MODIS NDVI and EVI products from the MOD13Q1.061 Terra Vegetation Indices 16-Day Global 250 m dataset (Didan, K. 2021). The MOD09A1 product

provides a surface reflectance product for Terra MODIS bands 1–7 at a spatial resolution of 500 m and considers atmospheric conditions such as gases, aerosols, and Rayleigh scattering. The reflectance of each pixel is selected from the best value of multiple acquisitions within an 8-day composite based on factors such as high observation coverage, low view angle, no clouds or cloud shadows, and aerosol loading (Vermote, E. 2021). The MOD11A2 product offers the average land surface temperature (LST) over 8 days at a spatial resolution of 1 km. The average LST for each pixel is calculated by taking the simple average of all corresponding LST values collected from the MOD11A1 product within that specific 8-day period (Wan, Z. *et al.* 2021). The MOD11A2 product incorporates both daytime and night time surface temperature bands to account for long-term soil factors (Saravanan, V. and Tamburi, V.N. 2022). Meteorological data were obtained from Daymet (Thornton, M.M. *et al.* 2022) and included daily measurements of six parameters, of which four were selected as climatic factors: precipitation, vapour pressure, minimum temperature, and maximum temperature. These parameters are generated on a gridded surface with a resolution of 1 km × 1 km. *Table 1* presents an overview of the satellite and climatic data utilized in this study.

Data preprocessing

The above datasets were preprocessed and downloaded by using Google Earth Engine (GEE) *(Figure 3).* All datasets were aggregated to a temporal resolution of 16 days corresponding to the period of 14–31 July for consistency. This period was selected because it coincides with the peak vegetation phase of soybeans. We previously investigated the contributions of dynamic input features to the crop yield, including the growth stage and phenology. We found that VI data from mid-July are more significant to forecasting the soybean yield than from other periods. This period corresponds to the crucial pod-setting stage for soybeans. The significance of the dynamic input features implies that the presence of pods and leaves predominantly influences the soybean crop yield (Li, Y. *et al.* 2023). Thus, all data within this period should have a significant relationship with the crop yield.

First, a dataset (e.g., MODIS NDVI) and the CDL were loaded into the GEE environment. The region of interest was selected, and both datasets were clipped to that region. We used the eq() function to create a binary mask based on the CDL values. Pixels with CDL values that corresponded to cropland were assigned a value of 1, while all other pixels were assigned a value of 0. We used the updateMask() function to apply the CDL mask to the MODIS NDVI dataset, which masked out all NDVI values that corresponded to non-cropland areas and left only soybean pixels. We then calculated the mean values of input features for each dataset at the county level. The soybean yield and input features were merged for each year using the county and year as common columns.

Method

Machine learning models

We compared various ML models in an effort to find a relationship between geospatial data and the soybean yield. We selected four different ML models: RF, least absolute shrinkable and selection operator (LASSO) regression, extreme gradient boosting (XGBoost), and decision tree regression (DTR). In addition, we selected a one-dimensional convolutional neural network (1D-CNN) as a DL model. All models were trained, tested, and validated. Models were trained and tested on data for 2012–2016. The models were then validated by forecasting the soybean yield for 2017–2021. The ML models were implemented in Python 3.11.3 with the scikit-learn package (Pedregosa, F. *et al.* 2012). The 1D-CNN model was implemented in Keras

Table 1. Overview of the satellite and climatic data used in this study

Data source	Spatial resolution	Temporal resolution	Feature	Products description
MOD13Q1	250 m	16-day	NDVI	Vegetation index value at a per-pixel basis.
			EVI	
MOD09A1	500 m	8-day	Red	The surface spectral reflectance of Terra MODIS bands 1–7, accounting for atmospheric factors. It includes seven reflectance bands, a quality layer, and four observation bands. Pixel values are chosen based on criteria like extensive coverage, optimal view angle, clear sky conditions, and minimal aerosol.
			Nir	
			Blue	
			Green	
			Nir 1	
			Swir 1	
			Swir 2	
MOD11A2	1,000 m	8-day	LST	The 8-day period aligns with the ground track repeat period of the Terra and Aqua satellites. This product includes day- and night-time LST bands, quality indicator layers, additional MODIS bands, and observation layers.
Daymet	1,000 m	Daily	Precipitation	Daymet V4 is an updated version that offers gridded estimates of daily weather parameters for Continental North America, Hawaii, and Puerto Rico. It addresses known issues by reducing timing bias, enhancing regression models, and introducing a novel approach to handle high elevation temperature measurement biases.
			Water vapour	
			Temperature min.	
			Temperature max.	

(Ketkar, N. 2017), which is an open-source DL framework written in Python.

RF estimates the crop yield by combining multiple regression trees. Each regression tree captures relationships between the input features and the target variable. Subsamples are randomly selected from the training set, which comprises 70 percent recorded yield samples and 30 percent test data. Each subsample is fitted to a regression tree. The final forecast is obtained by averaging the forecasts of all trees. RF has been demonstrated to be effective at mitigating overfitting (Wang, H. *et al.* 2016). We employed the Gaussian kernel function to investigate the non-linear association between input features (i.e., climatic and remote sensing data) and the target variable (i.e., crop yield). We applied RF to identify the most important input features utilizing Python 3.11.3 and the scikit-learn library, which offers Random Forest Regressor classes.

LASSO regression uses linear regression to minimize the residual sum of squares while constraining the absolute values of coefficients below a specified threshold (Tibshirani, R. 1996). LASSO regression addresses overfitting by automatically selecting relevant input features, which leads to a more concise regression model.

XGBoost is designed for tree boosting, which involves constructing multiple weak learners and combining their results to improve the regression or classification performance. It incorporates regularization techniques to prevent overfitting, and the weak learners can be regression trees or linear models (Chen, T. and Guestrin, C. 2016;

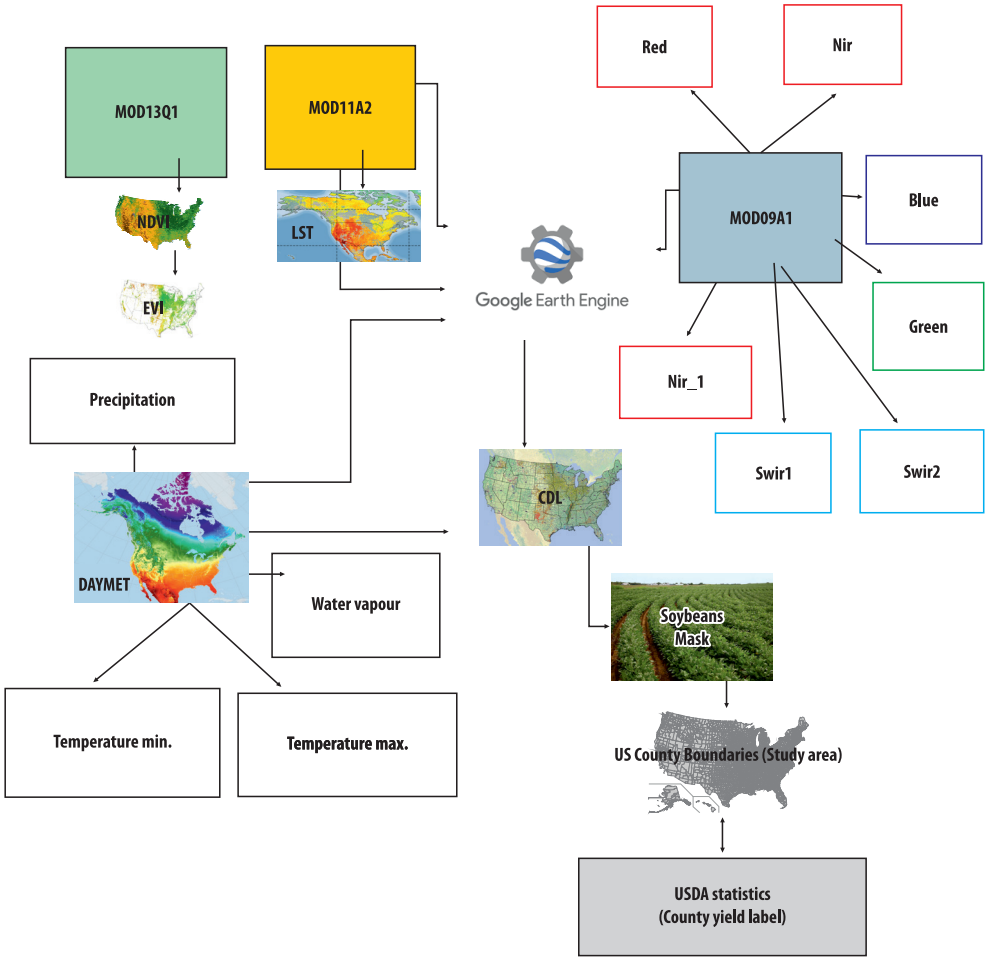

Fig. 3. GEE-based data preprocessing workflow

Song, Y. *et al.* 2019). We opted to use XGBoost based on decision trees. XGBoost makes forecasts by summing the weights of the leaves in all decision trees. We used the GridSearchCV package (Molinaro, A.M. *et al.* 2005) to determine the optimal parameters for XGBoost.

DTR constructs a tree structure based on input features in the training data to forecast the target variable. It is suitable for both classification and regression tasks and offers the benefit of interpretable results in the form of a tree. DTR utilizes binary splits to divide data into two groups and minimizes the sum of squared deviations from the mean within each group. This process is continued until a minimum node size specified by the user is achieved (San Millan-Castillo, R. *et al.* 2020).

Finally, 1D-CNN is a type of neural network commonly used for sequential data analysis (Kiranyaz, S. *et al.* 2021). Different filters are applied to the input data to extract meaningful input features, which allows the model to learn the representation more efficiently *(Figure 4).* The convolutional layers are followed by pooling layers that reduce the dimensions of data and only keep the

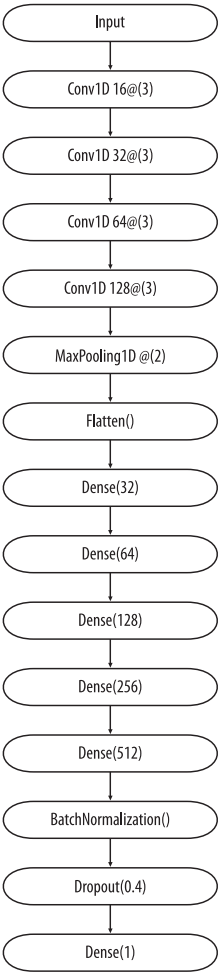

Fig. 4. 1D-CNN model architecture

useful information. This information is then passed to fully connected (FC) layers for the final forecast. We used a 1D-CNN comprising four convolutional layers, one max-pooling layer, and five FC layers followed by a dropout layer and then the final FC layer for crop yield forecasting. We used three convolutional layers with 16–128 filters. The FC layers had 32–512 neurons. The dropout rate was set to 0.4. In Keras, training a DL model requires tuning several hyper-parameters to find the optimal model, which include the learning rate, batch size, and optimization function. We considered learning rates of 0.00001–0.01, batch sizes of 16–128, and the Adam optimizer, which uses stochastic gradient descent to optimize the model performance and reduce the loss.

Model evaluation

We evaluated the model performances by using several metrics. We used the R^2 value to measure the proportion of variance explained by each model. We used the normalized root mean squared error (NRMSE%) and root mean squared error (NRMSE) to measure the forecasting error as a percentage area. We used the mean absolute error (MAE), which represents the average absolute difference between the forecasted and actual values, and the mean squared error (MSE), which measures the average squared difference between the forecasted and actual values. These metrics are calculated as follows:

$$R^2 = 1 - \frac{\sum_i \gamma_i^2}{\sum_i (y_i - \bar{y})^2} \quad (1)$$

$$RMSE = \sqrt{\frac{1}{m}\sum_{i=1}^{m}(yp^i - y^i)^2} \quad (2)$$

$$MAE = \frac{1}{m}\sum_{i=1}^{m}\left|yp^i - y^i\right| \quad (3)$$

$$MSE = \frac{1}{m}\sum_{i=1}^{m}(yp^i - y^i)^2 \quad (4)$$

$$NRMSE\% = \frac{RMSE}{y_{i,max} - y_{i,min}} \quad (5)$$

These metrics can be used to quantify the probability that a model correctly forecasts new samples from the underlying data distribution . The residuals (r_i) are the differences between the predicted values (yp^i) and actual labels (y^i) as well as the average of the labels ($\bar{y}$).

Results

Input feature importance

We identified surface reflectance (SR) band 2, EVI, and NDVI as the most influential input features with importance scores of 0.30, 0.29, and 0.13, respectively *(Figure 5).* These input features exhibited strong predictive power, which indicates their significance to the crop yield. The LST was found to have moderate importance with a score of 0.08. Conversely, climatic data and other SR bands had relatively low importance scores of 0.01–0.05. These findings emphasize the potential of incorporating MODIS LST and SR data with climatic data to enhance the accuracy of crop yield forecasting models.

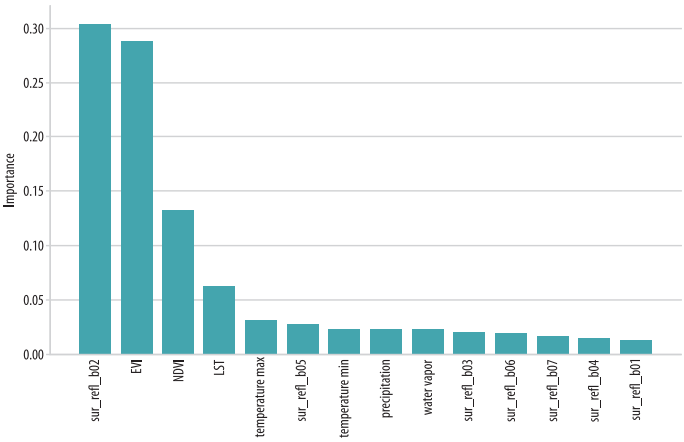

Fig. 5. Importance of input features according to the random forest model

1D-CNN performance

The 1D-CNN model was also applied to forecasting the soybean yield in the study area. *Table 2* presents the forecasting results for 2017–2021. Overall, the 1D-CNN model performed better than classical ML models with MSE values of 0.076–0.108 t/ha and R^2 values of 0.76–0.86. The highest R^2 value was in 2021 while the lowest R^2 value was in 2019. The scatterplots of the actual and forecasted yields were created for 2017–2021 *(Figure 8).*

Performance comparison of machine learning models

The RF model consistently demonstrated the best performance across all metrics *(Figure 6).* The RF model had the highest R^2 value of 0.75, which surpassed the R^2 values of XGBoost (0.70), DTR (0.59), and LASSO regression (0.60). The RF model also had the lowest RMSE of 0.342 t/ha, MAE of 0.264 t/ha, MSE of 0.117 t/ha, and NRMSE of 8.4 percent. XGBoost had the second-best performance with an RMSE of 0.373 t/ha, MAE of 0.287 t/ha, MSE of 0.139 t/ha, and NRMSE of 9.15 percent. Therefore, the RF model was selected for forecasting the soybean yield.

Crop yield forecasting

The year-to-year results indicated that the RF model achieved MAE values of 0.112–0.119 t/ha, RMSE values of 0.334–0.345 t/ha, R^2 values of 0.75–0.77, and NRMSE% values of 7.85–8.46 percent *(Figure 7).* The best results were obtained in 2021, for which the RF model achieved a MAE of 0.112 t/ha, RMSE of 0.334 t/ha, R^2 of 0.77, and NRMSE% of 7.85 percent.

Spatial patterns of crop yield forecasts

Spatial distribution of the forecasted soybean yields was generated over the period of 2017–2021 with the RF model *(Figure 9).* The soybean yield was forecasted as exceptionally high in the central and northeast (i.e., Iowa, Indiana, and Nebraska) at 1–5 t/ha while the observed yield was 1.0–4.5 t/ha. The error between the observed and forecasted yields was minimal, which indicated a high level of accuracy. The south (i.e., Arkansas and Mississippi) was forecasted with an average soybean yield of 2.0–3.5 t/ha, while Ohio in the west was forecasted with a soybean yield of 2.5–3.5 t/ha. The north (i.e., Minnesota and North Dakota) were forecasted with lower yields of 1.5–2.5 t/ha. The difference between the observed and forecast yields was not substantial. However, these results do suggest that the growing conditions in the north were less favourable for soybean cultivation than elsewhere in the study area. The variations in yield across different regions can be attributed to a multitude of factors, including climate, soil quality, agricultural practices, and other local conditions. The central and

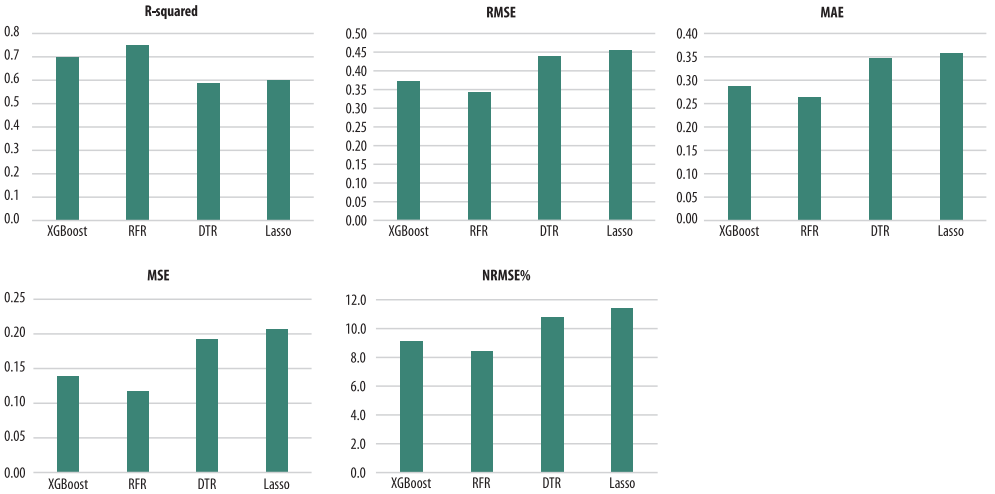

Fig. 6. Performance metrics of several ML models

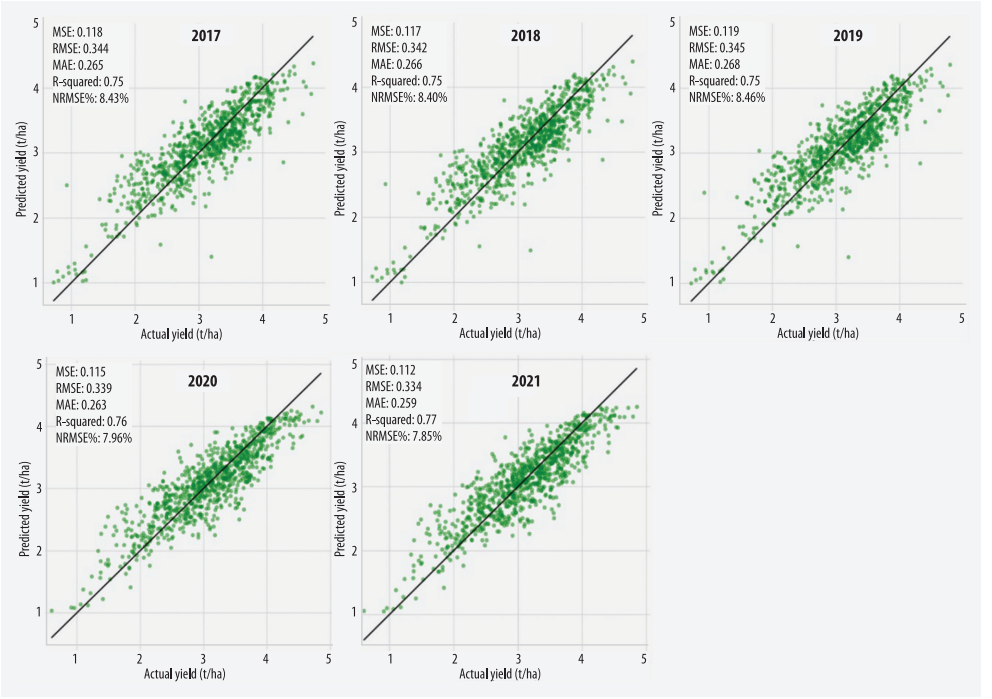

Fig. 7. Scatterplots between actual and forecasted soybean yields for 2017–2021 with the RF model

Table 2. Performance of the 1D-CNN soybean yield forecast model for 2017–2021.

Year	MSE	RMSE	MAE	R^2	NRMSE
	t/ha				%
2017	0.076	0.276	0.202	0.81	6.99
2018	0.079	0.280	0.208	0.83	6.96
2019	0.080	0.283	0.206	0.76	9.26
2020	0.090	0.300	0.222	0.80	6.74
2021	0.108	0.329	0.240	0.86	7.24

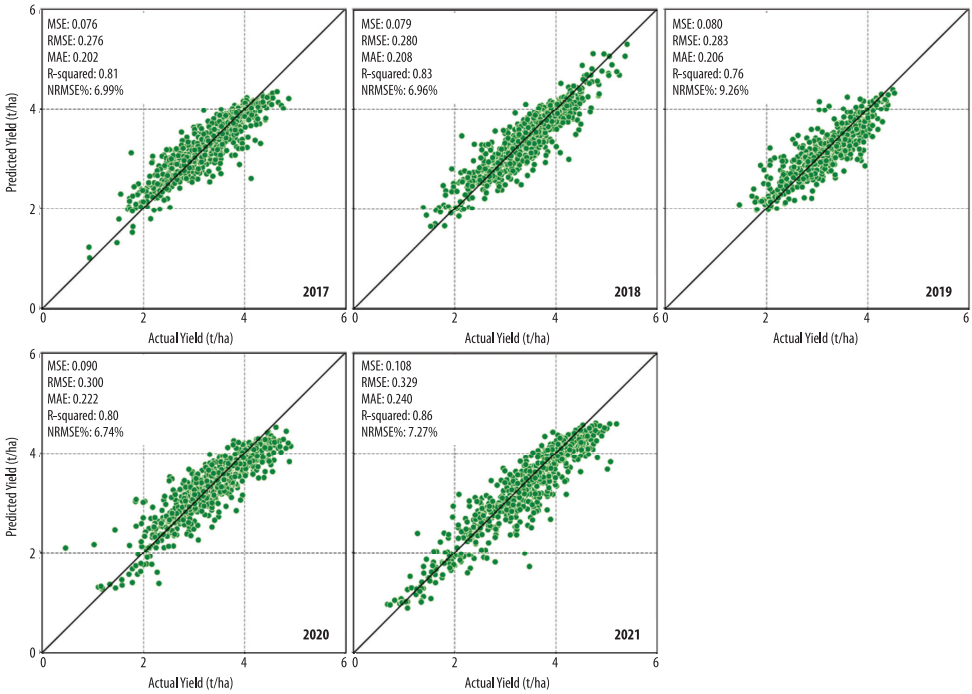

Fig. 8. Scatterplots between the actual and forecasted soybean yields for 2017–2021 with the 1D-CNN model

north-eastern states benefit from a highly conducive agricultural environment, which led to the forecast of higher yields. Conversely, the southern and northern states have less optimal conditions, which lowered the forecasted yields. Note that these forecasts were based on the RF model's analysis of historical data and other relevant factors. However, local factors, unforeseen events, and changes in agricultural practices can potentially affect the actual yield. Therefore, continuous monitoring and adjustment of the model's output to consider real-time data are essential for accurate and up-to-date forecasting.

Discussion

Input feature importance

The RF model found the SR band 2, EVI, and NDVI as the most influential input features

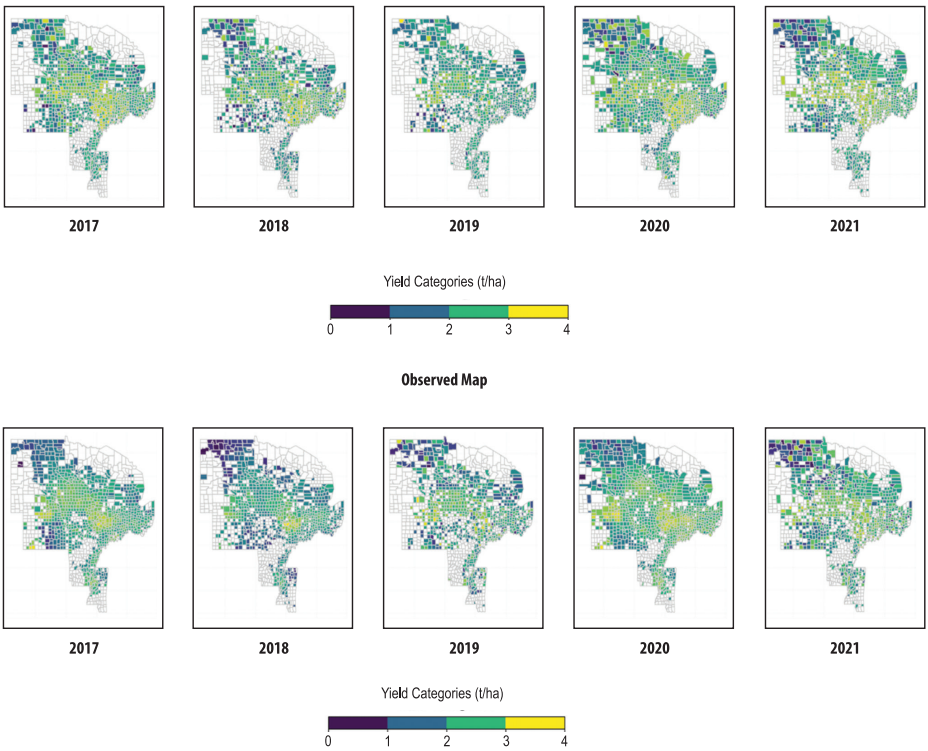

Fig. 9. Spatial distributions of the forecasted soybean yield with the RF model and the observed soybean yield for 2017–2021.

for forecasting the soybean yield in the study area, which is consistent with previous studies that have highlighted the importance of VI data on crop yield forecasting. Sun, J. *et al.* (2019) demonstrated a strong correlation between MODIS SR data and soybean yield. Kuwata, K. and Shibasaki, R. (2016) found that EVI exhibited a significant relationship with corn yield. Our study reinforces the existing literature by highlighting the significance of these VIs in different crop yield forecasting models. The LST was found to have moderate importance for forecasting the soybean yield. This aligns with previous studies that have emphasized the effect of temperature on crop development and productivity (Pede, T. *et al*. 2019; Mirhoseini, N. *et al.* 2022). Pede, T. *et al*. (2019) demonstrated the importance of MODIS LST to corn yield forecasting before the harvesting stage, especially during periods of extreme drought and water stress. Thus, our study reaffirmed the importance of considering temperature in crop yield forecasting. The climatic data and other SR bands were assigned a lower importance for soybean yield forecasting. This is consistent with previous studies that have shown mixed results regarding the contribution of climatic variables to crop yield forecasting (Cai, Y. *et al.* 2019; Hunt, M.L. *et al.* 2019; Farmonov, N. *et al.* 2022). Hunt, M.L. *et al.* (2019) found that climatic variables had limited predictive power of the wheat yield, but Cai, Y. *et al.* (2019) reported that climatic factors had a stronger influence on the wheat yield in Australia. These discrepancies may arise due to

variations in the crop type, geographic location, and specific weather variables considered. Nevertheless, our study highlights the potential of combining MODIS LST and SR data with climatic data to improve the accuracy of crop yiefigld forecasting models.

Model performance

We compared the performances of four ML models for soybean yield forecasting and found that the RF model consistently outperformed the others across all metrics with an RMSE value of 0.334 t/ha and R^2 value of 0.77. These results are consistent with those of Ji, Z. *et al.* (2022) who used an RF model to predict the corn and soybean yields in the Corn Belt with R^2 values of 0.55–0.75 and RMSE values of 1,000–1,500 kg/ha. Our findings align with previous studies that have reported the effectiveness of the RF model at crop yield prediction (Barbosa dos Santos, V. *et al.* 2022; Dhillon, M.S. *et al.* 2023). Barbosa dos Santos, V. *et al.* (2022) found that the RF model provided the most accurate soybean yield prediction in the Brazilian Cerrado with an R^2 value of 0.81 and RMSE value of 176.93 kg/ha, whereas Dhillon, M.S. *et al.* (2023) successfully applied the RF model to predicting the winter wheat and rapeseed yields in Germany. The robustness and flexibility of RF, combined with its ability to handle complex interactions and nonlinear relationships, make it a reliable choice for crop yield forecasting.

However, the comparison between the RF and 1D-CNN models revealed that the latter generally outperformed the former with an R^2 value of 0.86 in 2021 and RMSE value of 0.276 t/ha for 2017. This finding is consistent with other studies that have highlighted the effectiveness of DL models at crop yield prediction (Khaki, S. and Wang, L. 2019; Khaki, S. *et al.* 2020). Khaki, S. and Wang, L. (2019) employed a deep neural network for crop yield prediction and achieved better accuracy than with traditional ML models. Khaki, S. *et al.* (2020) developed a DL-based model to predict corn and soybean yields across the Corn Belt and demonstrated its superior performance. Our study adds to the growing body of literature supporting the potential of DL models for improving the accuracy of crop yield forecasting.

Conclusions

We explored the various contributions of dynamic input features to soybean yield forecasting and compared the performances of different ML models. The findings emphasized the importance of VI data from mid-July, particularly SR band 2, EVI, and NDVI, to the soybean yield, which align with previous studies. The RF model consistently outperformed the other ML models in forecasting the soybean yield. However, the 1D-CNN model performed even better, which highlights the potential of DL models for crop yield forecasting. The spatial patterns of the forecasted yields indicated higher yields in the central and north-eastern states and lower yields in the southern and northern states. These variations can be attributed to multiple factors, including the climate, soil quality, and local agricultural practices.

Overall, this study provides insights into the importance of different input features to crop yield forecasting and the performances of ML and DL models. These findings can help researchers, practitioners, and policymakers in making informed decisions to enhance crop productivity and ensure food security. Future research can focus on integrating additional variables and exploring advanced DL techniques to further improve the accuracy of crop yield forecasting.

Disclosure statement: The authors report there are no competing interests to declare.

Authors' ORCID:
Farmonov, N. – https://orcid.org/0000-0002-2491-9340
Amankulova, K. – https://orcid.org/0000-0001-6562-5616
Khan, S.N. – https://orcid.org/0000-0003-2185-7276
Szatmári, J. – https://orcid.org/0000-0002-7896-3363
Mucsi, L. – https://orcid.org/0000-0002-5807-3742

REFERENCES

Barbosa dos Santos, V., Moreno Ferreira dos Santos, A., da Silva Cabral de Moraes, J.R., de Oliveira Vieira, I.C. and de Souza Rolim, G. 2022. Machine learning algorithms for soybean yield forecasting in the Brazilian Cerrado. *Journal of the Science of Food and Agriculture* 102. (9): 3665–3672. Available at https://doi.org/10.1002/jsfa.11713

Boryan, C., Yang, Z., Mueller, R. and Craig, M. 2011. Monitoring US agriculture: The US Department of Agriculture, National Agricultural Statistics Service. Cropland data layer program. *Geocarto International* 26. (5): 341–358. Available at https://doi.org/10.1080/10106049.2011.562309

Cai, Y., Guan, K., Lobell, D., Potgieter, A.B., Wang, S., Peng, J. Xu, T. *et al.* 2019. Integrating satellite and climate data to predict wheat yield in Australia using machine learning approaches. *Agricultural and Forest Meteorology* 274. (August): 144–159. Available at https://doi.org/10.1016/j.agrformet.2019.03.010

Chen, T. and Guestrin, C. 2016. XGBoost: A scalable tree boosting system. In *Proceedings of the 22nd ACM SIGKDD International Conference on Knowledge Discovery and Data Mining*. San Francisco CA, USA, ACM. 785–794. Available at https://doi.org/10.1145/2939672.2939785

Dhillon, M.S., Dahms, T., Kuebert-Flock, C., Rummler, T., Arnault, J., Steffan-Dewenter, I. and Ullmann, T. 2023. Integrating random forest and crop modelling improves the crop yield prediction of winter wheat and oil seed rape. *Frontiers in Remote Sensing* 3. (January): 1010978. Available at https://doi.org/10.3389/frsen.2022.1010978

Didan, K. 2021. *MODIS/terra vegetation indices 16-day L3 global 250 m SIN grid V061.* NASA EOSDIS Land Processes DAAC. Available at https://doi.org/10.5067/MODIS/MOD13Q1.061

Farmonov, N., Amankulova, K., Szatmári, J., Urinov, J., Narmanov, Z., Nosirov, J. and Mucsi, L. 2023. Combining planet scope and Sentinel-2 images with environmental data for improved wheat yield estimation. *International Journal of Digital Earth* 16. (1): 847–867.Available at https://doi.org/10.1080/17538947.2023.2186505

Fernandes, J.L., Ebecken, N.F. and dalla Mora Esquerdo, J.C. 2017. Sugarcane yield prediction in Brazil using NDVI time series and neural networks ensemble. *International Journal of Remote Sensing* 38. (16): 4631–4644. Available at https://doi.org/10.1080/01431161.2017.1325531

Green, T.R., Kipka, H., David, O. and McMaster, G.S. 2018. Where is the USA Corn Belt, and how is it changing? *Science of The Total Environment* 618. (March): 1613–1618. Available at https://doi.org/10.1016/j.scitotenv.2017.09.325

Hunt, M.L., Blackburn, G.A., Carrasco, L., Redhead, J.W. and Rowland, C.S. 2019. High resolution wheat yield mapping using Sentinel-2. *Remote Sensing of Environment* 233. (November): 111410. Available at https://doi.org/10.1016/j.rse.2019.111410

Ji, Z., Pan, Y., Zhu, X., Zhang, D. and Wang, J. 2022. A generalized model to predict large-scale crop yields integrating satellite-based vegetation index time series and phenology metrics. *Ecological Indicators* 137. (April): 108759. Available at https://doi.org/10.1016/j.ecolind.2022.108759

Jones, J.W., Hoogenboom, G., Porter, C.H., Boote, K.J., Batchelor, W.D., Hunt, L.A., Wilkens, P.W., Singh, U., Gijsman, A.J. and Ritchie, J.T. 2003. The DSSAT Cropping System Model. *European Journal of Agronomy* 18. (3): 235–265. Available at https://doi.org/10.1016/S1161-0301(02)00107-7

Kang, Y., Ozdogan, M., Zhu, X., Ye, Z., Hain, C. and Anderson, M. 2020. Comparative assessment of environmental variables and machine learning algorithms for maize yield prediction in the US Midwest. *Environmental Research Letters* 15. (6): 064005. Available at https://doi.org/10.1088/1748-9326/ab7df9

Keating, B.A., Carberry, P.S., Hammer, G.L., Probert, M.E., Robertson, M.J., Holzworth, D.N., Huth, I. *et al.* 2003. An overview of APSIM, a model designed for farming systems simulation. *European Journal of Agronomy* 18. (3): 267–288. Available at https://doi.org/10.1016/S1161-0301(02)00108-9

Ketkar, N. 2017. Introduction to Keras. In *Deep Learning with Python*. Berkeley, CA, USA. Apress, 97–111. Available at https://doi.org/10.1007/978-1-4842-2766-4_7

Khaki, S. and Wang, L. 2019. Crop yield prediction using deep neural networks. *Frontiers in Plant Science* 10. (May): 621. Available at https://doi.org/10.3389/fpls.2019.00621

Khaki, S., Wang, L. and Archontoulis, S.V. 2020. A CNN-RNN framework for crop yield prediction. *Frontiers in Plant Science* 10. (January): 1750. Available at https://doi.org/10.3389/fpls.2019.01750

Khan, K., Iqbal, J., Ali, A. and Khan, S.N. 2020. Assessment of Sentinel-2-derived vegetation indices for the estimation of above-ground biomass/carbon stock, temporal deforestation and carbon emission estimation in the moist temperate forests of Pakistan. *Applied Ecology and Environmental Research* 18. (1): 783–815. Available at https://doi.org/10.15666/aeer/1801_783815

Khan, S.N., Li, D. and Maimaitijiang, M. 2022. A geographically weighted random forest approach to predict corn yield in the US Corn Belt. *Remote Sensing* 14. (12): 2843. Available at https://doi.org/10.3390/rs14122843

Khan, S.N., Khan, A.N., Tariq, A., Lu, L., Malik, N.A., Umair, M., Hatamleh, W.A. and Zawaideh, F.H. 2023. County-level corn yield prediction using supervised machine learning. *European Journal of Remote Sensing* 56. (1): 2253985. Available at https://doi.org/10.1080/22797254.2023.2253985

Khosla, E., Dharavath, R. and Priya, R. 2020. Crop yield prediction using aggregated rainfall-based modular artificial neural networks and support vector regression. *Environment, Development and Sustainability* 22. (6): 5687–5708. Available at https://doi.org/10.1007/s10668-019-00445-x

Kiranyaz, S., Avci, O., Abdeljaber, O., Ince, T., Gabbouj, M. and Inman, D.J. 2021. 1D convolutional neural networks and applications: A survey. *Mechanical Systems and Signal Processing* 151. (April): 107398. Available at https://doi.org/10.1016/j.ymssp.2020.107398

Kuwata, K. and Shibasaki, R. 2016. Estimating cord yield in the United States with MODIS EVI and machine learning methods. *ISPRS Annals of Photogrammetry, Remote Sensing and Spatial Information Sciences* III–8. (June): 131–136. Available at https://doi.org/10.5194/isprsannals-III-8-131-2016

Li, Y., Zeng, H., Zhang, M., Wu, B., Zhao, Y., Yao, X., Cheng, T., Qin, X. and Wu, F. 2023. A county-level soybean yield prediction framework coupled with XGBoost and multidimensional feature engineering. *International Journal of Applied Earth Observation and Geoinformation* 118. (April): 103269. Available at https://doi.org/10.1016/j.jag.2023.103269

Liakos, K., Busato, P., Moshou, D., Pearson, S. and Bochtis, D. 2018. Machine learning in agriculture: A review. *Sensors* 18. (8): 2674. Available at https://doi.org/10.3390/s18082674

Ma, Y., Zhang, Z., Kang, Y. and Özdoğan, M. 2021. Corn yield prediction and uncertainty analysis based on remotely sensed variables using a Bayesian neural network approach. *Remote Sensing of Environment* 259. (June): 112408. Available at https://doi.org/10.1016/j.rse.2021.112408

Mirhoseini, N., Mahdi, S., Abbasi-Moghadam, D., Sharifi, A., Farmonov, N., Amankulova, K. and Mucsi, L. 2022. Multi-spectral crop yield prediction using 3D-convolutional neural networks and attention convolutional LSTM approaches. *IEEE Journal of Selected Topics in Applied Earth Observations and Remote Sensing* 1–14. Available at https://doi.org/10.1109/JSTARS.2022.3223423

Molinaro, A.M., Simon, R. and Pfeiffer, R.M. 2005. Prediction error estimation: A comparison of resampling methods. *Bioinformatics* 21. (15): 3301–3307. Available at https://doi.org/10.1093/bioinformatics/bti499

Panda, S.S., Ames, D.P. and Panigrahi, S. 2010. Application of vegetation indices for agricultural crop yield prediction using neural network techniques. *Remote Sensing* 2. (3): 673–696. Available at https://doi.org/10.3390/rs2030673

Paudel, D., Boogaard, H. de Wit, A., Janssen, S., Osinga, S., Pylianidis, C. and Athanasiadis, I.N. 2021. Machine learning for large-scale crop yield forecasting. *Agricultural Systems* 187. 103016. Available at https://doi.org/10.1016/j.agsy.2020.103016

Pede, T., Mountrakis, G. and Shaw, S.B. 2019. Improving corn yield prediction across the US Corn Belt by replacing air temperature with daily MODIS land surface temperature. *Agricultural and Forest Meteorology* 276–277. (October): 107615. Available at https://doi.org/10.1016/j.agrformet.2019.107615

Pedregosa, F., Varoquaux, G., Gramfort, A., Michel, V., Thirion, B., Grisel, O., Blondel, M. *et al.* 2012. Scikit-learn: Machine learning in Python. *Journal of Machine Learning Research* 12. 2825–2830. Available at https://doi.org/10.48550/ARXIV.1201.0490

Piekutowska, M., Niedbała, G., Piskier, T., Lenartowicz, T., Pilarski, K., Wojciechowski, T., Pilarska, A.A. and Czechowska-Kosacka, A. 2021. The application of multiple linear regression and artificial neural network models for yield prediction of very early potato cultivars before harvest. *Agronomy* 11. (5): 10.3390. Available at https://doi.org/10.3390/agronomy11050885

San Millan-Castillo, R., Morgado, E. and Goya-Esteban, R. 2020. On the use of decision tree regression for predicting vibration frequency response of handheld probes. *IEEE Sensors Journal* 20. (8): 4120–4130. Available at https://doi.org/10.1109/JSEN.2019.2962497

Saravanan, V. and Tamburi, V.N. 2022. Assessment of land surface temperature (LST) using MODIS MOD11A2 thermal satellite images using zero to null pixel averaging method for the Bengaluru urban district. Preprint. In Review. Available at https://doi.org/10.21203/rs.3.rs-1932983/v1

Shahhosseini, M., Hu, G. and Archontoulis, S.V. 2020. Forecasting corn yield with machine learning ensembles. *Frontiers in Plant Science* 11. 1120. Available at https://doi.org/10.3389/fpls.2020.01120

Song, Y., Jiao, X., Qiao, Y., Liu, X., Qiang, Y., Liu, Z. and Zhang, L. 2019. Prediction of double-high biochemical indicators based on LightGBM and XGBoost. In *Proceedings of the 2019 International Conference on Artificial Intelligence and Computer Science*. Wuhan, Hubei Province, China, ACM, 189–193. Available at https://doi.org/10.1145/3349341.3349400

Sun, J., Di, L., Sun, Z., Shen, Y. and Lai, Z. 2019. County-level soybean yield prediction using deep CNN-LSTM model. *Sensors* 19. (20): 4363. Available at https://doi.org/10.3390/s19204363

Tantalaki, N., Souravlas, S. and Roumeliotis, M. 2019. Data-driven decision making in precision agriculture: The rise of Big Data in agricultural systems. *Journal of Agricultural & Food Information* 20. (4): 344–380. Available at https://doi.org/10.1080/10496505.2019.1638264

Thornton, M.M., Shrestha, R., Wei, Y., Thornton, P.E., Kao, S-C. and Wilson, B.E. 2022. *Daymet: Daily surface weather data on a 1-km grid for North America. Version 4 R1.* NetCDF, November, 0 MB. Available at https://doi.org/10.3334/ORNLDAAC/2129

Tibshirani, R. 1996. Regression shrinkage and selection via the Lasso. *Journal of the Royal Statistical Society: Series B (Methodological)* 58. (1): 267–288. Available at https://doi.org/10.1111/j.2517-6161.1996.tb02080.x

Tripathy, R., Chaudhari, K.N., Bairagi, G.D., Pal, O., Das, R. and Bhattacharya, B.K. 2022. Towards fine-scale yield prediction of three major crops of India using data from multiple satellite. *Journal of the Indian Society of Remote Sensing* 50. (2): 271–284. Available at https://doi.org/10.1007/s12524-021-01361-2

Vermote, E. 2021. *MODIS/terra surface reflectance 8-day L3 global 500 m SIN grid V061*. NASA EOSDIS Land Processes DAAC. Available at https://doi.org/10.5067/MODIS/MOD09A1.061

Wan, Z., Hook, S. and Hulley, G. 2021. *MODIS/terra land surface temperature/emissivity 8-day L3 global 1 km SIN grid V061*. NASA EOSDIS Land Processes DAAC. Available at https://doi.org/10.5067/MODIS/MOD11A2.061

Wang, H., Yang, F. and Luo, Z. 2016. Once measures. *BMC Bioinformatics* 17. 60. Available at https://doi.org/10.1186/s12859-016-0900-5

Zeng, W., Xu, C., Gang, Z., Wu, J. and Huang, J. 2018. Estimation of sunflower seed yield using partial least squares regression and artificial neural network models. *Pedosphere* 28. (5): 764–774. Available at https://doi.org/10.1016/S1002-0160(17)60336-9

DOI: 10.15201/hungeobull.72.4.5 Hungarian Geographical Bulletin **72** 2023 (4) 399–414.

European Green Deal + Poland + hydroelectric plants = Future?

Adam PIASECKI[1]

Abstract

This study considers the current state of hydropower in Poland and the legal and environmental conditions for its development. The research objective was to provide insights into the future of hydropower in Poland. An attempt was made to determine the direction of hydropower development in Poland by 2050, taking into account the requirements of the European Green Deal. The basic method used is logical argumentation, which is in turn based on a critical analysis of planning documents and scientific papers. Statistical data on the production and consumption of hydropower were also analysed. Currently, Poland's potential for hydropower production is not being fully exploited. The main reasons for this are a lack of political support and socio-ecological issues associated with the need to take over inhabited areas or areas of high natural value. The analysis of the state of hydropower in Poland indicates that urgent intervention is required in many areas. This applies, especially, to issues of the control, modernisation and technical condition of hydropower plants and damming facilities. The potential for the development of hydropower in Poland is assessed to be very small. Environmental, socio-economic and legal conditions are unfavourable to the construction of new, large hydropower plants. The exception is pumped-storage power plants, which, acting as energy storage facilities, should in the future constitute an important element of the Polish energy system. The possibility of using defunct lignite mining pits for this purpose is indicated. It is shown that some of Poland's former lignite mines are also conveniently located. The possible beneficial impact of building pumped-storage power plants into the water ecosystem of central Poland is emphasised.

Keywords: water, renewable energy, pumped-storage power plants, Poland, European Union

Received July 2023, accepted November 2023.

Introduction

Hydropower was one of the first sources of energy to be used by humans to facilitate and speed up various types of work. It is based on the simple principle of harnessing the kinetic energy of falling water to drive a turbine. In this way, the movement of the water is converted into mechanical and electrical energy. It is a simple process that can provide electricity very efficiently and reliably (Egré, D. and Milewski, J.C. 2002). This renewable energy source varies in popularity around the world, mainly due to differences in individual regions' potential in terms of size of water resources and appropriate topography. In Europe, it has increased in importance significantly in the last 20–30 years due to many countries' change in approach to climate protection. Countries of the European Union (EU) have particularly ambitious climate protection plans. This is reflected in the fact that 37.5 percent of the electricity consumed in the EU came from renewable sources in 2021. Hydropower accounted for, in turn, 32.1 percent of that, making it the second largest renewable source in total EU electricity consumption (Eurostat, 2021). Gaudard, L. and Romeiro, F. (2014) note that hydropower seems to have a promising future and can play an important role in Europe's energy transformation. However, in recent years,

[1] Department of Geomatics and Cartography, Faculty of Earth Sciences and Spatial Management, Nicolaus Copernicus University in Toruń. Lwowska 1, 87-100 Toruń, Poland. E-mail: piasecki@umk.pl

hydropower has been developing most dynamically in Asian countries (Zimny, J. *et al.* 2013). Globally, despite various other renewable energy sources growing rapidly, hydropower remains the largest renewable source of electricity, generating more than all other renewable technologies combined. In 2021, global electricity production from hydropower was 4,327 TWh (IEA, 2022).

In December 2019, the European Commission presented the European Green Deal. It is a package of legislative proposals to adapt the EU's climate, energy, transport and tax policies to meet the goal of reducing net greenhouse gas emissions by at least 55 percent by 2030. As an EU member, Poland is obliged to implement common policies in many areas, as defined by relevant regulations, directives and other legal acts. One area to which common EU policy applies is broadly understood environmental protection, including that relating to climate change. For Poland, the most important elements of the European Green Deal include guidelines for decarbonising the EU energy system. The main objective is to reduce, in the EU, greenhouse gas emissions from the use and production of energy (European Commission, 2019). Poland, whose electricity generation is based on bituminous coal and lignite (about 70%), must implement measures to meet the requirements set out in the European Green Deal. It should be noted that Poland has long been working to transform its energy system towards renewable energy sources.

With this in mind, consideration should be given to the place of hydropower in electricity generation in Poland for the coming years. Of the arguments supporting the importance of hydropower in Poland's energy mix, three are perhaps most important. One is the fact that it is far less sensitive to weather variability and seasonality than the other renewable energy sources that are currently most popular (wind and solar). This is an extremely important factor for maintaining the stability of the country's energy system. Another relates to the issue of Poland's limited water resources in the context of changing climatic conditions these resources can be increased by slowing down outflow with hydroelectric dams. A third important argument is the long history of hydropower in Poland. This applies especially to small hydropower plants, as discussed in detail later in the text. These arguments and the need to implement the guidelines contained in the European Green Deal allow us to pose the following research questions: What is the future of the Polish hydropower industry? Is hydropower needed in Poland? Is the European Green Deal the last chance to develop hydropower in Poland? In what direction should hydropower develop in Poland, bearing in mind the environmental, socio-economic and legal conditions? The present work aims to answer these questions. The following specific objectives were helpful in this regard:

– to analyse the current state of hydropower in Poland,
– to analyse the legal and environmental conditions for the development of hydropower in Poland,
– to indicate possible directions for hydropower development in Poland until 2050, taking into account the requirements of the European Green Deal.

Methods and materials

The research issues discussed herein are considered comprehensively, taking into account environmental, socio-economic and legal conditions. This required the use of several research methods. The basic method was logical argumentation, which was based on a critical analysis of planning documents and scientific papers – in total, about 100 of them were collected (all were available online). Ultimately, only a portion of these studies were used in the work, mainly due to the validity of the data and information they contained. *Table 1* summarises the most important planning documents and reports used in the work. The remaining literature (scientific articles) included in the study are cited in the body of the text. The descriptive method and the formal dogmatic method were used in

Table 1. The most important planning documents and reports used in the work

Document name	Document type	Main focus	Scale	Year of issue	EU connection
National renewable energy action plan	Planning and design	Information on goals and course for the use of renewable energy in Poland until 2020	National	2011	Reflecting EU values
Water management in Poland in 2020–2021	Report on completed task	Contains information on state of water resources in Poland and implementation of water management plans in river basin areas	National	2022	Reflecting local legal regulations
National energy and climate plan for 2021–2030	Planning and design	Sets Poland's climate and energy targets for 2030	National	2019	–
Poland's energy policy until 2040	Planning and design	Sets the framework for energy transformation in Poland up to 2040	National	2021	Implementation of EU energy and climate policy
Report: Small hydropower plants in Poland	Conceptual	Report contains proposals for regulatory changes to support development of small hydropower plants	National	2022	Reflecting local legal regulations
National Development Strategy	Conceptual	Development goals for the country	National	2019	Reflecting EU values
Krakow spatial plan	Planning and design	Technical realisation for infrastructure	Local	2022	Reflecting local legal regulations
Energy transformation in Poland	Report	Contains analysis of energy market in Poland over the last 10+ years	National	2023	Reflecting EU values
Report: Polish energy transition path	Report	Presents Poland's achievements in energy transformation. Also indicates near-future challenges for energy sector	National	2022	Reflecting local legal regulations and reflecting EU values

the legal analysis. The legal analysis also included comparative legal remarks. The legal analysis cites relevant legal acts. To achieve the research goal, research techniques such as literature review, geo-analysis and data interpretation were used. The literature review was used to determine the current state of knowledge about the research problem. The geo-analysis included data on electricity generation in Poland and on the relationship between electricity consumption and generation by voivodeship. These data were obtained from the Local Data Bank of Statistics Poland. The data were interpreted and the spatial relationships between them and selected natural conditions were identified.

Environmental conditions for hydropower development in Poland

For water to play a significant role as an energy source in a country, appropriate natural conditions are required. The most important

elements in this respect are adequate water resources and topography. Poland has some of the lowest water resources in Europe. The average annual sum of precipitation is 600 mm. Long-term average total surface water resources do not exceed 62 km^3. Most of Poland has a typical lowland topography. Only the south is decidedly more diverse, with an upland and mountainous character. The arrangement of southern uplands and central and northern lowlands means that the main direction of water outflow is northward. As a result, 95 percent of Poland belongs to the Baltic Sea catchment basin (Gutry-Korycka, M. *et al.* 2014).

An important factor limiting the development of hydropower in Poland is the spatial differentiation of surface water resources. This is well portrayed by the unit outflow coefficient, which ranges from 4 dm^3/s/km^2 in the Wielkopolskie-Kujawskie Lakeland to over 50 dm^3/s/km^2 in the mountain areas. The average value for Poland is 5.5 dm^3/s/km^2 (Jokiel, P. 2004). Attention should also be paid to the high seasonal and annual variability of precipitation sums. For example, in the city of Toruń in north-central Poland, over the last 15 years, annual precipitation has varied between 380 mm (2015) and 832 mm (2010).

The location of large hydropower plants in Poland has been determined by the presence of the most favourable natural conditions. In the case of small hydropower plants (SHPs), regional cultural considerations and histories have been an additional important factor. This results directly from the original function of dams on small watercourses in what is today Poland. They were used to drive water mills that ground grain into flour and groats.

The current state of hydropower in Poland

The potential for hydropower in Poland is small, ranging, according to various sources, from 8 to 14 TWh per year (Kowalczyk, K. and Cieśliński, R. 2018). At the same time, it is estimated that about 5 TWh falls on SHPs of up to 10 MW each (Gajda, P. 2022). These values are very small relative to European or global resources (rational European resources are technically estimated at about 1,120 TWh/year, and global resources at 8,000–26,000 TWh) (Szulc, P. and Skrzypacz, J. 2022). Poland's hydropower potential is concentrated mainly in the basins of its two largest rivers, i.e., the Vistula basin and the Odra basin, which account for 9.3 and 2.5 TWh per year, respectively *(Figure 1).* Meanwhile the potential of the Vistula river itself is 6.2 TWh per year. Taking into account Poland's annual electricity consumption of about 180 TWh (which translates into 4,700 kWh *per capita*), this hydropower potential is very small. The share of hydropower in electricity generation in Poland has been below 2 percent for many years.

Hydropower in Poland is mainly based on run-of-river power plants, conventional impoundment plants and pumped-storage plants (Novak, P. *et al.* 2007). In the 1920s and 1930s, there were over 6,800 hydropower plants operating in the country. After World War II, the number decreased, but until the 1950s there were an estimated 6,500 hydropower plants (Wiatowski, M. and Rosik-Dulewska, C. 2012). Currently, there are 788 hydropower plants operating in Poland, only 18 of whose capacity exceeds 5 MW *(Figure 2).*

The largest hydropower plant in Poland in terms of power (excluding pumped-storage power plants) is the Włocławek Power Plant. It has six hydropower units with a total installed capacity of 160.2 MW (Igliński, B. 2019). Other power plants have a much lower capacity, ranging from a few (e.g., Bielkowo Power Plant – 7.2 MW) to a few tens of MWs (Rożnów Power Plant). The capacity of commercial hydroelectric power plants in Poland is 2,042 MW, but as much as 1,366 MW is at pumped-storage power plants (Małecki, Z.J. *et al.* 2015). There are currently six pumped-storage power plants operating in Poland *(Table 2, Figure 2).* They are tasked with stabilising the power grid during the day (Igliński, B. *et al.* 2022). The total capacity of hydropower plants in Poland is 2,042 MW, of which the vast majority (~ 67%) is in pumped storage, which is best suited to catering to peak demand (Kalda, G. 2014).

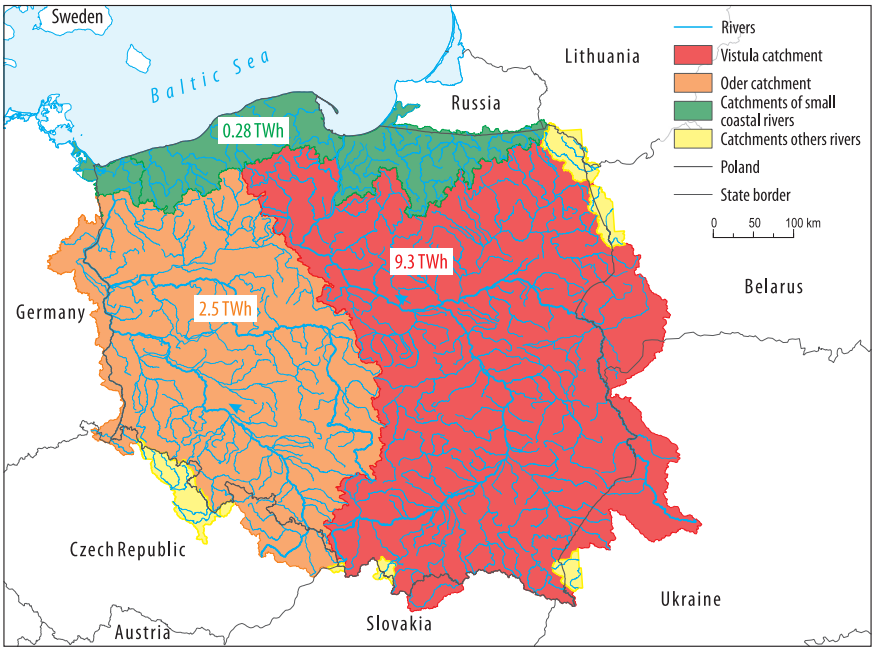

Fig. 1. Hydropower potential of Polish rivers

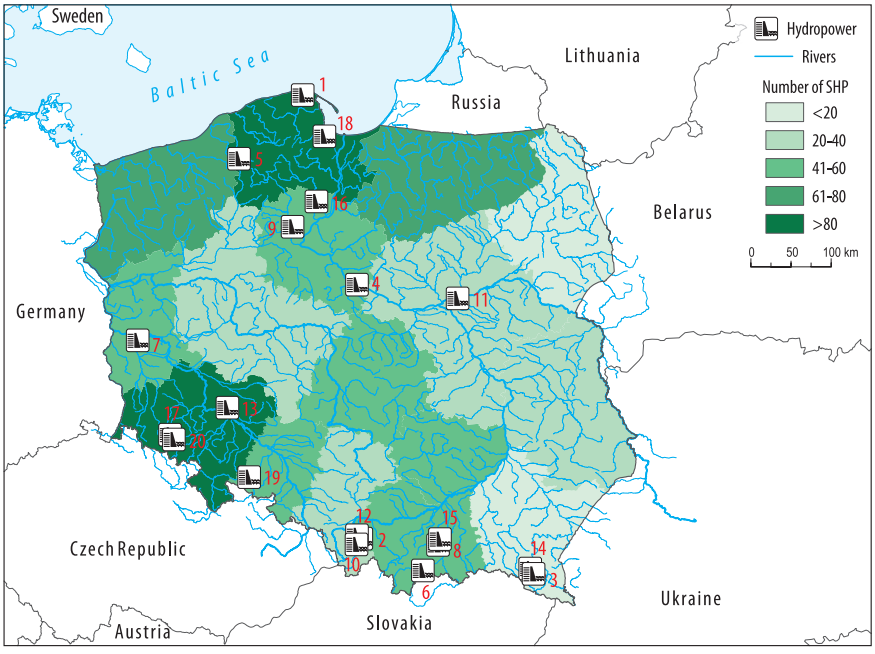

Fig. 2. Locations of the largest hydroelectric power plants in Poland and concentrations of small hydropower plants (SHPs) of ≤ 5 MW by voivodeship. 1–20 in red colour = numbering of power plants (see *Table 2.*)

Table 2. The largest hydroelectric power plants in Poland

Number	Hydroelectric power plant	Power plant type	River/Lake	Installed power, MW	Reservoir volume*, million m^3	Year of built
1	Żarnowiec	pumped-storage	Żarnowieckie	716.0	13.8	1983
2	Porąbka - Żar	pumped-storage	Soła	500.0	2.0	1979
3	Solina	pumped-storage	San	200.0	472.0	1969
4	Włocławek	run-of-river	Vistula	160.2	408.0	1970
5	Żydowo	pumped-storage	Jezioro Kamienne/ Jezioro Kwiecko	157.0	8.9	1971
6	Niedzica	pumped-storage	Dunajec	92.7	168.6	1997
7	Dychów	pumped-storage	Bóbr	88.0	4.0	1951
8	Rożnów	impoundment	Dunajec	50.0	165.0	1941
9	Koronowo	impoundment	Brda	26.0	80.6	1961
10	Tresna	impoundment	Soła	21.0	94.6	1966
11	Dębe	run-of-river	Narew	21.0	94.3	1963
12	Porąbka	impoundment	Soła	12.6	26.6	1954
13	Brzeg Dolny	run-of-river	Odra	9.8	5.3	1912
14	Myczkowice	run-of-river	Soła	8.3	10.9	1960
15	Czchów	run-of-river	Dunajec	8.0	8.0	1951
16	Żur	run-of-river	Wda	8.0	16.0	1930
17	Pilchowice	impoundment	Bóbr	7.9	50.0	1912
18	Bielkowo	impoundment	Radunia	7.2	no data	1930
19	Otmuchów	impoundment	Nysa Kłodzka	4.8	130.0	1933
20	Bobrowice	impoundment	Bóbr	2.5	54.0	1925

*For pumped-storage plants, the usable volume of the upper reservoir is given.

There are 770 SHPs of capacity up to 5 MW in Poland. These are significantly fewer SHPs than the 6,800 SHPs of the 1920s and 1930s. However, it should be noted that a significant proportion of the SHPs from the beginning of the 20th century were water mills that used mechanical energy to, for example, grind grain into flour. The requirements for and purposes served by SHP were entirely different at the beginning of the 20th century than today. This should, thus, be taken into consideration when comparing current numbers of SHPs against those of over 100 years ago. Currently, most are located in northern Poland, where precipitation, topography and geological structure are favourable. The second area with a higher density of SHPs is the mountain and foothill areas in the south of the country. The high hydropower potential of these areas results from their having significant differences in terrain elevation and the country's largest sums of precipitation.

The total installed capacity of SHP is 255.5 MW, i.e., 26.2 percent of the total capacity of hydropower plants in Poland. In terms of the breakdown of electricity production in Poland, hydroelectric power plants supply only about 2 percent of energy to the system (Marszelewski, M. and Piasecki, A. 2022). In 2021, over 180 GWh of energy was produced by small hydropower plants. This source provided 34 percent of the energy generated by all small renewable energy sources (RES) installations in Poland (Energy Regulatory Office, 2022).

As noted by Kasperek, R. (2020), Poland is currently using about 20 percent of its technical hydropower potential. Of the approximately 14,000 dams in Poland whose head exceeds 0.7 m, less than 5 percent is used for energy purposes (Gajda, P. 2022). Therefore, Poland has significant opportunities for hydropower development, especially in SHPs.

The development of hydropower in Poland until 2050

Strategic plans for the development of Poland's energy system, including hydropower, must take into account global changes in the approach to obtaining, storing and transmitting energy. In this regard, attention should be paid to the approach of the International Energy Agency (IEA). This institution's publications are the most authoritative source of analyses and forecasts of energy supply and demand for the coming decades. In one of its latest reports, the IEA drew attention to the need for more work on obtaining net-zero emissions by 2050 as the basic thrust of activities. The goal is to limit global warming to 1.5 °C and avoid the worst impacts of climate change (IEA, 2021). This approach is fully in line with EU actions and the European Green Deal. In its report, the IEA emphasises that hydropower is the largest source of renewable energy in terms of power and generation. At the same time, the observed upward trends in power generation are insufficient to place the energy source on a trajectory congruent with the net-zero scenario. The reason is the too-slow increase in hydropower capacity, along with the simultaneous increasing disruptions to water availability caused by climate change. Another important element is the poor technical condition of many hydropower plants as a result of their long-term operation. Many developed countries' hydropower plants were built mainly in the 1960s and 1980s (Farfan, J. and Breyer, C. 2017). It is estimated that almost 40 percent (476 GW) of the world's hydropower plants are at least 40 years old (the average age is 32). When hydropower plants are 45–60 years old, major upgrades and renovations are required (IEA, 2022). Environmental and legal changes since most power plants were commissioned also constitute an important issue. This mainly concerns changes in the flow (ensuring the minimum flow required to maintain ecological status in the watercourse), as well as detailed environmental protection regulations. These factors mean that it may not always be possible to temporarily shut down hydropower plants for refurbishment and then restart them at the previous level. Under current legal and environmental conditions, some hydropower plants may be able to produce only a certain percentage of the energy previously generated.

When planning the development of hydropower in Poland, experiments – and changes – in the approach to this energy source in other highly developed countries should be taken into account. The United States is a good example, where The New Deal initiated in the 1930s contributed to, among other things, the construction of many hydropower plants. As a result, within 20 years, hydropower generation tripled, providing about 40 percent of the electricity in the United States. In the following years, rapid growth in nuclear, gas and coal-fired power plants saw the share of hydropower in the USA fall to ~ 6 percent. However, importantly, since the 1990s there has been a rapid increase in the number of damming structures being liquidated in the USA. According to O'Connor, J.E. *et al.* (2015), 147 dams were closed in the years 1986–1995, 298 dams in 1996–2005, and 548 ones in 2006–2014. The reason was the poor technical condition of many dams built before 1950. They require urgent repair, which in many cases is too expensive. Furthermore, many of them no longer fulfil their original function, and their negative environmental impacts have become unacceptable. A similar trend towards liquidating dams is seen in Europe (Moran, E.F. *et al.* 2018). In the European Union, much of the available hydropower potential was developed in the 20th century. As noted by Kougias, I. *et al.* (2019) Europe's aging hydropower plants will soon need refurbishing to extend their lifespan, resolve ownership and operational issues, and increase safety. These activities should focus mainly on electromechanical instrumentation and control systems.

Currently, new hydropower plants are mainly being built in developing countries, where environmental standards are much lower or entirely disregarded. These are

very commonly huge projects that often repeat mistakes already identified in highly developed countries. This applies particularly to disrupting river ecology, deforestation, loss of water through evaporation, loss of terrestrial biodiversity, and the displacement of thousands of people (Stone, R. 2011; Fearnside, P.M. and Pueyo, S. 2012; Benchimol, M. and Peres, C.A. 2015; Moran, E.F. *et al.* 2018; Frolova, M. *et al.* 2019). In Europe, hydroelectric power plants are considered to have a negative impact on protected areas. Their interference in the natural environment is also one of the reasons for the failure of many river sections to be assessed as satisfactory according to Water Framework Directive indices (Lange, K. *et al.* 2018). Furthermore, according to recent studies, hydropower reservoirs annually emit methane, carbon dioxide and other greenhouse gases approximately equivalent to 1.07 Gtons of carbon dioxide (Harrison, J.A. *et al.* 2021; Mikulski, A. 2022). Particularly large amounts of greenhouse gases are generated by hydroelectric power plants located in tropical regions (Fearnside, P.M. 2005). Studies have confirmed that this negative phenomenon also applies to the reservoirs of hydropower plants in temperate climatic zones (Trojanowska, A. *et al.* 2009; Scherer, L. and Pfister, S. 2016; Miller, B.L. *et al.* 2017).

In the last few years, along with the EU's increasing promotion of the zero-emission policy and the adoption of the European Green Deal strategy, interest in small hydropower plants has increased in Poland. According to Renewable Energy Sources Transforming Our Regions (RESTOR) Hydro, an EU-funded project, there are over 8,000 potential locations for the construction of SHPs in Poland (Marszelewski, M. and Piasecki, A. 2022). According to another study prepared for the Minister of the Environment, nearly 13,500 damming structures have been identified in Poland that, for socio-economic reasons, can be used for energy purposes (Malicka, E. 2022). A great advantage of SHP is its location close to its energy consumers. This eliminates the energy losses to transmission, transformation and distribution that large power plants incur and that in Poland amount to more than ten percent (Igliński, B. 2019). Other positive aspects of the construction of SHPs are efficiency, safety and being based on a domestic energy source. Importantly, however, in many cases, SHPs are created in places that have already been transformed by man for the needs of watermills, sawmills, etc. (Radtke, G. *et al.* 2012). SHPs also negatively affect the natural ecosystem by disturbing existing hydrological and hydro-morphological processes. They can also significantly change and deplete flora along dammed sections of rivers (Jansson, R. 2002) and cause declines in invertebrate taxa (Growns, I.O. and Growns, J.E. 2001). However, it should be emphasised that the occurrence of any of these negative effects related to the construction and operation of an SHP is conditioned by local natural factors and technical solutions applied.

In March 2021, the document *Polish Energy Policy until 2040* was published. It sets out a framework for the energy transformation in Poland. It contains a strategy for selecting technologies for the construction of a low-emission energy system. The study clearly shows that, due to its low potential in Poland, hydropower will not play a significant role in the country's energy transformation. The document concludes that generation by hydropower plants in Poland will increase from 2.4 TWh in 2020 to 3.1 TWh in 2040 – an increase of just 0.7 TWh. The analogous increases for wind and solar generation are estimated at 31.7 and 12.8 TWh, respectively.

The age and technical condition of Poland's hydropower plants accord with the IEA's description of the world's hydropower plants. Most hydropower plants in Poland were built in the 1960s and 1970s. Inspections of structures that permanently dam water (and, thus, not only hydroelectric power plants) carried out in the years 2000–2009 showed that the condition of 17 structures was hazardous, and 82 structures were potentially hazardous. The main reasons, apart from the aging of the construction, were insufficient financial outlays

for renovations, and the theft and vandalism of construction elements (Świderska, I. and Lebiecki, P. 2011). The rating for the largest run-of-river power plant in Poland, i.e., the Włocławek power plant, should be considered particularly disturbing. It has indicated that the Włocławek dam may pose a threat to safety (Świderska, I. and Lebiecki, P. 2011). This is mainly due to the Włocławek facility being operated in completely different hydraulic conditions than were originally assumed in its design. The dam in Włocławek was designed as part of the Lower Vistula Cascade of eight dams planned in the lower section of the Vistula. The plans were not implemented, and only one stage was built. This has had many unfavourable consequences – in particular, accelerated erosion of the riverbed causing rapid and excessive lowering of the bottom. As a result, the water level in the river was lowered over a more-than-30-km section downstream of the dam. The lowering of the bottom has already exceeded the projected values several times over (Bagiński, L. 2007). Inspections of the technical condition of dams in Poland in successive years have confirmed the poor condition of some of them.

According to a report by the Supreme Audit Office (2016), which covered only the most important damming structures in Poland (122 first- and second-class objects were assessed), the safety condition of 12 constructions was assessed as potentially dangerous and one as dangerous. The main reasons for the deteriorating technical condition of the constructions were: age (about 70% are more than 30 years old), design errors, faulty execution of works and delays in renovation and modernisation works (SAO, 2016). The last assessment of the technical condition of dams, covering 313 structures, was carried out in 2020–2021 and showed that the condition of 19 structures poses a threat to safety (Ministry of Infrastructure, 2022). With this in mind, one might be concerned that increasing the number of such facilities will further degrade the technical condition of the damming structures. One of the main reasons for this assessment is that the limited financial resources would have to be allocated to a larger number of facilities.

Pumped-storage power plants are the exception to these remarks concerning the development of hydropower in Poland. Such hydropower plants have the potential to significantly increase in importance in the Polish energy system. The main reason is related to the dynamic growth in other renewable energy sources in Poland – particularly of wind and photovoltaic energy. Wind and solar energy entail problems stemming from their heavy dependence on inherently unpredictable weather conditions. This variability means that they do not generate a reliably steady supply of energy. This is one of the biggest drawbacks of renewable energy. In Poland, despite the still relatively small amount of energy from renewable sources, there have been days on which energy production needed to be curtailed (mainly on wind farms). Therefore, installations that allow electricity to be stored temporarily are urgently required. Pumped-storage power plants are a very good such solution. It should be noted that their construction and operation also have a significant environmental impact, but one that is usually significantly lower than for run-of-river power plants. In Poland, the area with the most urgent need to build pumped-storage power plants is the north. In this area, the temporary overproduction of energy from renewable sources is most common. This is due to the area having the most favourable conditions for wind farms (onshore and offshore) but lower-than-average energy consumption (fewer large cities and energy-intensive industries).

Piasecki, A. and Krzywda, M. (2018) have indicated 37 potential locations for pumped-storage power plants in northern Poland. They also determined their storage potential at 62.8 GWh. Another interesting direction for the expansion of pumped-storage power plants is to exploit disused coal-mining pits. This solution helps limit interference with the environment, while also significantly reducing total project costs (those related

to the purchase of land, the construction of a reservoir basin, etc.). There are open-pit lignite mines in central and south-western Poland. Of particular importance may be open-pit lignite mines exploited in central Poland, within the Wielkopolsko-Kujawskie Lake District *(Figure 3).*

In recent years, this area has seen a dynamic growth in wind and photovoltaic power plants. This fact should be assessed as very positive, given the insufficient level of electricity generation in this part of the country. In all voivodeships of western Poland (except West Pomeranian Voivodeship) there is an electricity generation deficit in excess of 20 percent (see *Figure 3*). The shortfall in energy must be sent from other parts of the country, resulting in losses to transmission networks. Nevertheless, the continued rapid growth in power plants generating energy from renewable sources in the area will, over time, create conditions for the construction of energy storage facilities. The use of disused mining pits for this purpose seems like the best solution. Especially if we also consider this area's difficult water relations. This is due to low precipitation totals (about 500 mm) and to evaporation that is both high and, in recent years, trending upwards (Piasecki, A. and Marszelewski, W. 2014). The construction of pumped-storage power plants will allow a large amount of water to be retained in this area and will somewhat stabilise the water table. At the same time, there will be a significant increase in evaporation from the water surface. However, the resulting water losses could be largely compensated by retaining the elevated amounts of precipitation that every few years occur in the area. This would require the introduction of appropriate solutions for the management of local water resources. This topic requires a detailed analysis and additional research that are beyond the scope of this study and will therefore be developed in a separate study. Therefore, in the publication below, this solution should be treated as a concept of sorts. Nevertheless, simulations and models of the operation of pumped-storage power plants in disused mining pits in Poland have confirmed the significant potential of this solution (Jurasz, J. *et al.* 2018; Oprychał, L. and Bąk, A. 2022).

Summarising the above considerations, it needs to be clearly recognised that significant growth in hydropower in the coming years is very unlikely in Poland (other than pumped storage power plants). The main reason is the low hydropower potential of Polish rivers. Social and environmental aspects are also extremely important. As indicated, the greatest hydropower potential in Poland is to be found in the Vistula river, particularly its lower section and the unfinished plan for the so-called Lower Vistula Cascades. However, any serious attempt to implement the abandoned plans would be met with numerous protests from local communities and pro-ecological circles, as has been the case in other countries (Operacz, A. 2017). This is especially so given that the area that would be flooded is currently covered by various forms of nature protection, e.g. reserves, Natura 2000 areas (bird areas, habitat areas), landscape parks and ecological land uses. There is a much better chance of measures aimed at building new SHPs being implemented. It should be emphasised that, even if all the locations indicated in the aforementioned studies were developed, this would allow for only a relatively small increase in the amount of energy generated – estimates say about 5 TWh (Gajda, P. 2022).

Discussion

Compared to other countries in Europe and the world, Poland has a relatively low hydropower potential (Kjaerland, F. 2007; Berkun, M. 2010; Cyr, J.F. *et al.* 2011; Pereira, M.G. *et al.* 2012; Kowalczyk, K. and Cieśliński, R. 2018). The main reason for this is the country's natural conditions, which, as already mentioned, largely determine the technical and economic possibilities. According to the *Hydropower-Europe Report* (2022) (implemented as part of the European Union's Horizon

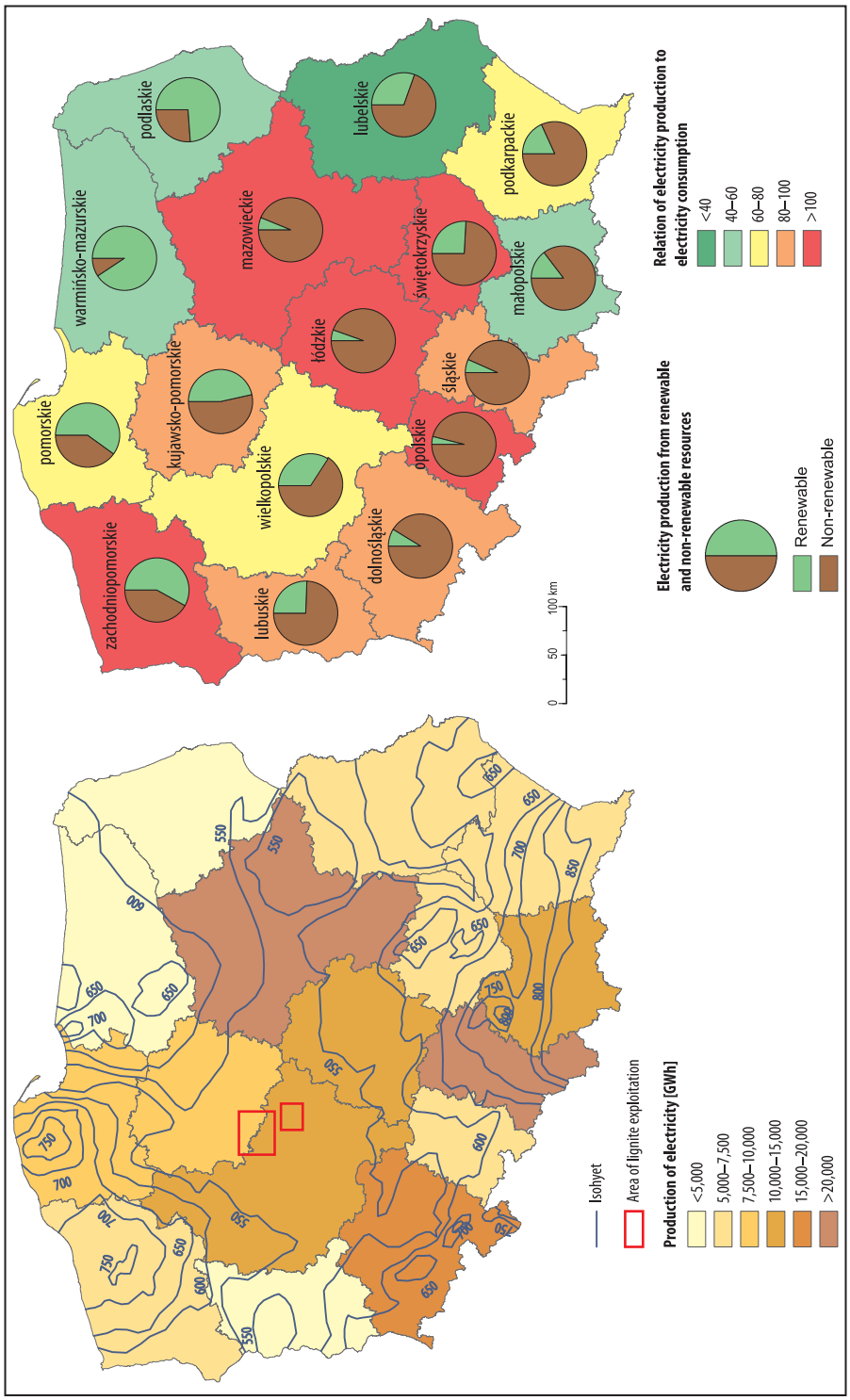

Fig. 3. Selected electricity production data for Poland by voivodeship against the background of precipitation conditions and lignite mining locations

2020), Poland is only 24th in Europe in terms of hydropower potential and 25th in terms of the amount of energy generated from hydroelectric power plants. At the same time, many authors point out that only 20 percent of the technical potential of Poland's hydropower industry is currently being used (Baczyński, D. and Kosiński, K. 2018; Kasperek, R. 2020; Piwowar, A. and Dzikuć, M. 2022). As already shown, no dramatic increase in the use of hydropower potential should be expected in the coming years in Poland. Poland is not alone in this regard; this conclusion can be generalised to all EU countries.

The implementation of the *Water Framework Directive* 2000/60/EC (WFD) and the *Habitats Directives* 92/43/EEC26 and 2009/147/EC have significantly limited the possibility of building new hydroelectric plants in the EU. Many countries that planned to develop hydropower as part of the energy transformation had to change their plans. One example is Slovakia, where more than a decade ago there were plans to build several large hydroelectric power plants. Similarly, Hungary decided to limit the development of hydropower to SHPs, and, thus, uses 5 to 6 percent of its potential (Steller, J. and Malicka, E. 2020). Moreover, attention should be paid to the increasingly frequent demolition of hydropower facilities in Europe. This applies especially to small plants, about 5,000 of which have been removed in the last 25 years (Wagner, B. *et al.* 2019). The international initiative "Dam Removal Europe" (DRE, 2023) is very important in this respect. In 2022 alone, it contributed to the removal of 325 dams on rivers in 16 countries in Europe. However, it should be emphasised that even building SHPs at all possible locations (as indicated, for example, in the RESTOR Hydro programme) would not significantly affect the structure of electricity production in Poland and other EU countries. The amount of energy that new SHPs could generate is decidedly too small, as the example of Poland shows.

Currently, in Poland (and most EU countries), the only significant and realistic potential in the field of hydropower lies in pumped-storage power plants. One of the consequences of the energy transformation underway in Poland and other EU countries is temporary difficulties in balancing the demand and supply sides of the electricity market. The reason is that the most frequently used renewable energy sources – wind and solar – are dependent on weather conditions, which are inherently unstable (Gøtske, E.K. and Victoria, M. 2021). This reality necessitates the temporary storage of generated electricity. The promotion of solutions based on energy storage in the form of batteries and accumulators in the public debate is controversial. Pumped-storage power plants, even small ones, can store much more energy than currently available battery storage facilities. As already mentioned, the construction of pumped-storage power plants involves interfering with the natural environment. However, it should be noted that the production and disposal of batteries used for energy storage also have negative environmental consequences (Mrozik, W. *et al.* 2021).

Many of the mineral raw materials used to produce batteries come from underdeveloped countries, where generally low environmental protection standards apply. In the case of building pumped-storage power plants in EU countries, the legal regulations minimise negative environmental consequences. Moreover, some of these negative consequences can be reduced by using existing facilities. One such solution involves the use of lignite mines in Poland, a discussed in the previous chapter. In addition to the capacity to temporarily store energy, pumped storage also increases local water resources. Another solution exploits the large height differences provided by some mixed-use blocks in cities. In the work of Jurasz, J. *et al.* (2022), it was demonstrated on the example of the city of Toruń (Poland) how to effectively use tall buildings in the city to build an energy storage facility operating on a principle similar to that of pumped-storage power plants.

The construction and operation of run-of-river hydroelectric power plants involve significant interference in the natural en-

vironment, as discussed in detail in earlier chapters. Most rivers in the EU are covered by various forms of nature protection, which further complicates the possibility of implementing hydropower projects. In this context, we provide the example of the Vistula river and the unfinished cascade of dams on its lower section. However, similar examples of unimplemented or only partially completed investments can also be found in Hungary, Slovakia, Romania and Serbia (Nakamichi, M. 1997; Szabó, M. and Kiss, Á. 2014; Năstase, G. *et al.* 2017). It should be noted that modern technological solutions can minimise some of the negative consequences of the operation of the type of hydropower plants that we have discussed here. A good example is the use of solutions that ensure free passage for fish and free flow of sediments. This also applies to the use of the latest technological solutions, including damless hydrokinetic energy conversion systems (Wagner, B. *et al*. 2019). The use of these solutions usually significantly increases investment costs, so they are not always profitable. Therefore, investments in hydroelectric power plants usually require additional financial support from state institutions. In the case of EU countries, financial support is mainly dedicated to SHP. For example, in Poland, the "Energy for the countryside" programme came in operation in 2023, providing beneficiaries with funding for investments in hydropower with a capacity of no more than 1 MW. In the case of large run-of-river power plants, co-financing is provided for projects related to modernisation and improved efficiency of operation.

In recent years, the energy transformation process has become more dynamic in EU countries. This was largely due to external factors. This applies especially to the war in Ukraine and the limitation or cessation of imports of Russian raw materials for energy generation. In early 2023, EU lawmakers reached a provisional agreement on the *Renewable Energy Directive* (*RED III*) (European Council, 2023). The goal of *RED III* is to increase the share of renewable energy in total energy consumption in the EU to 42.5 percent by 2030. The current structure of electricity production in individual EU countries is highly diversified. With some exceptions (Romania, Croatia, Lithuania and Latvia), the largest share of renewable energy in the energy production structure (above 35%) is recorded in the so-called old union (Eurostat, 2023). Only in Belgium and France is the percentage of energy from renewable sources lower (27 and 25%, respectively), due to the very high share of nuclear energy (above 45%). In Poland, the share of renewable energy in the electricity production structure is 22 percent.

The legal regulations contained in *RED III* are intended to help achieve the ambitious EU goals for energy from renewable sources. They will provide member countries the opportunity to designate renewable energy acceleration areas in which renewable energy projects will be subject to a simplified and expedited permit process. If hydropower were included among these acceleration areas, it would be possible to implement many investments related to hydropower (European Council, 2023). It should be noted, however, that already at the beginning of 2023, several hundred NGOs operating within Living Rivers Europe asked the EU authorities to at least exclude hydropower from "target areas" and apply strict sustainability criteria to it. Since appeals by environmental organisations are often acted upon by the EU, it is difficult to assume that hydropower will ultimately be included as target areas for renewable energy acceleration.

Conclusions

The analysis of the state of hydropower in Poland indicates that it requires urgent intervention in many areas. This applies particularly to issues of the control, modernisation and technical condition of hydropower plants and damming facilities. The potential for the development of hydropower in Poland is assessed to be very small. Environmental, socio-economic and legal conditions are unfavourable to the

construction of new, large hydropower plants. The exception is pumped-storage power plants, which, acting as energy storage facilities, should in the future constitute an important element of the Polish energy system. The possible development of small hydropower plants is also indicated, provided that appropriate incentives and financial assistance, as well as favourable legal conditions, are provided.

Poland faces challenges related to the country's energy transformation towards renewable energy sources. According to the assumptions of *RED III*, in less than a decade the country should double the share of green energy in the total production structure. Wind and solar energy will probably play the largest part in Poland's energy transformation. However, due to their specificity, both of these energy sources require the creation of local energy-storage facilities. Thus, the European Green Deal may contribute indirectly to the significant development of hydropower in Poland. Currently, it is impossible to provide an unambiguous answer to the titular question of this study, because it depends largely on state policy. Nevertheless, the European Green Deal is a great opportunity for the development of hydropower (in the field of electricity storage) in Poland, which would be worth taking advantage of for many reasons indicated in the article.

REFERENCES

Baczyński, D. and Kosiński, K. 2018. Possibility of power generation control in small hydro installations for a period of several days. *Energy Policy Journal* 4. 65–86.

Bagiński, L. 2007. Selected problems of the safety status of the Włocławek barrage. *Nauka Przyroda Technologie* 1. (2): 12.

Benchimol, M. and Peres, C.A. 2015. Widespread forest vertebrate extinctions induced by a mega hydroelectric dam in Lowland Amazonia. *PLoS One* 10: e0129818.

Berkun, M. 2010. Hydroelectric potential and environmental effects of multidam hydropower projects in Turkey. *Energy for Sustainable Development* 14. (4): 320–329. Available at https://doi.org/10.1016/j.esd.2010.09.003

Cyr, J.F., Landry, M. and Gagnon, Y. 2011. Methodology for the large-scale assessment of small hydroelectric potential: Application to the Province of New Brunswick (Canada). *Renewable Energy* 36. (11): 2940–2950. Available at https://doi.org/10.1016/j.renene.2011.04.003

DRE 2023. *Dam Removal Europe 2023. An international initiative*. Powered by WFMF. Available at https://damremoval.eu/

Egré, D. and Milewski, J.C. 2002. The diversity of hydropower projects. *Energy Policy* 30. (14): 1225–1230.

Energy Regulatory Office 2022. *Report of the President of the Energy Regulatory Office for 2020 – Electricity generation in Poland in small renewable energy installations.* Warsaw, ERO. Available at https://www.ure.gov.pl/download/3/14992/RAPORTART17ZA2021.pdf

European Commission 2019. *Communication from the Commission to the European Parliament, the European Council, the Council, the European Economic and Social Committee and the Committee of the Regions – The European Green Deal.* Brussels, 11.12.2019 COM (2019) 640 final. Document 52019DC0640.

European Council 2023. *Renewable Energy Directive* (*RED III*). Brussels, European Commission. Available at https://www.consilium.europa.eu/en/press/press-releases/2023/03/30/council-and-parliament-reach-provisional-deal-on-renewable-energy-directive/

Eurostat 2021. Renewable energy statistics. Brussels, European Commission. Available at https://ec-europa-eu.translate.goog/eurostat/statistics-explained/index.php?title=Renewable_energy_statistics&_x_tr_sl=en&_x_tr_tl=pl&_x_tr_hl=pl&_x_tr_pto=wapp#Wind_and_water_provide_most_renewable_electricity.3B_solar_is_the_fastest-growing_energy_source

Eurostat 2023. Renewable energy statistics. Brussels, European Commission. Available at https://ec.europa.eu/eurostat/databrowser/view/NRG_CB_PEM__custom_5180368/default/table?lang=en

Farfan, J. and Breyer, C. 2017. Aging of European power plant infrastructure as an opportunity to evolve towards sustainability. *International Journal of Hydrogen Energy* 42. (28): 18081–18091.

Fearnside, P.M. 2005. Do hydroelectric dams mitigate global warming? The case of Brazil's Curuá-Una Dam. *Mitigation and Adaptation Strategies for Global Change* 10. 675–691.

Fearnside, P.M. and Pueyo, S. 2012. Greenhouse-gas emissions from tropical dams. *Nature Climate Change* 2. 382–384.

Frolova, M., Centeri, Cs., Benediktsson, K., Hunziker, M., Kabai, R., Scognamiglio, A., Martinopoulos, G., Sismani, G., Brito, P., Muñoz-Cerón, E., Słupiński, M., Ghislanzoni, M., Braunschweiger, D., Herrero-Luque, D. and Roth, M. 2019. Effects of renewable energy on landscape in Europe: Comparison of hydro, wind, solar, bio-, geothermal and infrastructure energy landscapes. *Hungarian Geographical Bulletin*

68. (4): 317–339. Available at https://doi.org/10.15201/hungeobull.68.4.1

Gajda, P. 2022. The role of small power plants in the Polish energy transformation. In *Small Hydropower Plants in Poland*. Eds.: Wyszkowski, K., Piwowarek, Z. and Pałejko Z., Warsaw, UN Global Compact Network Poland, 72–74. Available at https://ungc.org.pl/wp-content/uploads/2022/03/Raport_Male_elektrownie_wodne_w_Polsce.pdf

Gaudard, L. and Romeiro, F. 2014. The future of hydropower in Europe: Interconnecting climate, markets and policies. *Environmental Science and Policy* 37. 172–181.

Gøtske, E.K. and Victoria, M. 2021. Future operation of hydropower in Europe under high renewable penetration and climate change. *Iscience* 24. (9): 102999. Available at https://doi.org/10.1016/j.isci.2021.102999

Growns, I.O. and Growns, J.E. 2001. Ecological effects of flow regulation on macroinvertebrate and periphytic diatom assemblages in the Hawkesbury-Nepean river, Australia. Regulated Rivers. *Research & Management* 17. (3): 275–293.

Gutry-Korycka, M., Sadurski, A., Kundzewicz, Z.W., Pociask-Karteczka, J. and Skrzypczyk, L. 2014. Water resources and their use. *Nauka* 1. (2014): 77–98. (in Polish)

Harrison, J.A., Prairie, Y.T. and Mercier-Blais, S. 2021. Year-2020 global distribution and pathways of reservoir methane and carbon dioxide emissions according to the greenhouse gas from reservoirs (G-res) model. *Global Biogeochemical Cycles* 35. e2020GB006888

Hydropower-Europe Report 2022. Final Project Report. London, International Hydropower Association. Available at https://hydropower-europe.eu/private/Modules/Tools/EUProject/documents/68/HPE_FinalProjRep_WP1_Rp_68_v2_1.pdf

IEA 2021. *World Energy Outlook*. Paris, International Energy Agency. Available at https://www.iea.org/reports/world-energy-outlook-2021

IEA 2022. *Hydroelectricity*. Paris, International Energy Agency. Available at https://www.iea.org/reports/hydroelectricity

Igliński, B. 2019. Hydro energy in Poland: The history, current state, potential, SWOT analysis, environmental aspects. *International Journal of Energy and Water Resources* 3. 61–72.

Igliński, B., Krukowski, K., Mioduszewski, J., Pietrzak, M.B., Skrzatek, M., Piechota, G. and Wilczewski, S. 2022. Assessment of the current potential of hydropower for water damming in Poland in the context of energy transformation. *Energies* 15. (3): 922.

Jansson, R. 2002. *The biological cost of hydropower*. CCB Report. Uppsala, Sweden, Coalition Clean Baltic.

Jokiel, P. 2004. *Water Resources of Central Poland on the Threshold of the 21st Century*. Łódź, Poland, Academic Press.

Jurasz, J., Dąbek, P.B., Kaźmierczak, B., Kies, A. and Wdowikowski, M. 2018. Large scale complementary solar and wind energy sources coupled with pumped-storage hydroelectricity for Lower Silesia, Poland. *Energy* 161. 183–192.

Jurasz, J., Piasecki, A., Hunt, J., Zheng, W., Ma, T. and Kies, A. 2022. Building integrated pumped-storage potential on a city scale: An analysis based on geographic information systems. *Energy* 242. 122966. Available at https://doi.org/10.1016/j.energy.2021.122966

Kalda, G. 2014. Analysis of the hydropower industry in Poland. *Journal of Civil Engineering, Environment and Architecture* 61. (4/14): 81–92.

Kasperek, R. 2020. Prospects for the development of hydropower in Poland. *Polish Journal for Sustainable Development* 24. (2): 29–38. Available at http://dx.doi.org/10.15584/pjsd.2020.24.2.3

Kjaerland, F. 2007. A real option analysis of investments in hydropower: The case of Norway. *Energy Policy* 35. (11): 5901–5908. Available at https://doi.org/10.1016/j.enpol.2007.07.021

Kougias, I., Aggidis, G., Avellan, F., Deniz, S., Lundin, U., Moro, A., Muntean, S., Novara, D., Perez-Diaz, J.I., Quaranta, E., Schild, P. and Theodossiou, N. 2019. Analysis of emerging technologies in the hydropower sector. *Renewable and Sustainable Energy Reviews* 113. 109257.

Kowalczyk, K. and Cieśliński, R. 2018. Analysis of the hydroelectric potential and the possibilities of its use in the Pomeranian Voivodeship. *Water-Environment-Rural Areas* 18. (1): 69–86.

Lange, K., Meier, P., Trautwein, C., Schmid, M., Robinson, C., Weber, C. and Brodersen, J. 2018. Basin-scale effects of small hydropower on biodiversity dynamics. *Frontiers in Ecology and Environment* 16. (7): 397–404. Available at https://doi.org/10.1002/fee.1823

Małecki, Z.J., Wira, J. and Małecka, I. 2015. Energy-efficient construction – RES future solutions? *Scientific Journals. Civil Engineering in Environmental Management* 13. 46–55. Available at https://biblioteka-nauki.pl/articles/407594.pdf

Malicka, E. 2022. The state and needs of changes in legal regulations related to the development of small water energy with respect for the environment In *Small Hydropower Plants in Poland.* Eds.: Wyszkowski, K., Piwowarek, Z. and Pałejko Z., Warsaw, UN Global Compact Network Poland, 72–74. Available at https://ungc.org.pl/wp-content/uploads/2022/03/Raport_Male_elektrownie_wodne_w_Polsce.pdf

Marszelewski, M. and Piasecki, A. 2022. Toward to Green Deal legal and natural aspects of the development of small hydropower plants: the example of Poland. *International Journal of Energy Economics and Policy* 12. (4): 249–262.

Mikulski, A. 2022. Wpływ tradycyjnej energetyki wodnej na środowisko (Environmental impact of traditional hydropower). In *Small Hydropower Plants in Poland.* Eds.: Wyszkowski, K., Piwowarek, Z. and

Pałejko Z., Warsaw, UN Global Compact Network Poland, 76–79. Available at https://ungc.org.pl/wp-content/uploads/2022/03/Raport_Male_elektrownie_wodne_w_Polsce.pdf

Miller, B.L., Arntzen, E.V., Goldman, A.E. and Richmond, M.C. 2017. Methane ebullition in temperate hydropower reservoirs and implications for US policy on greenhouse gas emissions. *Environmental Management* 60. 615–629. Available at https://doi.org/10.1007/s00267-017-0909-1

Ministry of Infrastructure 2022. *Water management in Poland in 2020–2021.* Warsaw, Poland, Publication of the Ministry of Infrastructure.

Moran, E.F., Lopez, M.C., Moore, N., Müller, N. and Hyndman, D.W. 2018. Sustainable hydropower in the 21st century. *Proceedings of the National Academy of Sciences* 115. (47): 11891–11898.

Mrozik, W., Rajaeifar, M.A., Heidrich, O. and Christensen, P. 2021. Environmental impacts, pollution sources and pathways of spent lithium-ion batteries. *Energy & Environmental Science* 14. (12): 6099–6121. Available at https://doi.org/10.1039/D1EE00691F

Nakamichi, M. 1997. The International Court of Justice decision regarding the Gabcikovo-Nagymaros Project. *Fordham Environmental Law Review* 9. (2): 337–372. Available at https://ir.lawnet.fordham.edu/cgi/viewcontent.cgi?referer=&httpsredir=1&article=1497&context=elr

Năstase, G., Şerban, A., Năstase, A.F., Dragomir, G., Brezeanu, A.I. and Iordan, N.F. 2017. Hydropower development in Romania. A review from its beginnings to the present. *Renewable and Sustainable Energy Reviews* 80. 297–312. Available at https://doi.org/10.1016/j.rser.2017.05.209

Novak, P., Moffat, A.I.B., Nalluri, C. and Narayanan, 2007. *Hydraulic Structures*. London, Taylor and Francis.

O'Connor, J.E., Duda, J.J. and Grant, G.E. 2015. 1000 dams down and counting. *Science* 348. 496–497.

Operacz, A. 2017. The term "effective hydropower potential" based on sustainable development – An initial case study of the Raba river in Poland. *Renewable and Sustainable Energy Reviews* 75. 1453–1463.

Oprychał, L. and Bąk, A. 2022. Is it worth building the Turów pumped-storage power plant? *Energetyka Wodna* 4. 20–22.

Pereira, M.G., Camacho, C.F., Freitas, M.A.V. and da Silva, N.F. 2012. The renewable energy market in Brazil: Current status and potential. *Renewable and Sustainable Energy Reviews* 16. (6): 3786–3802. Available at https://doi.org/10.1016/j.rser.2012.03.024

Piasecki, A. and Marszelewski, W. 2014. Dynamics and consequences of water level fluctuations of selected lakes in the catchment of the Ostrowo-Gopło Channel. *Limnological Review* 14. (4): 187–194.

Piasecki, A. and Krzywda, M. 2018. Use of pumped-storage hydroelectricity to compensate for the inherent and unavoidable variability of wind energy. *E3S Web of Conferences* 44. 00138.

Piwowar, A. and Dzikuć, M. 2022. Water energy in Poland in the context of sustainable development. *Energies* 15. (21): 7840. Available at https://doi.org/10.3390/en15217840

Radtke, G., Bernaś, R. and Skóra, M. 2012. Small hydropower stations – major ecological problems: some examples from rivers of northern Poland. *Let's Protect our Native Nature* 68. (6): 424–434.

SAO 2016. *Supervision over the technical condition and safety of water damming structures*. Warszawa, Najwyższa Izba Kontroli. Available at https://www.nik.gov.pl/plik/id,10236,vp,12559.pdf (in Polish).

Scherer, L. and Pfister, S. 2016. Hydropower's biogenic carbon footprint. *PLoS One* 11. (9): e0161947. Available at https://doi.org/10.1371/journal.pone.0161947

Steller, J. and Malicka, E. 2020. Poland and Eastern Europe in the UNIDO Hydropower Report. *Energetyka Wodna* 1. 36–42.

Stone, R. 2011. Mayhem on the Mekong. *Science* 333. 814–818.

Szabó, M. and Kiss, Á. 2014. Effects of renewable energy resources on the landscape. *Hungarian Geographical Bulletin* 63. (1): 5–16. Doi: 10.15201/hungeobull.63.1.1

Świderska, I. and Lebiecki, P. 2011. *Safety status of water damming structures in Poland at the end of 2009.* Paper for the 25th Scientific and Technical Conference "Building failures" Warsaw, STC, 24–27.

Szulc, P. and Skrzypacz, J. 2022. Small hydropower plants in Poland. In *Small Hydropower Plants in Poland.* Eds.: Wyszkowski, K., Piwowarek, Z. and Pałejko Z., Warsaw, UN Global Compact Network Poland, 12–14.

Trojanowska, A., Kurasiewicz, M., Plesniak, L. and Jedrysek, M.O. 2009. Emission of methane from sediments of selected Polish dam reservoirs. *Teka Komisji Ochrony i Kształtowania Środowiska Przyrodniczego* 6. 368–373.

Wagner, B., Hauer, C. and Habersack, H. 2019. Current hydropower developments in Europe. *Current Opinion in Environmental Sustainability* 37. 41–49. Available at https://doi.org/10.1016/j.cosust.2019.06.002

Wiatowski, M. and Rosik-Dulewska, C. 2012. Present status and the possibilities of hydropower industry development in the Opole Voivodeship. *Water–Environment–Rural Areas* 2. (38): 313–327.

Zimny, J., Michalak, P., Bielik, S. and Szczotka, K. 2013. Directions in development of hydropower in the world, in Europe and Poland in the period 1995–2011. *Renewable and Sustainable Energy Reviews* 21. 117–130.

BOOK REVIEW SECTION

Nowak, M.J. et al.: Spatial Planning Systems in Central and Eastern European Countries. Review and Comparison of Selected Issues. Cham, Springer, 2023. 112 p.

Central and Eastern Europe is a region where, over the last few decades, the understanding of planning, its approaches and principles, and the main planning concepts and institutional regulation have changed as much as the socio-political and spatial context of the region itself. Therefore, it has gone through a difficult path from the unwanted and contradictory legacy of socialism and planning as an ideological construct that is aimed at solving ideological issues and implementing economic plans, to planning as a policy and practice that is designed to interact with emerging challenges – restructurings and inequalities, new regulation, and new spatial development policy. Hence, the study of spatial planning systems enables to address the planning systems and planning cultures across the countries of Central and Eastern Europe and to unpack their evolution under transition and socio-political landscape changes, to illustrate approaches to planning and organization of planning process, and to exemplify certain planning instruments and practices.

The recently published book is the result of a collaboration of 14 authors from different countries of the region, which offers insight into the context and practice of planning in Bulgaria, the Czech Republic, Estonia, Hungary, Latvia, Lithuania, Poland, Romania, and Slovakia by examining how planning systems are functioning at the local level and thereby establishing a framework for comparing spatial planning systems within the region through a detailed and careful analysis of the planning process in different countries.

The authors of the monograph explore the relations between planning concepts, approaches to spatial planning, and regulations in different national contexts, and they are trying, in particular, to reflect how planning concepts are translated into regulations. For this reason, the analysis of the institutional environment and its historical background is supplemented by case studies of the detailed spatial planning arrangements. Describing specific spatial planning instruments and illustrating their use in relation to the spatial objectives, the authors of the monograph contribute in this way to the discussion on planning instruments, their effectiveness, and the implementation of sectoral policies. By providing a clearly structured analysis of the characteristics of the planning process at the local level and examining specific instruments and solutions in detail, this study ensures a comparative perspective and shows how planning systems are organized in the countries across the region and which concepts and instruments they rely on. Therefore, it offers new insights into discourses on declared concepts and the practices of implementing them.

The book starts with a brief discussion on the meaning and approaches of spatial planning. Such a discussion, which is a kind of reflection on the content and role of planning, is of crucial importance in the region, where such significant changes in the notion of planning and its agenda have taken place in recent decades relations between society, politics, and space. First, a shift from a highly centralized and hierarchized planning in the socialist period to weak planning took place during the transition of the 1990s and early 2000s, which was accompanied by the so-called "legitimacy crisis" of planning (Nedović-Budić, Z.

2001). Such a situation, along with spatial development challenges, created the need for "re-establishing" planning as a societal function across the region (Hirt, S. and Stanilov, K. 2009), which was followed by the search for new concepts in planning and development policy, the adaptation and implementation of these concepts, the "reinventing" (Tsenkova, S. 2007) and strengthening certain types of planning, particularly to manage spatial restructurings and foster collaborative decision-making.

By highlighting the approaches to spatial planning and concepts of planning in legal acts across Central and Eastern European countries, the authors show that various countries translate the objectives of spatial planning into the normative framework in different ways, and even the objectives themselves are often defined differently (p. 9). The same applies to the multidimensionality of planning and the approaches to it: as the authors argue, these vary significantly in different countries of the region (p. 4). Even more diverse are the instruments of planning, such as spatial plans and their composition and content (Chapter 1.3). In this volume, the authors focus on describing the prevailing types of instruments at the local level, which are mostly spatial plans, and their relation to other available instruments, their position in the planning system, and their relationship with development policies, which are in some cases integrated into spatial plans and serve as part of them.

The role and significance of such an analysis is well understood as a starting point for further discussions on the organization of the planning process at the local level, its regulation, and the ability to ensure the compliance of the declared goals, particularly during the land use. However, after considering how different countries are approaching the spatial plans, the authors suppose that an in-depth comparison of the planning systems should rather begin with investigating specific issues instead of specific documents (p. 13), which they treat as a response to current issues and challenges.

Based on the brief analysis of the conceptual and regulatory frameworks of spatial planning, planning tools at the local level, and the relationship between planning and development policy, the authors engage in dialogue on the classification of spatial planning systems, which is a reference point for their further comparative analysis. While emphasizing the difficulties of making comparisons, the authors at the same time underline the importance of such comparisons for various goals, particularly the Europeanization of spatial planning. As limits to such comparisons, the authors name diverse legal provisions and their interpretation, and different planning practices embedded into specific planning cultures. These two dimensions characterizing the planning system can be correlated with what Karel Maier called the "hardware" of formal institutions, instruments, and procedures, and the "software" of planning cultures (Maier, K. 2012).

Finally, the authors propose a set of issues which should be considered when classifying spatial planning systems. The first criterion they propose is the degree of centralization or decentralization of the planning system. Here, it is worthwhile to mention one of the comparative analyses conducted for the countries of the region in 2009 on the first twenty years of post-communist transition, which was dedicated to revisiting urban planning in transitional countries (Hirt, S. and Stanilov, K. 2009). When analyzing the institutional and regulatory framework in so-called transitional countries, particularly its implications for planning, in a long-term perspective, Sonia Hirt and Kiril Stanilov pointed out decentralized planning as a means of consensus-building in communities as well as more dynamic power balance between the central and the local governments.

Since the development of the new balances in the once centralized and hierarchical planning systems is an essential trait for their studying across the region, the levels of planning in spatial planning systems and linkages between them are considered by the authors of the study among the key criteria for classification and comparing of planning systems. This also applies to the relevant acts, instruments, and documents. Thereby, they reflect the concept of governance, the character of the political discourse around it, and planning practices, including formal and informal practices and their balance, which result from "specific configurations of formal and informal institutions in a specific context" (van Assche, K. *et al.* 2012) and reflect the functioning of planning systems. From this perspective, the criteria proposed by the authors – e.g., the consolidation of legislation, the development of documents, public participation, and spatial conflicts – not only characterize the planning system and process but also display how the discourse around them and planning systems themselves are transforming.

Despite a substantial number of shared features and tendencies in the restructuring of planning systems, the context of CEE countries demonstrates considerable variety in approaches to the organization of the planning process and specific instruments, in Chapter 2, the authors perform an overview of the planning systems in different CEE countries to provide a comparative understanding of different institutions, primarily focusing on the local level.

This chapter begins with a brief historical overview of planning and spatial development in the region, where among the common features of CEE countries, the authors suggest the difficulty of responding to the market pressure on the one hand and spatial challenges (like urban sprawl) on the other, which in one way or another manifest themselves in spatial conflicts. Undoubtedly, the narrative of modernization, which for long acted as an umbrella for any projects in a post-communist context, manifested it-

self in dramatic changes in the spatial structures and urban morphologies and even became a challenge for citizen empowerment, marginalizing it in favour of more technocratic governing as Anna Durnová (2021) showed. From this perspective, the analysis of planning systems and the relationship between spatial planning and spatial development policy, as well as specific instruments and their performance, may contribute to the discussion around planning system configurations and their ability to achieve the goal of more sustainable and inclusive spatial development.

The authors of the book organize an overview of the planning systems in the countries across the region as a detailed table, in which they provide diverse characteristics of the planning systems, illustrate the legal acts on spatial planning, give an overview of the relationships between acts at the local and regional levels, characterize related acts at the national level and identify specific solutions by giving examples and highlighting their results. However, the particular focus of this detailed description of the planning systems is made on the local level to explain the production of decisions and documents on spatial planning and their effect. To that end, the authors for the case of each country in the region review how public authorities at the local level participate in spatial planning and explain which acts define zones and land use parameters, indicate which acts at the local level shape the spatial development policy, and how planning acts include environmental conservation. Based on this analysis, different issues associated with spatial plans at the local level are further explained, including particular attention to the role of courts in planning acts.

Hence, the authors create a framework for comparison by critically reviewing how planning systems function in CEE countries. That enables considering specific practices to investment pressures and ensuring the expected role of spatial planning in achieving spatial development goals. During the analysis, it becomes clear that in most countries of the region, the problem of confusion and fragmentation of legal norms in spatial planning appears when various legal acts and even various sectoral regulations include specific provisions. In addition, changes to legislation in this field "occur too frequently" in most countries, further complicating the situation and making it even more confusing for interpretation when applied and complicated for the practice of planning and urban development, thereby causing regular court proceedings. Moreover, as emphasized by the authors, in the case of Romania or the Czech Republic, courts exert influence on the direction of local spatial policies (p. 59) and often shape spatial policy in practice (p. 34); therefore, the book considers the role of courts about planning as one of the criteria for comparing the planning systems.

Although the main planning instrument at the local level is the spatial plan, it is paradoxical that in some countries, such as Bulgaria or Poland, certain municipalities did not adopt the spatial plans, which opens the door to implementing investment projects but significantly challenges sustainable land use. Similarly, the interaction between different planning levels and the implementation of spatial planning regulations is quite challenging, since provisions are sometimes "too vague" (p. 59) for planning practice. The same applies to the relations with development policy and its translation into local spatial planning, which often faces numerous barriers when implemented, i.e., the overabundance of objectives and tasks (the Czech Republic) and the scarcity of a holistic view (Estonia).

It is noteworthy that for several countries at once, particularly the Czech Republic, Poland, and Latvia, the authors highlight the underrepresentation of the public interest in spatial planning and the "need for an in-depth dialogue" (p. 44). We should underline that the authors focus here mostly not on participation as such, which implies the various forms of involvement during the development of spatial planning documents but on the need and growing demand for proper representation and consideration of public interest. The constant coordination of efforts, which goes beyond the scope of statutory requirements on public participation in spatial planning, can significantly change approaches and decisions on spatial development, which the authors illustrate by giving the example of one of the towns in Bulgaria.

By providing a detailed overview of the planning systems in each of the countries, the authors have provided a framework for both comparing and discussing planning practices, planning instruments, and configurations of the planning systems across the region, as well as their relations with spatial development goals and their ability to put them in practice. Hence, in Chapter 3, the book's authors perform, on the one hand, the comparative analysis of planning systems (Chapter 3.2) and, on the other hand, employ individual case studies to illustrate the context of specific planning systems more deeply (Chapter 3.3). In this way, the authors open the possibilities for "the transfer of best planning and policy practices across systems, places, or countries" (van Assche, K. *et al.* 2020).

Before analyzing individual cases, the authors note that some planning systems lack an overall development concept or a proper translation of the concept into individual instruments (p. 78). Given this, the characteristics of planning instruments and their interaction with each other provide an essential insight into the planning process, its results, and its effectiveness.

In 2015, Sonia Hirt noted that regional planning could become "more instrumental in solving some of the serious challenges" (Hirt, S. 2015). That's why particular interest is the unpacking of the specific instruments – for instance, the analysis of general spatial plans for cases in Bulgaria, regulatory plans in the

Czech Republic, and the strategy of the Riga planning region, as well as individual decisions and planning practices, including outsourcing plan preparations in Estonia, specific environmental natural provisions within spatial plans in Hungary, and court rulings in Poland. The authors comprehensively examine in these cases the challenges, problems, and solutions in each of the planning systems in the CEE region, show their mosaic and diversity across the region, and the ability of different instruments and practices to deal with these challenges. Hence, the authors guide the discussion on the planning instruments and practices in CEE countries under the umbrella of what Tuna Tasan-Kok calls critical constructive thinking in contemporary planning studies (Tasan-Kok, T. 2019) to promote more effective approaches, decisions, and practices across the region.

Olena Denysenko[1]

REFERENCES

Durnová, A. 2021. Czech post-communist trouble with participatory governance. Toward an analysis of the cultural agency of policy discourses. *Policy Studies* 42. (1): 80–97.

Hirt, S. and Stanilov, K. 2009. *Twenty Years of Transition: The Evolution of Urban Planning in Eastern Europe and the Former Soviet Union, 1989–2009.* Nairobi, United Nations Human Settlements Programme.

Hirt, S. 2015. Planning during post-socialism. In *International Encyclopedia of the Social & Behavioral Sciences.* 2nd Edition, Vol. 18. Ed.: Wright, J. D., London, Elsevier, 187–192.

Maier, K. 2012. Europeanization and changing planning in East-Central Europe: An Easterner's view. *Planning Practice and Research* 27. (1): 137–154.

Nedović-Budić, Z. 2001. Adjustment of planning practice to the new Eastern and Central European context. *Journal of the American Planning Association* 67. (1): 38–52.

Tasan-Kok, T. 2019. Exploring critical constructive thinking in planning studies. *plaNext – next generation planning* 8. 40–44.

Tsenkova, S. 2007. Reinventing strategic planning in post-socialist cities: Experiences from Sofia. *European Planning Studies* 15. (3): 295–317.

van Assche, K., Beunen, R. and Duineveld, M. 2012. Formal/informal dialectics and the self-transformation of spatial planning systems: an exploration. *Administration & Society* 46. (6): 654–683.

van Assche, K., Beunen, R. and Verweij, S. 2020. Comparative planning research, learning, and governance: the benefits and limitations of learning policy by comparison. *Urban Planning* 5. (1): 11–21.

[1] Ukrainian Researches Society, Kyiv, Ukraine.
E-mail: denysenko.olena.o@gmail.com

Flint Ashery, S.: Micro-residential Dynamics: A Case Study of Whitechapel, London. The Urban Book Series. Cham, Springer, 2019. 130 p.

Micro-residential Dynamics is a book containing niche studies in micro-segregation research, from the point of view of using both quantitative and qualitative methods. In the study of segregation, smaller scales than neighbourhoods, such as street and building levels, have been coming to the fore since the 2000s, one result of which is the introduction of suburban areas as a scale of inquiry into the scientific discourse. One of the main motives of these studies is that, unlike previous research, they do not neglect scrutinising socio-economic and cultural differences within streets and argue that if we do not consider such micro-spaces homogeneous, we will see a much more diverse society. As a result, micro-segregation research is one of the defining aspects of urban research nowadays where, due to the rudimentary nature of the topic, mainly quantitative studies have been conducted to present the phenomenon.

Micro- and vertical segregation studies on European cities such as Budapest (Kovács, Z. *et al.* 2022), Bucharest (Marcinczak, S. and Hess, B.D. 2022), Naples (Dines, N. and Mattiucci, C. 2022), Athens (Maloutas, T. *et al.* 2023), have been complemented in the literature by South American and Near and Far Eastern settlements such as Tel Aviv (Shamur, T. and Yacobi, H. 2022) or Hong Kong (Ho, H.K. and Yip, M. 2022). Flint Ashery's book on London's Whitechapel neighbourhood has expanded previous research on micro-segregation to include views of small-scale segregation, vertical residential segregation, and social differences perceived by local populations. The readers can get acquainted with the topical question of how the image and causes of segregation between commonly known neighbourhoods can be interpreted on a micro scale. The answer is made possible by the long-time series statistical analyses presented in the study, while the longitudinal description of the socio-economic and ethnic composition of the pilot area and the interviews reveal the underlying reasons, which are mostly site-specific but sometimes generalisable to other areas.

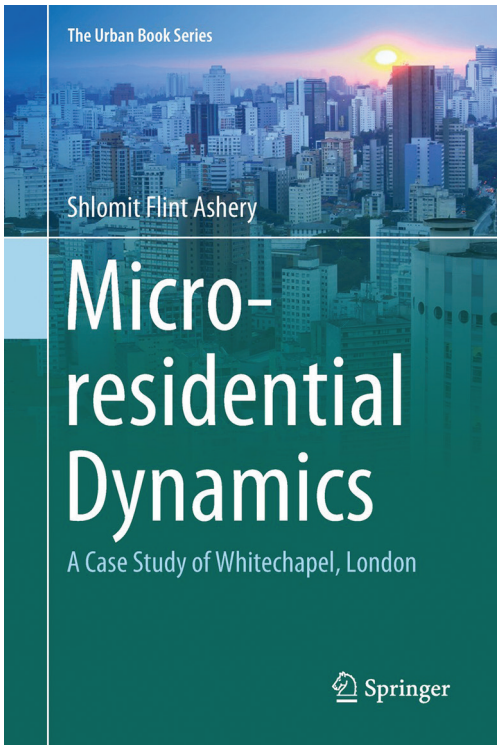

Based on this dual approach, the book consists of two separate parts where Flint Ashery examines issues related to the topic of micro-segregation. It should be emphasised that the book deals with the relationship between private and public property in the light of micro-segregation. Therefore, the majority of the studies focus on the private sector and, although with less emphasis, the author presents the role of the public sector. The book begins with an introduction to the model area of Whitechapel, so the reader can learn how the area has developed and changed and gain a general picture of the ethnic and religious complexity of the district. The novel approach of the book is supported by its limited emphasis on describing the physical environment, which often dominates traditional segregation research.

In the first part of the book, entitled *Private Realm*, the author presents the impact of social diversity on the development and existence of micro-segregation through four studies. The studies reveal the positive and negative relationships that can develop between different social groups such as illegal immigrants and indigenous locals, or the impact of the real estate market on immigration and immigrants. The author devotes a separate chapter to examining the pattern of horizontal and vertical segregation on a small scale.

In the second chapter, we can learn the background of the choice of residence, which proves that socio-cultural and economic reasons can be traced back to who chooses which place of residence. The historical connection between ethnic and/or religious groups plays an important role in making housing decisions in the study area. Another decisive aspect is the proximity of friends living in the area. In the chapter on

horizontal segregation, the author concludes that inside buildings, newcomers look for close acquaintances who belong to their own group, while they regard other people living there as "enemies". It is an interesting observation of the researcher that the same phenomenon and pattern, however, cannot be observed at the neighbourhood level. Flint Ashery's research does not explain why this phenomenon occurs but it provides a new opportunity within micro-segregation research.

The third chapter of the book, dealing with vertical segregation, is perhaps one of the most important parts of the work, because it summarises academic literature on the topic. The author analyses several concepts and processes of vertical segregation and differentiation, which raise the question of which statistical criteria in which study can be used for interpreting segregation. The chapter states that vertical segregation and differentiation are based on income disparities and employment group categories, but Flint Ashery expands on this knowledge. As a result of primary research the author investigates the inner guiding force of verticality in the studied part of the city. She reveals why people of the Muslim religion prefer to choose the upper floor. As qualitative research confirms, the corridor is functioning as a kind of public and private space, which also becomes the place of prayer. The corridor builds the community of the given floor, where the dwellers will not be made vulnerable or discriminated because of their religion, and, thus, the number of conflict situations with other groups will remain moderate. The author complements what previous analyses identified as the causes of vertical segregation with his study results, i.e., that identity and belonging to a specific social group also determine social separation within the building.

In the fourth chapter, the author presents the situation of micro-segregation in the light of public and private homes. In this section, Flint Ashery explores several processes, some of which are present in the real estate market globally. The number of state-owned properties in the pilot area of Whitechapel is insufficient, but the number of people living in social housing is increasing. Another important aspect is that since the EU enlargement in 2004, people arriving from EU Member States have much better prioritised social housing than other nations (e.g., of Somali and Irish origin). The gentrification process has also started in the pilot area. People with low income are crowded out, which is manifested in the fact that more and more people and families live together in the same real estate. These dynamics is also confirmed by the so-called overcrowding index, which measures the number of people living in one apartment, and indicates an accelerating growth. As a result, informal letting of real estate has started in the area, which in turn plays a role in maintaining micro-segregations. Although a general solution to the problem is yet to be found, the author briefly presents some possible solutions at the end of the chapter.

In the last, fifth chapter of the first part of the book, the author presents informal housing in more detail, so the reader can understand the situation of the affected residents and their motivations. Flint Ashery visited and made interviews with immigrants who do not have official papers and therefore live informally in an apartment. The result is helpful for micro-segregation research and urban planning because we can learn that: „Most of the undocumented population prefer to live close to the centre and amongst their 'friends'". However, there is a lack of cohesion between the title and the content of the chapter.

The second and shorter part is entitled *Public Realm.* It consists of two chapters, one of which deals with the role of decision-makers in the diversity and micro-segregation of Whitechapel. The second chapter serves as a summary of the book as a whole. The chapter entitled *Whitechapel Road: Between Group Behaviour and Planning Policy* draws attention to that one should not only keep in mind what has been decided, but also what has not been decided and why, while examining the decision-making behaviour of city managers. In the pilot area of Whitechapel, the aforementioned changes in the real estate market brought about the transformation of social groups and increasing tension between them. Despite the fact that both the local population and the local city administration are aware of the situation, nothing has changed, which results rather from the preservation of the territorial status quo instead of a compromise between the groups.

For those interested in micro-segregation, I recommend Flint Ashery's book because it provides a comprehensive overview of available research on the topic and enriches small-scale social segregation studies with its qualitative research results. The reader can learn about the ethnic and religious diversity of the Whitechapel pilot area as well as the problems and conflict situations arising from it. The book examines the relationship between the private and public spheres in the light of micro-segregation, but these two strands do not have equal weight. In most cases, the private sphere comes to the fore, while only one chapter analyses the public sector. The complexity of the topic is indicated by that the author examines micro-segregation from several perspectives. Yet, as the im balance between investigating the public and private sectors illustrates, many aspects of the problems affecting communities are still to be explored, and these would further expand our knowledge about horizontal and vertical segregation and micro-segregation.

The book *Micro-residential Dynamics* may contain less maps than what a geographer expects, but the author fills this gap with illustrative images and figures. In addition, the 322 in-depth interviews will help researchers better understand how and why micro-

segregation develops, and why different ethnic and religious groups choose to live side by side. Although the author answers many questions, she also raises many new ones, which confirms that micro-scale segregation is still a process to be explored – but I think *Micro-residential Dynamics* will be one of the defining studies in the future.

Acknowledgement: Supported by the ÚNKP-23-2 New National Excellence Program of the Ministry for Culture and Innovation from the source of the National Research, Development and Innovation Fund.

Ramóna Vámos[1]

REFERENCES

Dines, N. and Mattiucci, C. 2022. Constantly evoked but under-researched: the conundrum of vertical stratification in Naples. In *Vertical Cities*. Eds.: Maloutas, T. and Karadimitriou, N., Cheltenham, Edward Elgar, 23–38.

Ho, H.K. and Yip, M. 2023. From micro- to nano-segregation: policy-led vertical urbanism in Hong Kong. *International Journal of Housing Policy* 1–15.

Kovács, Z., Székely, J. and Szabó, B. 2022. Vertical micro-segregation in apartment buildings in Budapest. In *Vertical Cities*. Eds.: Maloutas, T. and Karadimitriou, N., Cheltenham, Edward Elgar, 189–203.

Maloutas, T., Spyrellis, S., Szabó, B. and Kovács, Z. 2023. Vertical segregation in the apartment blocks of Athens and Budapest: A comparative study. *European Urban and Regional Studies* 30. (1): 72–90.

Marcinczak, S. and Hess, B.D. 2022. Vertical separation in high-rise apartment buildings: evidence from Bucharest and Budapest under state socialism. In *Vertical Cities*. Eds.: Maloutas, T. and Karadimitriou, N., Cheltenham, Edward Elgar, 173–188.

Shamur, T. and Yacobi, H. 2022. Compulsory social mix, micro-scale segregation and gentrification: the case of Gan HaHashmal neighbourhood, Tel Aviv. In *Vertical Cities*. Eds.: Maloutas, T. and Karadimitriou, N., Cheltenham, Edward Elgar, 253–269.

[1] University of Szeged, Department of Economic and Social Geography, Szeged, Hungary.
E-mail: vamos.ramona@geo.u-szeged.hu

GUIDELINES FOR AUTHORS

Hungarian Geographical Bulletin (formerly Földrajzi Értesítő) is a double-blind peer-reviewed English-language quarterly journal publishing open access **original scientific works** in the field of physical and human geography, methodology and analyses in geography, GIS, environmental assessment, regional studies, geographical research in Hungary and Central Europe. In the regular and special issues also discussion papers, chronicles and book reviews can be published.

Manuscript requirements

We accept most word processing formats, but MSWord files are preferred. Submissions should be single spaced and use 12pt font, and any track changes must be removed. The paper completed with abstract, keywords, text, figures, tables and references should not exceed **7,000 words**.

The Cover Page of the article should only include the following information: title; author names; a footnote with the affiliations, postal and e-mail addresses of the authors in the correct order; a list of 4 to 8 keywords; any acknowledgements.

An abstract of up to **300 words** must be included in the submitted manuscript. It should state briefly and clearly the purpose and setting of the research, methodological backgrounds, the principal findings and major conclusions.

Figures and tables

Submit each illustration as a separate file. Figures and tables should be referred in the text. Numbering of figures and tables should be consecutively in accordance with their appearance in the text. Lettering and sizing of original artwork should be uniform. Convert the images to TIF or JPEG with an appropriate resolution: for colour or grayscale photographs or vector drawings (min. 300 dpi); bitmapped line drawings (min.1000 dpi); combinations bitmapped line/photographs (min. 500 dpi). Please do not supply files that are optimised for screen use (e.g., GIF, BMP, PICT, WPG). Size the illustrations close to the desired dimensions of the printed version. Be sparing in the use of tables and ensure that the data presented in tables do not duplicate results described elsewhere in the article.

REFERENCES

Please ensure that every reference cited in the text is also present in the reference list (and vice versa).

Reference style

Text: In the text refer to the author's name (small capitals with initials) and year of publication. References should be arranged first chronologically and then further sorted alphabetically if necessary. More than one reference from the same author(s) in the same year must be identified by the letters 'a', 'b', placed after the year of publication.
Examples: (Ridgewell, A.J. 2002; Maher, B.A. *et al.* 2010) or Ridgewell, A.J. (2002); Maher, B.A. *et al.* (2010).

Journal papers:
Aagaard, T., Orford, J. and Murray, A.S. 2007. Environmental controls on coastal dune formation; Skallingen Spit, Denmark. *Geomorphology* 83. (1): 29–47.

Books:
Pye, K. 1987. *Aeolian Dust and Dust Deposits.* London, Academic Press.

Book chapters:
Kovács, J. and Varga, Gy. 2013. Loess. In *Encyclopedia of Natural Hazards.* Ed.: Bobrowsky, P., Frankfurt, Springer, 637–638.

Book reviews

Book reviews should be between 2,000 and 3,000 words (including references).

Submission

Submission to this journal occurs online. Please submit your article via http://ojs3.mtak.hu/index.php/hungeobull/about/submissions

All correspondence, including notification of the Editor's decision and requests for revision, takes place by e-mail.

Publisher:
Research Centre for Astronomy and Earth Sciences
1121 Budapest, Konkoly Thege Miklós út 15–17., Hungary

Editorial office:
Geographical Institute, Research Centre for Astronomy and Earth Sciences
1112 Budapest, Budaörsi út 45., Hungary
Phone, fax: +36 1 309 2628
E-mail: geobull@mtafki.hu, kovacs.zoltan@csfk.org
Distribution: GABRIELLA PETZ, petz.gabriella@csfk.org
Full text is available at https://ojs3.mtak.hu/index.php/hungeobull

Typography: ESZTER GARAI-ÉDLER
Technical staff: FANNI KOCZÓ, ANIKÓ KOVÁCS, GÁSPÁR MEZEI

Cover design: ANNA REDL
Printed by: Premier Nyomda Kft.

HU ISSN 2064–5031
HU E-ISSN 2064–5147

Distributed by the Geographical Institute, Research Centre for Astronomy and Earth Sciences

Subscription directly at the Geographical Institute, Research Centre for Astronomy and Earth Sciences (H-1112 Budapest, Budaörsi út 45), by postal order or transfer to the account IBAN: HU24 10032000-01730841-00000000. Individual copies can be purchased in the library of the Institute at the above address.